

MICROBUBBLE-ASSISTED ULTRASOUND FOR RETINAL DRUG DELIVERY



Charis Rousou

Microbubble-assisted ultrasound for retinal drug delivery

Charis Rousou

Copyright 2022 © **C. Rousou**

The Netherlands. All rights reserved. No parts of this thesis may be reproduced, stored in a retrieval system or transmitted in any form or by any means without permission of the author.

DOI: <https://doi.org/10.33540/1626>

ISBN: 978-94-6458-901-6

Provided by thesis specialist Ridderprint, ridderprint.nl

Printing: Ridderprint

Cover design: Collin Wetzel, collinwetzel.com

Layout and design: Eduard Boxem, persoonlijkproefschrift.nl

Microbubble-assisted ultrasound for retinal drug delivery

Door microbellen ondersteund ultrageluid voor retinale medicijnafgifte

(met een samenvatting in het Nederlands)

Proefschrift

ter verkrijging van de graad van doctor aan de
Universiteit Utrecht
op gezag van de
rector magnificus, prof.dr. H.R.B.M. Kummeling,
ingevolge het besluit van het college voor promoties
in het openbaar te verdedigen op

woensdag 8 maart 2023 des middags te 2.15 uur

door

Charis Rousou

geboren op 10 januari 1992
te Nicosia, Cyprus

Promotoren:

Prof. dr. G. Storm

Prof. dr. C.T.W. Moonen

Prof. dr. E. Mastrobattista

Copromotor:

Dr. R.H.R. Deckers

Beoordelingscommissie:

Prof. dr. S. de Smedt

Prof. dr. R. Masereeuw

Prof. dr. S.M. Imhof

Prof. dr. R.M. Schiffelers

Dr. K. Kooiman PhD

Dit proefschrift werd (mede)mogelijk gemaakt met financiële steun van het onderzoeks- en innovatieprogramma Horizon 2020 van de Europese Unie onder de Marie Skłodowska-Curie-subsidieovereenkomst nr. 722717 (OCUTHER).

Table of Contents

Chapter 1	General introduction and thesis outline	10
Chapter 2	Ultrasound and microbubbles for the treatment of ocular diseases: From preclinical research towards clinical application	22
Chapter 3	The effect of microbubble-assisted ultrasound in molecular permeability across cell barriers	76
Chapter 4	A technical protocol for an experimental <i>ex vivo</i> model using arterially perfused porcine eyes	108
Chapter 5	Microbubble-mediated drug delivery in the retina using a clinical ultrasound system	132
Chapter 6	Summary and general discussion	150
List of abbreviations		162
Appendices	Nederlandse samenvatting	166
	List of publications	169
	Acknowledgements	170
	About the author	174

To my parents and the victims of the COVID-19 pandemic.

1

General Introduction And Thesis Outline

INTRODUCTION

This thesis aims to investigate the potential of microbubble-assisted ultrasound as a means of drug delivery to the retina. In this introductory chapter three retinal diseases, which were selected based on their potential to be treated with ultrasound and microbubbles (USMB), are briefly discussed. The standard methods currently used in the clinic for their treatment and the associated challenges are then presented. Next, the definition of USMB therapy is given, which is proposed as a potential therapeutic method to face the current challenges in retinal drug delivery. Finally, the structure of this thesis is presented.

ANATOMY AND FUNCTION OF THE RETINA

The retina is a semi-transparent tissue constructed by multiple cell types in laminar arrangement (Figure 1). Light beams that enter the eye are converted by the retina into electric signals, which are sent along the optic nerve to the brain and are processed to finally form images. The retina can be subdivided into the neural retina and the retinal pigment epithelium (RPE). The cell layers of the neural retina from inside to outside are: inner limiting membrane, nerve fiber layer, retinal ganglion cells, inner plexiform layer, inner nuclear layer, outer plexiform layer, outer nuclear layer, outer limiting membrane and photoreceptor layer. Adjacent to the photoreceptors is the RPE, an epithelial cell monolayer that is pigmented owing to the presence of melanin. One of the main roles of RPE is to phagocytose debris and waste products from the photoreceptors. The Bruch's membrane is an extracellular matrix located between the RPE and choroid. The choroid is a dense vascular network that provides the outer retina with nutrients. Like the RPE, choroid cells in humans are highly pigmented, a property that contributes to increase the absorbance of light.

To protect the retina from harmful substances present in the blood circulation and regulate the exchange of molecules with the bloodstream in a controlled manner, a specialized barrier function takes place in the vascular endothelium and epithelium of the retina [1]. Tight junctions present at the level of the RPE and retinal endothelium form the outer and inner blood-retina barrier, respectively.

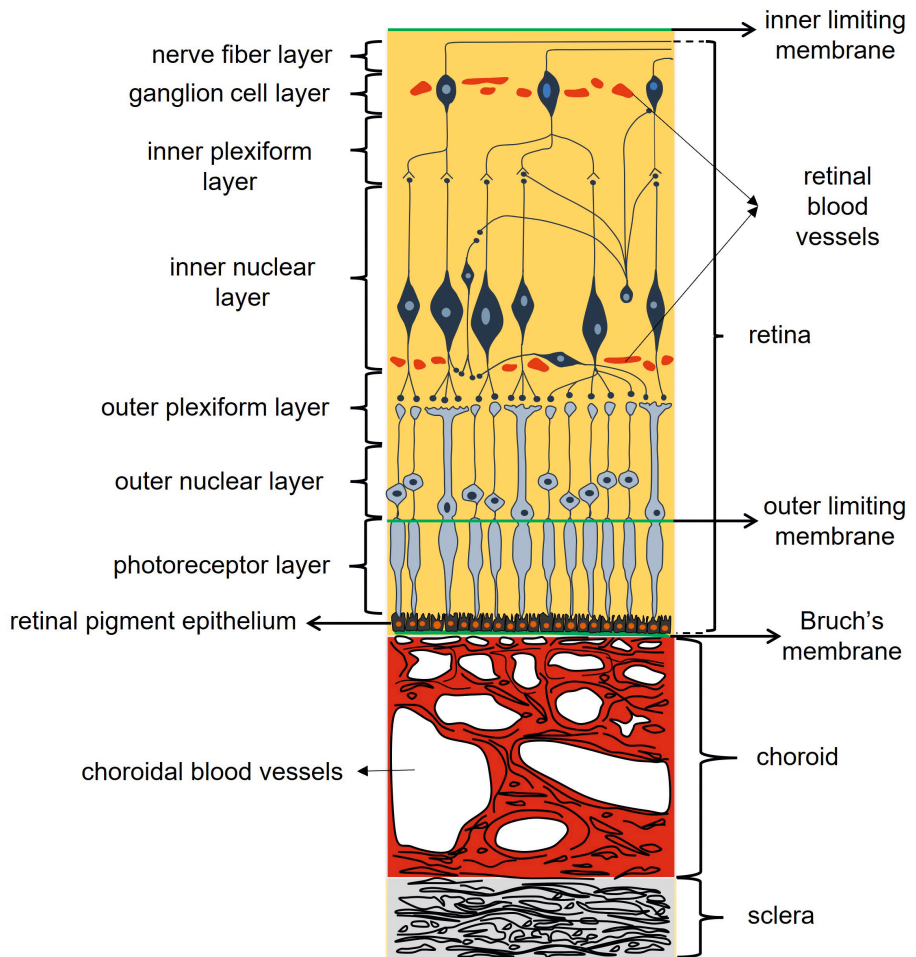


Figure 1. Anatomy of the retina. Figure not to scale. Adapted from [2].

RETINAL DISEASES

Retinal diseases can affect any part of the retina, can cause visual impairment and, if left untreated, blindness. Although some retinopathies are considered acquired, the great majority of them have an inherited basis as they result from the interaction between a particular genotype and the environment [3]. Since 1986, when the retinoblastoma-associated RB1 gene was identified and cloned, over 270 genes have been associated with retinal diseases [4]. Genetic complexity and heritability vary among retinopathies. For instance, Sorsby fundus dystrophy is a highly heritable retinal disease with a single genetic etiology, in contrast to age-related macular degeneration (AMD) and diabetic

retinopathy (DR), which are influenced by other factors (e.g., environment, lifestyle, age) in addition to multiple genetic variants [4–8]. As a result, AMD and DR are sometimes labeled as acquired retinopathies. Below, three examples of retinopathies are discussed based on the potential to be treated with microbubble-assisted ultrasound.

AMD is the most common cause of vision loss among people older than 60 years, accounting for 8.7% of all blindness globally [9]. It is expected that 288 million people will be affected by AMD by 2040 [9–12]. AMD is caused by the deposition of acellular polymorphous debris (drusen) between the RPE and Bruch's membrane. In AMD the area of the macula is damaged, therefore the central vision is affected and patients lose the ability to see fine details (Figure 2, middle).

DR is another retinal disorder that affects almost all diabetic patients with type 1 diabetes and more than 60% of patients with type 2 diabetes. Globally, DR accounts for 2.6% of blindness [13]. Depending on the disease stage, DR is characterized by microaneurysms and hemorrhages and in more severe form by retinal neovascularization [14,15]. Patients with DR experience blurry vision, floating spots in their vision (Figure 2, right) or blindness.

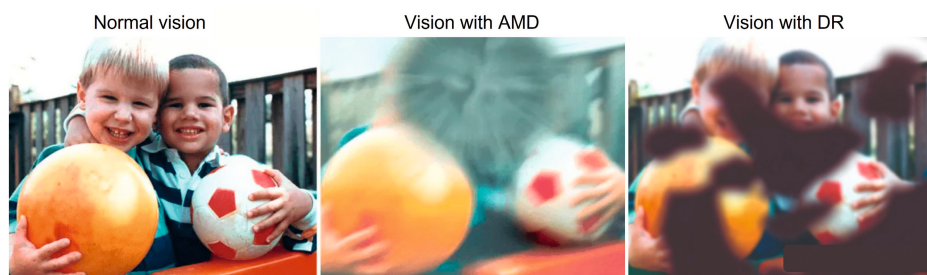


Figure 2. Simulation of normal vision (left), vision affected by AMD (middle, adapted from [16]) and DR (right, adapted from [17]). AMD: age-related macular degeneration, DR: diabetic retinopathy

Retinoblastoma (RB) is the primary intraocular malignancy in children, caused by a mutation in the RB1 gene. The incidence of RB is 1 in 15,000–20,000 live births, of which 92% occur in developing countries [18]. Patients in countries with low national income level are diagnosed at an older age compared to those in developed countries and have a higher proportion of locally advanced disease due to delayed diagnosis and treatment [19].

CURRENT STANDARDS IN RETINAL DRUG DELIVERY

The standard care of treatment of AMD is intravitreal injection of anti-vascular endothelial growth factor (anti-VEGF) agents [20]. DR is typically treated with laser therapy [21], however following the improved therapeutic results in the treatment of AMD, anti-VEGF agents are currently also used in the treatment of DR [22].

RBs are typically treated with intravenous chemotherapy in order to prevent metastases. In case of extensive unilateral tumors and tumors with seeds, intraarterial chemotherapy is administered. Intraarterial injections enable ten times higher dose to the eye compared to the intravenous route and are associated with reduced systemic toxicity [23,24].

OPEN CHALLENGES IN RETINAL DRUG DELIVERY

Despite the improvements in the treatment of retinal diseases, there are various challenges to face in terms of therapeutic efficacy and specificity. The half-lives of anti-VEGF agents after intravitreal injections are limited to a couple of days (2-9 days depending on the anti-VEGF agent) [25,26], which creates the need for repeated eye injections (monthly or bi-monthly) in order to manage chronic diseases like AMD and DR. Intravitreal injections are frequently associated with patient discomfort and other adverse effects, such as increased intraocular pressure, retinal detachment, endophthalmitis and retinal hemorrhages [27,28]. In addition, the presence of the inner limiting membrane (the vitreoretinal border) hinders the delivery of some therapeutic molecules that are intravitreally injected [29,30].

Intravenous and intraarterial injections of chemotherapeutic agents for the treatment of RB often result in inadequate drug penetration in the tumor, causing the presence of vitreous and subretinal seeds that form recurrent and chemoresistant tumors [23,31]. Consequently, there is a clear need for novel drug delivery methods that are targeted and enable more efficacious drug deposition in the disease side.

Targeting the retina from the blood circulation is a less invasive method as compared to intravitreal injections. Molecules that are intravenously administered and circulate in the choroid are in closer proximity to the disease side (i.e., choroidal endothelial cells, RPE cells and cells of the neural retina) compared to intravitreally administered drugs,

which need to penetrate through multiple cell layers in the retina before they reach the target cells. In addition, using the intravenous route, the inner limiting membrane is bypassed. However, intravenously administered drug molecules need to bypass the BRB in order to have access to the neural retina. Thus, a method that enables disruption of the BRB in a safe and reversible manner could potentially be combined with intravenously administered drugs. Due to the anatomy of the eye, an externally applied trigger, such as ultrasound waves, would be suitable to be used to facilitate targeted delivery of drugs to the retina.

ULTRASOUND AND MICROBUBBLES (USMB) AS A MEANS FOR DRUG DELIVERY

Ultrasound relates to sound waves with frequencies above the human audible frequency range (above 20 kHz). Ultrasound is used as a non-invasive medical imaging modality in various diagnostic applications. In ophthalmology, ultrasound imaging is used for the diagnosis of intraocular tumors, and the detection of structural changes in glaucoma and retinal detachment. Additionally, high frequency ultrasound (35–70 MHz) is used to construct high resolution images of the anterior eye.

Microbubbles are spherical particles with size in the micrometer range (diameter between 0.5 and 10 μm) and a gaseous core [32]. They are intravenously administered and used as ultrasound contrast agents as they improve the blood-to-tissue contrast during ultrasound imaging. Due to their size, microbubbles remain in the vascular space, when the vasculature is intact. Contrast-enhanced ultrasound (CEUS) is a microbubble-specific imaging method with various clinical applications, such as imaging of carotid arterial, liver and kidney disorders [33–35].

In addition to their use in diagnostic imaging, microbubbles in combination with ultrasound, can be used for therapeutic purposes. When exposed to ultrasound waves, microbubbles undergo oscillations that induce various bioeffects on the surrounding structures. These bioeffects can be used to improve the local distribution and/or uptake of drugs and genes [36,37]. Recently, preclinical investigations of the therapeutic use of ultrasound and microbubbles (USMB) have been conducted in the field of ophthalmology, where there is a clear need for improved new delivery methods [38–41].

AIM AND OUTLINE OF THIS THESIS

This thesis aims to investigate the potential of USMB therapy as a means of treatment of retinal diseases, the major challenge in the field of ophthalmology.

In **Chapter 2** the mechanisms underlying the therapeutic properties of USMB are discussed in more depth. Furthermore, an extensive overview is given of the *in vitro* and *in vivo* studies that investigated the efficacy and safety of USMB in ocular drug delivery. According to the available literature, USMB can (i) temporarily disrupt the blood–retina barrier in order to enhance the delivery of systemically administered drugs into the eye, (ii) induce intracellular uptake of anticancer drugs and macromolecules and (iii) achieve targeted delivery of genes, for the treatment of ocular malignancies and degenerative diseases. Finally, the safety and tolerability aspects of USMB, essential for the translation of USMB to the clinic for drug delivery applications, are discussed.

The USMB-mediated transport efficacy of five molecules with different (i) hydrophilicities and (ii) molecular weights across an epithelial cell barrier was studied in **Chapter 3**. The transwell model was used to investigate the permeability of the selected molecules across the *in vitro* barrier. Furthermore, the effect of USMB on the permeability of the barrier was investigated using a clinically relevant molecule (anti-CXCR4 nanobody) as a model drug for the treatment of RB.

To study the efficacy of USMB in a more physiologically representative system than an *in vitro* model, an experimental platform using arterially perfused *ex vivo* porcine eyes was developed. In **Chapter 4** a detailed description of the steps taken in this method starting from eye enucleation to cannulation of the ophthalmic artery and perfusion is given.

Using *ex vivo* eyes that were prepared as described in chapter 4, the effect of USMB on the porcine retina was investigated in **Chapter 5**. A clinical ultrasound system and FDA/EMA approved microbubbles were used for the treatment. Intracellular accumulation of model drugs with different molecular weights was compared between eyes treated with USMB and eyes that received ultrasound only.

In **Chapter 6** the findings of this thesis are summarized and future perspectives of USMB in retinal drug delivery are discussed.

The research described in this thesis was financially supported by the European Union's Horizon 2020 research and innovation program under the Marie Skłodowska-Curie grant agreement No 722717 (OcuTher) [38]. The objective of this three year project was to educate early-stage researchers in a European network, consisting by academic and industrial partners, where they received tailored, multi-disciplinary and inter-sectoral education in preclinical ocular drug development.

REFERENCES

1. O’Leary, F.; Campbell, M. The Blood–retina Barrier in Health and Disease. *FEBS J.* 2021, doi:10.1111/febs.16330.
2. Rousou, C.; Schuurmans, C.C.L.; Urtti, A.; Mastrobattista, E.; Storm, G.; Moonen, C.; Kaarniranta, K.; Deckers, R. Ultrasound and Microbubbles for the Treatment of Ocular Diseases: From Preclinical Research towards Clinical Application. *Pharmaceutics* 2021, 13, 1782, doi:10.3390/pharmaceutics13111782.
3. Seiple, W.; Greenstein, V.C.; Holopigian, K.; Noble, K.G. Chapter 15 Acquired Retinopathies. In *Handbook of Clinical Neurophysiology*; Elsevier, 2005; Vol. 5, pp. 295–327 ISBN 9780444512338.
4. Sergouniotis, P.I. Inherited Retinal Disorders: Using Evidence as a Driver for Implementation. *Ophthalmologica* 2019, 242, 187–194, doi:10.1159/000500574.
5. Stöhr, H.; Anand-Apte, B. A Review and Update on the Molecular Basis of Pathogenesis of Sorsby Fundus Dystrophy. In *Retinal Degenerative Diseases*; LaVail, M.M., Ash, J.D., Anderson, R.E., Hollyfield, J.G., Grimm, C., Eds.; Springer US: Boston, MA, 2012; Vol. 723, pp. 261–267 ISBN 978-1-4614-0630-3, 978-1-4614-0631-0.
6. Fritsche, L.G.; Fariss, R.N.; Stambolian, D.; Abecasis, G.R.; Curcio, C.A.; Swaroop, A. Age-Related Macular Degeneration: Genetics and Biology Coming Together. *Annu. Rev. Genomics Hum. Genet.* 2014, 15, 151–171, doi:10.1146/annurev-genom-090413-025610.
7. Anantharaman, G.; Jain, A. Genetics in Age-Related Macular Degeneration. In *Genetics of Ocular Diseases*; Nema, H.V., Nema, N., Eds.; Springer Nature Singapore: Singapore, 2022; pp. 125–134 ISBN 978-981-16-4246-3, 978-981-16-4247-0.
8. Bhatwadekar, A.D.; Shughoury, A.; Belamkar, A.; Ciulla, T.A. Genetics of Diabetic Retinopathy, a Leading Cause of Irreversible Blindness in the Industrialized World. *Genes* 2021, 12, 1200, doi:10.3390/genes12081200.
9. Wong, W.L.; Su, X.; Li, X.; Cheung, C.M.G.; Klein, R.; Cheng, C.-Y.; Wong, T.Y. Global Prevalence of Age-Related Macular Degeneration and Disease Burden Projection for 2020 and 2040: A Systematic Review and Meta-Analysis. *Lancet Glob. Health* 2014, 2, e106–e116, doi:10.1016/S2214-109X(13)70145-1.
10. Klein, R.; Klein, B.E.; Cruickshanks, K.J. The Prevalence of Age-Related Maculopathy by Geographic Region and Ethnicity. *Prog. Retin. Eye Res.* 1999, 18, 371–389, doi:10.1016/s1350-9462(98)00025-1.
11. Keel, S.; Xie, J.; Foreman, J.; van Wijngaarden, P.; Taylor, H.R.; Dirani, M. Prevalence of Age-Related Macular Degeneration in Australia: The Australian National Eye Health Survey. *JAMA Ophthalmol.* 2017, 135, 1242, doi:10.1001/jamaophthalmol.2017.4182.
12. Klaver, C.C.; Assink, J.J.; van Leeuwen, R.; Wolfs, R.C.; Vingerling, J.R.; Stijnen, T.; Hofman, A.; de Jong, P.T. Incidence and Progression Rates of Age-Related Maculopathy: The Rotterdam Study. *Invest. Ophthalmol. Vis. Sci.* 2001, 42, 2237–2241.
13. Leasher, J.L.; Bourne, R.R.A.; Flaxman, S.R.; Jonas, J.B.; Keeffe, J.; Naidoo, K.; Pesudovs, K.; Price, H.; White, R.A.; Wong, T.Y.; et al. Global Estimates on the Number of People Blind or Visually Impaired by Diabetic Retinopathy: A Meta-Analysis From 1990 to 2010. *Diabetes Care* 2016, 39, 1643–1649, doi:10.2337/dc15-2171.

14. Antonetti, D.A.; Silva, P.S.; Stitt, A.W. Current Understanding of the Molecular and Cellular Pathology of Diabetic Retinopathy. *Nat. Rev. Endocrinol.* 2021, 17, 195–206, doi:10.1038/s41574-020-00451-4.
15. Kusahara, S.; Fukushima, Y.; Ogura, S.; Inoue, N.; Uemura, A. Pathophysiology of Diabetic Retinopathy: The Old and the New. *Diabetes Metab. J.* 2018, 42, 364, doi:10.4093/dmj.2018.0182.
16. Rami Reddy, R. A Simple Guide to Understand Age-Related Macular Degeneration Available online: <https://neoretina.com/blog/a-simple-guide-to-understanding-age-related-macular-degeneration/> (accessed on 14/9/2022)
17. The Discovery Eye Foundation Diabetic Retinopathy Available online: <https://discoveryeye.org/eye-conditions/diabetic-retinopathy/> (accessed on 14/9/2022)
18. Gallie, B.L.; Zhao, J.; Vandezande, K.; White, A.; Chan, H.S.L. Global Issues and Opportunities for Optimized Retinoblastoma Care. *Pediatr. Blood Cancer* 2007, 49, 1083–1090, doi:10.1002/pbc.21350.
19. Global Retinoblastoma Study Group; Fabian, I.D.; Abdallah, E.; Abdullahi, S.U.; Abdulqader, R.A.; Adamou Boubacar, S.; Ademola-Popoola, D.S.; Adio, A.; Afshar, A.R.; Aggarwal, P.; et al. Global Retinoblastoma Presentation and Analysis by National Income Level. *JAMA Oncol.* 2020, 6, 685, doi:10.1001/jamaoncol.2019.6716.
20. Kovach, J.L.; Schwartz, S.G.; Flynn, H.W.; Scott, I.U. Anti-VEGF Treatment Strategies for Wet AMD. *J. Ophthalmol.* 2012, 2012, 1–7, doi:10.1155/2012/786870.
21. Everett, L.A.; Paulus, Y.M. Laser Therapy in the Treatment of Diabetic Retinopathy and Diabetic Macular Edema. *Curr. Diab. Rep.* 2021, 21, doi:10.1007/s11892-021-01403-6.
22. Chatziralli, I.; Loewenstein, A. Intravitreal Anti-Vascular Endothelial Growth Factor Agents for the Treatment of Diabetic Retinopathy: A Review of the Literature. *Pharmaceutics* 2021, 13, 1137, doi:10.3390/pharmaceutics13081137.
23. Ancona-Lezama, D.; Dalvin, L.; Shields, C. Modern Treatment of Retinoblastoma: A 2020 Review. *Indian J. Ophthalmol.* 2020, 68, 2356, doi:10.4103/ijo.IJO_721_20.
24. Manjandavida, F.; Stathopoulos, C.; Zhang, J.; Honavar, S.; Shields, C. Intra-Arterial Chemotherapy in Retinoblastoma – A Paradigm Change. *Indian J. Ophthalmol.* 2019, 67, 740, doi:10.4103/ijo.IJO_866_19.
25. Xu, L.; Lu, T.; Tuomi, L.; Jumbe, N.; Lu, J.; Eppler, S.; Kuebler, P.; Damico-Beyer, L.A.; Joshi, A. Pharmacokinetics of Ranibizumab in Patients with Neovascular Age-Related Macular Degeneration: A Population Approach. *Investig. Ophthalmology Vis. Sci.* 2013, 54, 1616, doi:10.1167/iovs.12-10260.
26. Nguyen, Q.D.; Das, A.; Do, D.V.; Dugel, P.U.; Gomes, A.; Holz, F.G.; Koh, A.; Pan, C.K.; Sepah, Y.J.; Patel, N.; et al. Brolicizumab: Evolution through Preclinical and Clinical Studies and the Implications for the Management of Neovascular Age-Related Macular Degeneration. *Ophthalmology* 2020, 127, 963–976, doi:10.1016/j.ophtha.2019.12.031.
27. Ghasemi Falavarjani, K.; Nguyen, Q.D. Adverse Events and Complications Associated with Intravitreal Injection of Anti-VEGF Agents: A Review of Literature. *Eye* 2013, 27, 787–794, doi:10.1038/eye.2013.107.
28. Schargus, M.; Frings, A. Issues with Intravitreal Administration of Anti-VEGF Drugs. *Clin. Ophthalmol.* 2020, Volume 14, 897–904, doi:10.2147/OPTH.S207978.

29. Dalkara, D.; Kolstad, K.D.; Caporale, N.; Visel, M.; Klimczak, R.R.; Schaffer, D.V.; Flannery, J.G. Inner Limiting Membrane Barriers to AAV-Mediated Retinal Transduction From the Vitreous. *Mol. Ther.* 2009, 17, 2096–2102, doi:10.1038/mt.2009.181.
30. Del Amo, E.M.; Rimpelä, A.-K.; Heikkinen, E.; Kari, O.K.; Ramsay, E.; Lajunen, T.; Schmitt, M.; Pelkonen, L.; Bhattacharya, M.; Richardson, D.; et al. Pharmacokinetic Aspects of Retinal Drug Delivery. *Prog. Retin. Eye Res.* 2017, 57, 134–185, doi:10.1016/j.preteyeres.2016.12.001.
31. Shields, C.L.; Bianciotto, C.G.; Jabbour, P.; Griffin, G.C.; Ramasubramanian, A.; Rosenwasser, R.; Shields, J.A. Intra-Arterial Chemotherapy for Retinoblastoma: Report No. 2, Treatment Complications. *Arch. Ophthalmol. Chic. Ill* 1960 2011, 129, 1407–1415, doi:10.1001/archophthalmol.2011.151.
32. Frinking, P.; Segers, T.; Luan, Y.; Tranquart, F. Three Decades of Ultrasound Contrast Agents: A Review of the Past, Present and Future Improvements. *Ultrasound Med. Biol.* 2020, 46, 892–908, doi:10.1016/j.ultrasmedbio.2019.12.008.
33. Clevert, D.A.; Sommer, W.H.; Zengel, P.; Helck, A.; Reiser, M. Imaging of Carotid Arterial Diseases with Contrast-Enhanced Ultrasound (CEUS). *Eur. J. Radiol.* 2011, 80, 68–76, doi:10.1016/j.ejrad.2010.12.103.
34. Dietrich, C.F.; Tana, C.; Caraianni, C.; Dong, Y. Contrast Enhanced Ultrasound (CEUS) Imaging of Solid Benign Focal Liver Lesions. *Expert Rev. Gastroenterol. Hepatol.* 2018, 12, 479–489, doi:10.1080/17474124.2018.1464389.
35. Erlichman, D.B.; Weiss, A.; Koenigsberg, M.; Stein, M.W. Contrast Enhanced Ultrasound: A Review of Radiology Applications. *Clin. Imaging* 2020, 60, 209–215, doi:10.1016/j.clinimag.2019.12.013.
36. Qin, P.; Han, T.; Yu, A.C.H.; Xu, L. Mechanistic Understanding the Bioeffects of Ultrasound-Driven Microbubbles to Enhance Macromolecule Delivery. *J. Controlled Release* 2018, 272, 169–181, doi:10.1016/j.jconrel.2018.01.001.
37. Deprez, J.; Lajoinie, G.; Engelen, Y.; De Smedt, S.C.; Lentacker, I. Opening Doors with Ultrasound and Microbubbles: Beating Biological Barriers to Promote Drug Delivery. *Adv. Drug Deliv. Rev.* 2021, 172, 9–36, doi:10.1016/j.addr.2021.02.015.
38. Touhri, Y.; Dixit, R.; Kofoed, R.H.; Miloska, K.; Park, E.; Raeisossadati, R.; Markham-Coultes, K.; David, L.A.; Rijal, H.; Zhao, J.; et al. Focused Ultrasound as a Novel Strategy for Noninvasive Gene Delivery to Retinal Müller Glia. *Theranostics* 2020, 10, 2982–2999, doi:10.7150/thno.42611.
39. Sonoda, S.; Tachibana, K.; Yamashita, T.; Shirasawa, M.; Terasaki, H.; Uchino, E.; Suzuki, R.; Maruyama, K.; Sakamoto, T. Selective Gene Transfer to the Retina Using Intravitreal Ultrasound Irradiation. *J. Ophthalmol.* 2012, 2012, 1–5, doi:10.1155/2012/412752.
40. Zheng, X.; Du, L.; Wang, H.; Gu, Q. A Novel Approach to Attenuate Proliferative Vitreoretinopathy Using Ultrasound-Targeted Microbubble Destruction and Recombinant Adeno-Associated Virus-Mediated RNA Interference Targeting Transforming Growth Factor- β 2 and Platelet-Derived Growth Factor-B: Attenuate PVR Using UTMD and RNAi Targeting TGF- β 2 and PDGF-B. *J. Gene Med.* 2012, 14, 339–347, doi:10.1002/jgm.2629.
41. Kowalczyk, L.; Boudinet, M.; El Sanharawi, M.; Touchard, E.; Naud, M.-C.; Saïed, A.; Jeanny, J.-C.; Behar-Cohen, F.; Laugier, P. In Vivo Gene Transfer into the Ocular Ciliary Muscle Mediated by Ultrasound and Microbubbles. *Ultrasound Med. Biol.* 2011, 37, 1814–1827, doi:10.1016/j.ultrasmedbio.2011.07.010.
42. OcuTher Available online: <https://www.ocuther.eu/> (accessed on 14/9/2022)

2

Ultrasound and microbubbles for the treatment of ocular diseases: From preclinical research towards clinical application

Charis Rousou ^{1,2}, Carl C. L. Schuurmans ^{1,3}, Arto Urtti ^{4,5,6}, Enrico Mastrobattista ¹, Gert Storm ^{1,7,8}, Chrit Moonen ², Kai Kaarniranta ^{9,10}, Roel Deckers ²

¹ Department of Pharmaceutics, Utrecht University, The Netherlands

² Division of Imaging and Oncology, University Medical Center Utrecht, The Netherlands

³ Department of Pharmacology, Utrecht University, The Netherlands

⁴ School of Pharmacy, University of Eastern Finland, Finland

⁵ Division of Pharmaceutical Biosciences, University of Helsinki, Finland

⁶ Institute of Chemistry, Saint Petersburg State University, Russia

⁷ Department of Biomaterials Science and Technology, University of Twente, The Netherlands

⁸ Department of Surgery, National University of Singapore, Singapore

⁹ Department of Ophthalmology, Kuopio University Hospital, Finland

¹⁰ Department of Ophthalmology, University of Eastern Finland, Finland

ABSTRACT

The unique anatomy of the eye and the presence of various biological barriers make efficacious ocular drug delivery challenging, particularly in the treatment of posterior eye diseases. This review focuses on the combination of ultrasound and microbubbles (USMB) as a minimally invasive method to improve the efficacy and targeting of ocular drug delivery. An extensive overview is given of the *in vitro* and *in vivo* studies investigating the mechanical effects of ultrasound-driven microbubbles aiming to: (i) temporarily disrupt the blood–retina barrier in order to enhance the delivery of systemically administered drugs into the eye, (ii) induce intracellular uptake of anticancer drugs and macromolecules and (iii) achieve targeted delivery of genes, for the treatment of ocular malignancies and degenerative diseases. Finally, the safety and tolerability aspects of USMB, essential for clinical translation, are discussed.

INTRODUCTION

Ophthalmic ultrasound as a research field started in 1956, when researchers Mundt and Hughes, using an ultrasonic reflectoscope, found that they could calculate the horizontal distance between ocular tissues based on sent ultrasound waves and received echoes in a single axis (a technique known as A-mode ultrasonography) [1]. Since then, ocular ultrasound has flourished, and became one of the standard imaging techniques clinically applied in ophthalmology. Some examples of modern ophthalmic ultrasound applications in the clinic include the diagnosis of intraocular tumors, the detection of structural changes in glaucoma and retinal detachment and the use of high frequency ultrasound (35–70 MHz) to construct high resolution images of the anterior eye (a method known as ultrasound biomicroscopy, UBM) [2,3,4].

Around the same time (mid-1960s), microbubbles made their entrance into the ultrasound field [5]. Microbubbles are gas-filled spheres with a diameter typically between 0.5 and 10 μm [6]. They are intravenously administered and used as ultrasound contrast agents as they improve blood-to-tissue contrast during ultrasound imaging. Microbubbles dissolve in blood after injection and, if the vasculature is intact, they circulate in the bloodstream until they are eliminated by exhalation or phagocytosis [7,8]. Microbubble-specific imaging methods, so-called contrast enhanced ultrasound (CEUS), have been developed and are currently used as a diagnostic tool in the clinic. An in-depth explanation of the diagnostic applications of CEUS can be found elsewhere [7,9]. Microbubbles first entered the field of ophthalmology in 1994, to enhance the blood flow signal in ocular and orbital malignancies [10,11]. Other clinical examples of CEUS in ophthalmology include imaging of the microcirculation in benign ocular lesions, differentiation between subretinal hemorrhage and hypovascular tumors, and quantification of perfusion-specific parameters [12,13,14,15]. Extensive reviews on the different microbubble imaging methods used in ophthalmology can be found elsewhere [4,16,17,18].

Microbubbles can also be used in therapeutic ultrasound applications. Microbubbles exposed to ultrasound waves undergo oscillations that induce various bioeffects on the surrounding structures. These bioeffects can be exploited to improve the local administration of drugs and genes. Recently, preclinical investigations of the therapeutic use of ultrasound and microbubbles (USMB) have been conducted in the field of ophthalmology, where there is a clear need for improved new delivery methods. The

aim of this review is to provide an overview of the different therapeutic applications of USMB in ophthalmology (Figure 1). These can be divided into two distinct applications: (i) disruption of the blood–retina barrier and extravasation of drugs/genes that circulate in the bloodstream, and (ii) intracellular uptake of drugs/genes in various ocular cells.

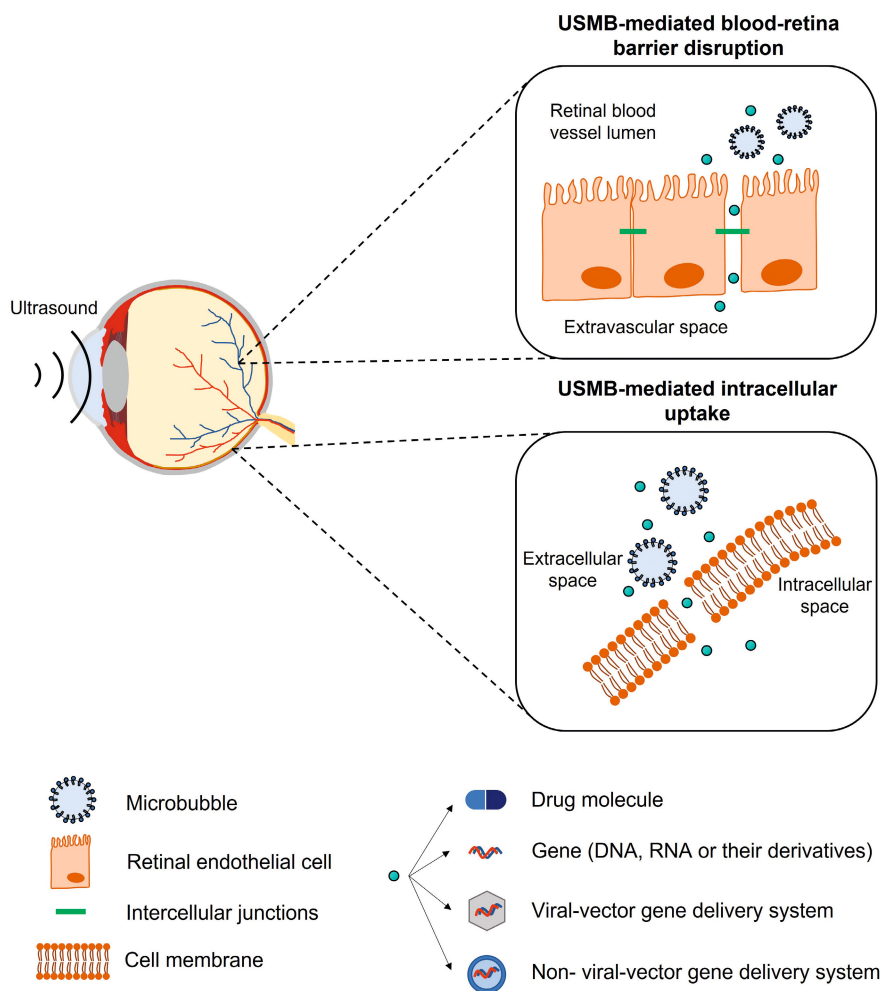


Figure 1. Schematic illustration of the therapeutic applications of USMB.

The structure of this review is as follows: first, a brief introduction on the mechanisms that underlie USMB-mediated therapy is given, followed by an overview of the effect of biological barriers on the pharmacokinetics of ocular drug delivery. Various studies that investigated the application of USMB in the treatment of different ocular diseases are

presented. Finally, safety and tolerability aspects important in the clinical translation of USMB and future directions are discussed.

MECHANISMS UNDERLYING THE THERAPEUTIC USE OF ULTRASOUND AND MICROBUBBLES

Microbubbles exposed to ultrasound waves will alternate between contraction and expansion due to their compressible nature. The amplitude of microbubble oscillation depends on the amplitude of the ultrasound pressure wave. Ultrasound amplitude may be expressed as acoustic pressure (measured in MPa), intensity (measured in W/cm²), or mechanical index (MI). The latter is a unitless parameter defined as the ratio of the peak negative pressure (P_{neg} , in MPa) over the square root of the transmitted ultrasound frequency (in MHz). A microbubble responds with linear oscillations at low ultrasound pressures. The microbubble starts oscillating asymmetrically with increased pressure, as the absolute microbubble radius change during expansion is larger than during contraction. This phenomenon is known as stable or non-inertial microbubble cavitation. Further increases in ultrasound pressure cause the microbubble to oscillate more violently, until it becomes unstable and collapses (also known as inertial microbubble cavitation).

Different biophysical events can occur depending on the oscillation regime of the microbubbles, which will have various effects on cells in close proximity. During stable cavitation, a microbubble pushes and pulls the membrane of the adjacent cell as a result of microbubble expansion and contraction, respectively. Furthermore, mechanical forces are developed on the cell membrane induced by microstreaming formation around the oscillating microbubble. Finally, inertial cavitation is associated with the formation of shock waves and liquid micro-jets that act as micro-syringes on the cell membrane during microbubble collapse [19,20]. These biophysical events can, in turn, lead to various bioeffects on the cells. Particularly interesting are the bioeffects induced by stable and inertial cavitation, as they are potent in (i) enhancing the membrane permeability of cells in close vicinity and improving the intracellular uptake of drugs, (ii) increasing the permeability of blood vessel linings and allowing for extravasation of drugs, and (iii) altering the flow of blood inside blood vessels.

The mechanical stresses caused by an oscillating or collapsing microbubble lead to the formation of pores in the cell membrane (Figure 2A), so-called sonoporation (or

sonopermeation). It has been shown that pore formation and the resulting intracellular uptake of molecules occur immediately or within a few minutes after USMB treatment [21,22,23]. USMB may also stimulate endocytosis (Figure 2A), though the mechanisms underlying this bioeffect are not yet fully understood [21]. Sonoporation and endocytosis can induce the uptake of molecules (fluorescent dextrans, calcein, propidium iodide, liposomes, plasmid DNA) that are otherwise not able to permeate intact cell membranes, because of their large size and/or low lipophilicity [24,25,26,27,28]. Similar to stable cavitation, sonoporation induced by inertial cavitation has been exploited to enhance the uptake of drugs and genes by cells [29,30,31,32]. Whether inertial cavitation can safely induce endocytosis still remains to be investigated. The pore size as a result of sonoporation highly depends on the microbubble cavitation regime (stable or inertial): low P_{neg} induces pores with sizes from several tens to a few hundred nanometers, while high P_{neg} results in pores with sizes of a few micrometers [21,33]. Similar to the size of pores, the kinetics of membrane resealing are defined by the acoustic pressure used and can vary between milliseconds and minutes [21]. Notably, the bioeffects caused by stable cavitation do not negatively affect cell viability, while the formation of larger pores correlates with reduced cell viability as a result of apoptosis [33,34].

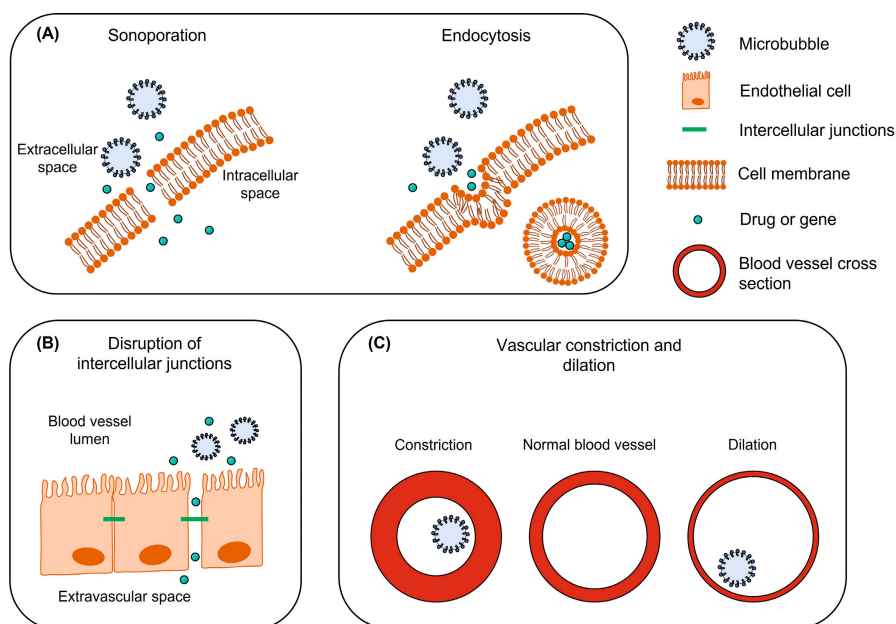


Figure 2. The mechanisms underlying the therapeutic use of USMB. **(A)** Intracellular uptake of drug/gene induced by sonoporation (left) and endocytosis (right). **(B)** Disruption of intercellular junctions and extravasation of drug/gene from blood vessel to the extravascular space. **(C)** Vascular constriction and dilation. Figure not to scale.

The endothelium in blood capillaries, with a diameter in the range of the size of microbubbles ($\sim 5 \mu\text{m}$), experiences mechanical forces exerted by the cavitating microbubbles. This mechanical activity increases the permeability of the endothelium by influencing the cytoskeleton arrangement in the endothelial cells and altering the expression of intercellular junction proteins (Figure 2B) [21,35]. A widely studied application of this USMB-induced bioeffect is the temporal disruption of the blood–brain barrier (BBB) and deposition/extravasation of drug molecules in the brain parenchyma [36,37]. In contrast to sonoporation-induced intracellular uptake, increases in the paracellular diffusion of compounds via intercellular gaps were found to be prolonged, on the time scale of several hours [35,38,39]. Preclinical studies have shown that the extent of BBB disruption is highly dependent on the frequency of the transmitted ultrasound waves, P_{neg} , and exposure time [40,41]. An *in vivo* animal study demonstrated that, for various P_{neg} , the opening size of tight junctions in the mouse brain endothelium ranged between 2 nm and approximately 50 nm [42]. It was previously observed that stable cavitation can induce BBB permeability without inducing side effects, while inertial cavitation induces both barrier disruption and extravasation of erythrocytes as a result of the more violent bioeffects and larger opening size [43]. Compared with sonoporation, less information is available on the kinetics of tight junction opening and resealing, due to the lack of adequate technology for microscopic imaging of the interaction between microbubbles and vascular endothelium [21].

A third mechanism induced by USMB is the alteration of blood flow inside the blood vessels. As a consequence of cavitating microbubbles activity in the vasculature, two contradictory phenomena have been reported: vascular invagination or shutdown and vascular dilation (Figure 2C). Chen *et al.* studied the behavior of cavitating microbubbles (11 MPa P_{neg}) in *ex vivo* microvessels using high-speed microscopy [44]. In a microvessel where microbubbles were in contact with the endothelium, microbubbles initially expanded, causing microvessel dilation, followed by immediate microbubble collapse and microvessel invagination (constriction). Immediately afterwards, microbubble remnants were observed outside the microvessel walls, indicating blood vessel rupture. In line with this study, Hwang *et al.* observed a positive correlation between inertial cavitation (1–9 MPa P_{neg}) and blood vascular damage *in vivo* [45]. This microbubble-driven blood vessel narrowing might explain the significant decrease in blood perfusion previously observed in numerous preclinical studies [46,47,48,49,50,51]. On the other hand, some studies have shown that USMB can induce blood vessel dilation and local increase in blood perfusion [50,52,53]. This phenomenon is known as vasodilation and

could be of great importance in the treatment of postischemic cardiac damage [52]. In their study, D'Souza *et al.* treated hepatocellular carcinoma-bearing rats with two different USMB doses [50]. The high USMB dose was at an intensity of 2.0 W/cm², with 6 minutes exposure time. In the low USMB dose group, ultrasound intensity and exposure time were reduced by half. Quantification of perfusion indicated a decrease in blood flow as a result of vascular disruption in the group that received the high-dose therapy. In contrast, the low USMB dose group showed an enhancement in tumor blood perfusion, but this result was not consistent. This study demonstrated that ultrasound settings and microbubble dose might be critical factors in balancing between USMB-induced vascular dilation and constriction. More extensive information on the mechanisms that underlie USMB-mediated drug delivery and the induced bioeffects can be found elsewhere [21,31,33].

THE EFFECT OF BIOLOGICAL BARRIERS ON THE PHARMACOKINETICS OF OCULAR DRUG DELIVERY

The eye is a unique sensory organ in terms of anatomy, physiology, and function. Anatomically, it can be divided into anterior and posterior segments (Figure 3A). The anterior eye consists of the tissues in the front third of the eyeball, which include the cornea, conjunctiva, anterior sclera, iris, ciliary body, lens and the anterior chamber. The posterior eye consists of the vitreous humor, neural retina, Bruch's membrane, choroid and posterior sclera. The retina can be subdivided into the neural retina and the retinal pigment epithelium (RPE) (Figure 3B). The retina is a semi-transparent tissue constructed by multiple neural cells in laminar arrangement. The RPE is an epithelial cell monolayer that is pigmented due to the presence of melanin. The main role of RPE is to phagocytose debris and waste products from photoreceptors and, as discussed below, to form the outer blood–retina barrier. Bruch's membrane, an extracellular matrix rich in collagen and elastin, is located between the RPE and the choroid (a network of blood vessels). More detailed information about ocular physiology and the function of the different neural retinal cell types can be found elsewhere [54,55,56].

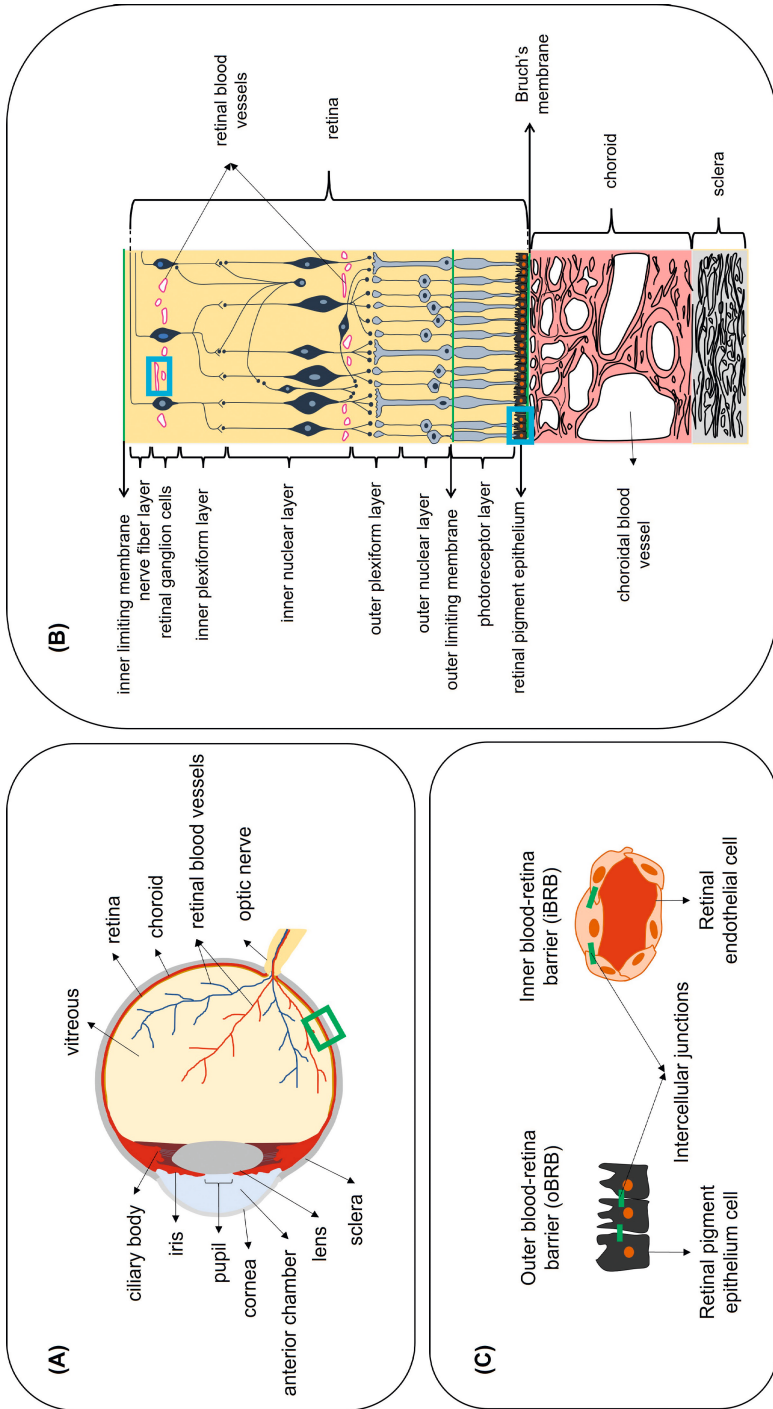


Figure 3. (A) Anatomy of the eye. **(B)** Boxed region (green line) in (A) showing a cross-section of the posterior eye with the different cell layers of the retina, Bruch's membrane, choroid and sclera. **(C)** Boxed regions in (B) (blue line) showing the locations where the outer and inner blood–retina barriers are formed, due to intercellular junctions between adjacent cells. Figure not to scale.

Due to the unique anatomy of the eye, i.e., the presence of the ocular barriers, the development of efficacious ocular therapeutics poses a major challenge in ophthalmology, especially in the treatment of retinal diseases. Here, we briefly discuss some of the main routes of drug administration in the eye and the main drawbacks of current treatments. Topical administration of eye drops is a traditional therapeutic modality for the treatment of anterior eye diseases such as inflammations and increased intraocular pressure (IOP), such as in the treatment of glaucoma. It is characterized by high patient compliance, as eye drops can easily be self-administered daily. However, the bioavailability of topically administered drugs is between 1 and 4% due to the rapid drainage from the surface of the eye and systemic absorption of fluids by the conjunctiva, making this delivery method unsuitable for the treatment of posterior eye diseases [57]. After intravitreal administration, drugs are eliminated by the anterior or posterior route [58]. Drug molecules first diffuse to the posterior vitreous chamber, then via outflow channels in the trabecular meshwork, and they are eliminated by the aqueous humor (anterior route). If a drug is capable of crossing the endothelia of the BRB and blood–aqueous barrier (BAB), i.e., it is smaller than 2 nm in size, it is eliminated via the posterior route. Generally, the half-life of intravitreally administered small molecules is between 1 to 10 hours, and several days for larger molecules such as proteins [59,60], creating a need for repeated injections. Periocular administration includes the injection of drug molecules in locations around the eyeball, and it results in improved bioavailability of drugs in the anterior tissues as compared to topical administration [58]. However, the retinal bioavailability of a small molecule is limited to only 0.1%, underscoring the challenge associated with replacing intravitreal with subconjunctival injections, despite the fact that the subconjunctival route is less invasive and less associated with adverse effects such as retinal detachment and increase in IOP [58,61].

In the human eye, the exchange of nutrients for normal function of the neural cell layers in the retina is maintained by two independent vascular networks: the retinal vasculature and the choroid. To protect the retina from harmful substances present in the blood circulation and to regulate the exchange of molecules with the bloodstream in a controlled manner, a specialized barrier function is situated between the vascular endothelium and epithelium of the retina. This retinal barrier resembles the BBB in terms of function and ultrastructure. Junctional complexes (tight and adherens junctions) are present at the level of the RPE and retinal endothelium and form the outer blood–retina barrier (oBRB) and inner blood–retina barrier (iBRB), respectively (Figure

3C). The iBRB allows only molecules that are smaller than 2 nm to freely permeate, such as mannitol (molecular radius of 0.4 nm [62]) and carboxyfluorescein (molecular radius of 0.5 nm [63]) [58]. The permeability of molecules across the oBRB is highly dependent on their hydrophilicity. Indicatively, the apparent permeability coefficient for betaxolol (LogD 1.59, MW 307 Da) was calculated in *ex vivo* bovine RPE-choroid to be 16.7×10^{-6} cm/s, while the corresponding value for carboxyfluorescein (LogD -3.15, MW 376 Da) was 0.96×10^{-6} cm/s, showing that the higher the hydrophilicity, the less the transport across the oBRB [64]. While the presence of these natural barriers protects the eye from the invasion of foreign substances and regulates the environment of ocular tissues, it also hinders the delivery of therapeutics in the case of ocular disease. Intravenous administration for ocular drug targeting is generally characterized by higher patient compliance compared to intraocular injections, as it is a less invasive method. Additionally, it is not associated with increased IOP and intraocular hemorrhage, retinal detachment or vitreous hemorrhage or other side effects commonly associated with intravitreal injections [65,66,67]. In addition to the iBRB and oBRB, another biological factor that regulates drug transfer from the bloodstream to the retina is the high blood flow in the choroid relative to the tissue (peak systolic velocity of about 10 mm/s measured in healthy human eyes [68]). However, quantitative information about retinal bioavailability after intravenous administration is not available. Some physiological characteristics, such as fenestrations in choriocapillaries with size 70–80 nm [58], and the active RPE internalization of compounds such as low-density lipoprotein [69], make targeted retinal drug delivery from the bloodstream an interesting drug delivery approach.

OCULAR PATHOLOGIES THAT COULD BENEFIT FROM THERAPEUTIC ULTRASOUND AND MICROBUBBLES

In this section, we summarize the studies that investigated the use of USMB to overcome the biological barriers discussed in the previous section and enhance, thereby, the ocular delivery of drugs and genes for the treatment of various ocular diseases (Table 1). In each subsection, we provide information about the pathologic characteristics of each disease, along with the most frequently used drug treatment methods and the associated challenges. Finally, we discuss the main findings from *in vitro* and *in vivo* animal studies reported in the literature and how these can contribute to improve ocular drug delivery.

Wet Age-Related Macular Degeneration

Age-related macular degeneration (AMD) is a progressive chronic disease of the neural retina and choriocapillaris caused by the deposition of acellular polymorphous debris (drusen) between the RPE and Bruch's membrane. Histochemical characterization of drusen revealed that they are composed of a mucopolysaccharide (sialomucin) and a cerebroside lipid [70]. Tissue metalloproteinase inhibitor 3, clusterin, vitronectin, serum albumin, crystallin and complement proteins are rich in AMD drusen [71]. Drusen develop with age as a result of RPE degeneration and their size is used to determine the grade of AMD [72]. Advanced AMD is classified into (i) non-neovascular/dry/atrophic, which is characterized by geographic atrophy and drusen formation that extend to the center of the macula, and (ii) neovascular/wet/exudative, where choroidal neovascularization is additionally present. Another clinical hallmark of wet AMD is retinal hemorrhage (Figure 4B).

Currently, the most common treatment method for wet AMD is intravitreal injection of anti-vascular endothelial growth factor (anti-VEGF) drugs. The first Food and Drug Administration (FDA)-approved anti-VEGF was Pegaptanib (Macugen, Pfizer), an oligonucleotide drug that binds the VEGF-163 isoform, followed by ranibizumab (Lucentis, Genentech/Novartis), an antibody fragment that binds all VEGF isoforms. Bevacizumab (Avastin, Genentech) is a full-length antibody that binds all VEGF isoforms that are currently approved for systemic malignancies; however, it is also used off-label for the treatment of wet AMD. Aflibercept (VEGF Trap-Eye, Regeneron/Bayer) is a recently FDA-approved engineered protein that binds VEGF [73]. The last addition to anti-VEGF treatments for wet AMD is brolucizumab [74]. The limited half-lives of anti-VEGF drugs after intravitreal administration (9 days for ranibizumab and about 5 days for bevacizumab, estimated 7 days for aflibercept [75,76,77], and about 3 days for brolucizumab [78]) create a need for repeated injections (monthly or bi-monthly), which are frequently associated with patient discomfort due to injection-related pain and adverse effects (e.g., hemorrhages, retinal detachment, endophthalmitis) [58,76]. Intravenous administration, on the other hand, is a less invasive and more patient-compliant delivery method; however, this approach is currently limited by the low permeability of the BRB for many drugs. Considering the functional and structural similarities between the BBB and BRB, USMB has the potential to enhance the efficacy of intravenously administered drugs against AMD. In addition, other ocular disorders with the pathology site in close proximity with the BRB, such as diabetic retinopathy or retinoblastomas, may also benefit from USMB-induced BRB disruption.

The first study to determine the feasibility of BRB opening using USMB was performed by Hirokawa *et al.* in 2007 [79]. Rabbit eyes were treated with USMB at a frequency of 2 MHz, at two different MIs (0.2 and 1.7). Comparison between fluorescein fundus angiography and fundus photography images acquired pre- and post-treatment revealed alteration in the diameter of the uveal blood vessels in 20% of the eyes treated at low MI. In contrast, 80% of the eyes treated at high MI had altered uveal vessels. In addition, the average retinal vein (but not the artery) diameter was significantly reduced in the high MI-treated eyes after treatment, suggesting the occurrence of vasoconstriction. At high MI, leakage of fluorescein (MW 332 Da) was observed in the fundus of one eye, suggesting increased permeability of blood vessels (Figure 5A). No bleeding was observed, though microscopic hemorrhage could not be excluded. Similarly, Park *et al.* investigated the effect of USMB on BRB permeability in rat eyes by investigating the extravasation of gadolinium (Gd, MW 938 Da) [80]. USMB treatment was performed at 0.69 MHz frequency and three different pressures (0.81, 0.88 and 1.10 MPa, corresponding to MI 0.98, 1.06 and 1.32, respectively). Quantification of Gd-enhanced magnetic resonance images revealed that signal intensity increased immediately after USMB treatment for all three MIs and was the highest for 1.1 MPa, indicating disruption of the BRB. A second Gd injection 3.5 hours after treatment did not result in signal enhancement, showing for the first time that this BRB disruption was reversible at 0.81 and 0.88 MPa, but not at 1.10 MPa. Retinal microscopic examination revealed the presence of extravasated erythrocytes in the nuclear retinal layer 24 hours after treatment. Most retinal damage was observed at the highest pressure. Touahri *et al.* investigated the effect of USMB on the extravasation of macromolecules with different sizes: Evans blue (MW 66 kDa after binding to serum albumin), immunoglobulin G (IgG) monomer (MW 150 kDa) and immunoglobulin M (IgM) pentamer (MW 970 kDa) [81]. BRB disruption was investigated in rats at MIs ranging between 0.3 and 0.8, and frequency 1.1 MHz. In five out of six rats, all three macromolecules were localized in the deep and superficial vascular plexi (INL and RGC layers) as a result of iBRB permeabilization. In contrast, no evidence indicating extravasation from the choroidal plexus and penetration of molecules to the neural retina through the oBRB was found. Evidence for neuroinflammation and presence of erythroid cells was found in 33% of the eyes, 30 minutes after treatment with USMB, and co-localization with Evans blue was observed. Hematoxylin and eosin (H&E) staining of retinal sections revealed no morphological alterations in 83% of the animals.

In addition to increasing the permeability of the BRB, USMB can also increase the permeability of plasma membranes and increase the intracellular concentration of drug molecules. Numerous research groups have investigated the effect of USMB in the intracellular uptake of macromolecules [82], genes [83,84,85,86,87,88,89] and nanoparticles [90,91] by the neural retina and RPE. Although these studies are discussed here as drug delivery applications against AMD, the same principles could be applied for the treatment of other retinal diseases discussed later in this section, such as retinitis pigmentosa.

Thakur *et al.* studied the intracellular delivery of a model IgG in three retinal cell lines (human RPE cells and human-derived Müller glia and mouse-derived photoreceptors) [82]. These *in vitro* experiments were conducted using custom-made nanobubbles (NBs) activated by ultrasound at a frequency of 1 MHz. They found that ultrasound in combination with nanobubbles (USNB) significantly increased the uptake of the macromolecule in retinal cells compared with ultrasound only or USMB (using conventional microbubbles). However, the increase in the intracellular uptake was significant only for the two human-derived cell lines, showing that induced effects are cell line-dependent. Furthermore, shorter exposure time in combination with higher ultrasound intensity (20 s at 1.0 W/cm² vs. 30 s at 0.5 W/cm²) had a more significant effect on intracellular uptake, showing that USNB efficacy is highly dependent on these two ultrasound parameters.

The effect of ultrasound parameters in the intracellular uptake of macromolecules/genes in retinal cells was also investigated by Wan *et al.* [83]. Specifically, they determined how ultrasound intensity, exposure time and the ratio of microbubbles to cells affected cell viability and intracellular uptake of a positively charged complex (PEI/pEGFP). They observed that increased ultrasound intensity resulted in higher amounts of EGFP-positive cells but also more extensive cell damage. The exposure time was inversely proportional to cell viability. These *in vitro* results were confirmed *in vivo* by injecting PEI/pEGFP alone or combined with USMB (frequency 1 MHz, intensity 2 W/cm², exposure time 5 minutes) subretinally in rat eyes. Examination of frozen tissues revealed that, in the group treated with USMB, 7 out of 12 retinas appeared with diffused EGFP-positive cells, mainly distributed in the neural retina. Using the same ultrasound parameters as Wan *et al.*, Li *et al.* examined the differences in EGFP expression after subretinal injection of microbubbles and ultrasound treatment [84]. A significantly greater number of GFP-positive cells was found in eyes treated with plasmid + USMB

compared with plasmid alone, plasmid + microbubbles and plasmid + ultrasound. GFP-signal was distributed in the neural retina and RPE. Differences in fluorescent signal between PEI/pDNA and PEI/pDNA + USMB were significant during the first 5 days post-treatment, showing that USMB enhanced and accelerated the expression of EGFP by allowing PEI/pDNA to enter the cytoplasm earlier via sonoporation.

In contrast to the studies discussed above where ultrasound was externally applied, Sonoda *et al.* developed a miniature ultrasound probe to be intraocularly positioned after vitrectomy in rabbit eyes [85]. Bubble liposomes (BLs) were injected intravitreally in combination with a GFP-plasmid. Fluorescence microscopy imaging revealed that the eyes treated with plasmid + USBL (frequency 3 MHz, intensity 0.15 W/cm², exposure time 60 s) had 8 times greater numbers of GFP-positive cells per visual field (32 cells) compared with plasmid + BL (0 cells) or plasmid + ultrasound (4 cells). GFP-positive cells were co-localized with the sonicated area and mainly appeared in the outer nuclear area (Figure 5B). Eye physiology was examined 1 and 3 days post-treatment, with no obvious tissue damage, which was confirmed by histology. Applying ultrasound using an intraocular probe can help to reduce acoustic energy attenuation by the anterior tissues and provide more precise control of the area exposed to ultrasound compared with externally applied probes. However, it remains open for investigation whether these arguments are enough to compensate for inducing the need for vitrectomy, that, unlike externally applied ultrasound using an ocular probe, is an invasive procedure that needs to be performed by a retinal surgeon. Moreover, precise localization of the ultrasound probe is needed so that retinal injury is avoided.

The transduction efficiency of recombinant adeno-associated virus (rAAV) vectors expressing EGFP in combination with USMB was investigated in RPE cells by Li *et al.* and Zheng *et al.* [86,87]. *In vitro* experiments were conducted using human-derived (Li *et al.*) and rat-derived (Zheng *et al.*) RPE cells. Li *et al.* reported that exposure to ultrasound only was not enough to increase the number of GFP-positive cells. When USMB was applied, an increase of about 10% was observed in the RPE cells compared with ultrasound alone. On the other hand, Zheng *et al.* observed an increase in number of GFP-positive cells in rAAV + ultrasound (approximately 22% of control cells), but not in rAAV + USMB treatment (about 9% of control cells). This might be due to differences in the sensitivity between the two cell-lines in microbubble-induced bioeffects. Despite this difference in the *in vitro* studies, USMB-combined treatment with rAAV resulted in the highest expression of EGFP following subretinal administration of microbubbles

in rat eyes. In both studies, the GFP signal in the rAAV + USMB group was significantly higher than in all other groups in the first 35 days after treatment. In the study of Zheng *et al.*, GFP signal could be detected 120 days post-treatment (Figure 5C). No alterations were observed in retinal morphology in either study.

An *in vivo* study on the delivery of fluorescently labelled lipofectamine-formulated-siRNA (L/siRNA) in rat retinas was performed by Zheng *et al.* [88]. Microscopic examination of retinas performed 12 hours after treatment revealed that the highest ratio of transfected cells for the group that received L/siRNA + USMB was 57.8%, compared with the group that received L/siRNA + ultrasound (19.7%), L/siRNA (12.6%) and naked siRNA + USMB (4.3%). No signs of tissue damage, inflammation or photoreceptor loss were seen twelve hours post-treatment.

Using RPE cells *in vitro*, Li *et al.* compared the improvement in efficiency of USMB-mediated transfection/transduction between different genes (pDNA, siRNA) and different delivery vectors (chemical: PEI/pDNA, L/siRNA and biological: rAAV) [89]. Cells were exposed to different USMB parameters (frequency 1 MHz, intensity 1–3 W/cm², microbubble-to-cell ratio 20:1–70:1, exposure time 1–2 minutes, duty cycle 20–100%) and cell viability was determined. Viability was lowered with increasing ultrasound intensity, duty cycle and microbubble concentration. Furthermore, the authors demonstrated that not all delivery vectors had increased transfection efficiency when combined with USMB. PEI/pDNA + USMB led to the highest transfection efficiency compared with the control, followed by rAAV + USMB. Transfection efficiency using L/siRNA was not enhanced by USMB compared with the control.

The intracellular enhancement of uptake of fluorescently labelled siRNA encapsulated in mPEG-PLGA-PLL nanoparticles by rat RPE cells was investigated by Du *et al.* [90]. The authors observed a 1.5-fold increase in nanoparticle uptake (48.39%) when cells were treated with ultrasound alone (1 MHz frequency, 0.5 W/cm² intensity, 60 s exposure time) compared with the untreated control group (32.17%). Interestingly, nanoparticle uptake did not differ significantly between the cells treated with ultrasound and USMB groups, which was attributed to possible damage in the microstructure of RPE cells (microvilli or caveolae) induced during microbubble cavitation. In 2017, the same research group conducted an *in vivo* animal study to investigate the transfection efficiency of the same nanoparticles loading PDGF-BB siRNA [91]. In contrast to their *in vitro* uptake study, higher values of ultrasound intensity and exposure time were used

(intensity 2 W/cm², exposure time 5 minutes). *In vivo* results indicated an enhanced nanoparticle uptake when combined with USMB (transfection efficiency 18.22%), which was significantly greater than eyes treated with nanoparticles + ultrasound (10.67%) or nanoparticles alone (3.74%). Histological examination of enucleated eyes showed that retinal layers were well preserved without any damage in the photoreceptor layer or inflammation.

In conclusion, the above studies have demonstrated that USMB can induce a reversible disruption of the BRB, enhance the extravasation of molecules to the neural retina, and improve the intracellular uptake of macromolecules, genes and nanoparticles in retinal cells. The chosen ultrasound parameters are crucial for the efficacy, as well as the safety of the treatment. As seen in the following sections, this is a common observation among all USMB applications.

Glaucoma

Glaucoma refers to a group of eye neuropathies characterized by retinal ganglion cell (RGC) damage and apoptosis. One of the clinical hallmarks of glaucoma is optic disc excavation (Figure 4C). It is the second leading cause of blindness worldwide (following cataract), with the most common type being primary open-angle glaucoma. Multiple factors are associated with the development of glaucoma, such as age, family history, diabetes, treatment with steroids and hypertension [92,93]. Reducing intraocular pressure (IOP) is the most common approach for the prevention of glaucoma progression, which is typically performed via topical administration of eye drops (prostaglandin analogues, beta blockers, alpha 2-adrenergic agonists, carbonic anhydrase inhibitors) [94,95,96,97]. Topical administration of eye drops is characterized by low bioavailability due to the rapid elimination of eye drop solutions and systemic drug absorption through blood vessels in the conjunctiva [58]. In addition, this treatment method is associated with compliance rates of approximately 55% of patients, in chronic treatment of glaucoma, related to patient-perceived problems such as forgetting doses [98]. Other treatment methods are surgical interventions such as cyclo-cryocoagulation, laser treatment (laser trabeculoplasty and cyclophotocoagulation), filtration and non-filtration surgeries [99]. Despite the efficacy of these treatment methods to reduce IOP, the need to treat RGCs and optic nerve degeneration is still unmet.

A number of studies focused on the USMB-mediated treatment of glaucoma by enhancing the delivery of neuron growth factors and genes that can prevent RGC

apoptosis and enhance optic nerve protection. Shen *et al.* investigated the uptake of mouse neuron growth factor (mNGF) by RGCs in a rabbit model for intraocular hypertension [100]. They have shown that USMB (1 MHz frequency, 0.5 W/cm² intensity, 1 minute exposure time) in combination with mNGF significantly improved the flash visual evoked potential (F-VEP) scores (F-VEP assesses the function of optic nerve myelin and axons by measuring the electric potential generated upon application of a light stimulus). In addition, retinal thickness was significantly increased compared with controls; photoreceptors had normal appearance without degeneration, and RGCs were normal in structure both in the retina and optic nerve.

The potential of USMB-mediated gene transfection of RGCs was investigated *in vitro* and *in vivo* [101,102]. Li *et al.* investigated the delivery of the bcl-xl gene (i.e., the main gene from the bcl-2 family expressed in the rat retina, known for its anti-apoptotic activity) to RGCs and its role in the prevention of cell apoptosis [101]. Non-transfected RGCs were shrunken, rounded and detached, showing extensive apoptosis. On the other hand, USMB-combined delivery of bc1-xl reduced the number of apoptotic cells, showing that USMB could partially prevent RGC death. Gene delivery of the rAAV-EGFP gene to RGCs was investigated in a study by Xie *et al.* [102]. USMB treatment was performed after intravitreal injection of the gene with or without lipid microbubbles (ultrasound frequency 0.3 MHz, intensity 0.5 W/cm², exposure time 1 minute). Examination of retinas 28 days after treatment revealed that the highest RGCs transduction rate was observed in the eyes that received combined gene delivery and USMB (rAAV-EGFP 12.75%, rAAV-EGFP + ultrasound 15.78%, rAAV-EGFP + USMB 19.48%).

A different application of USMB in the treatment of glaucoma was demonstrated by Yamashita *et al.* by showing that the delivery of genes to the anterior eye could improve and accelerate wound healing following one of the invasive methods used for the treatment of glaucoma, such as trabeculoplasty [103]. First, the transfection efficiency of pDNA (pEGFP-N2 gene) in combination with ultrasound bubble liposomes (USBL) was investigated *in vitro* in corneal epithelial cells. Cells were treated at 1 MHz ultrasound frequency and exposure time of 20 s. Ultrasound intensity varied between 0.8 and 1.2 W/cm². The highest number of GFP-positive cells was found at the highest ultrasound intensity, with no significant changes in cell viability. Next, transfection efficiency was compared between bubble liposomes (BLs) and conventional microbubbles (Optison™, GE Healthcare), revealing that the ratio of GFP-positive cells over the total amount of cells treated with USBL was approximately 2 times higher than for the cells treated with

USMB. Gene expression in rat eyes was then compared between USBL- and USMB-mediated delivery. *In vivo* results were in agreement with the *in vitro* study, indicating that plasmid + USBL resulted in a higher number of GFP-positive cells compared with plasmid alone, plasmid + ultrasound and plasmid + USMB. USBL-mediated GFP-positive cells were mostly located beneath the conjunctival epithelium in the area that was treated with ultrasound and GFP was found localized in the cytosol (Figure 5D). The structure of the conjunctiva was well preserved, and no hemorrhage or edema was found.

In conclusion, the studies discussed above have shown the potency of USMB to enhance the delivery of a neuron growth factor and various genes and enhance the protection of RGCs in glaucoma.

Diabetic Retinopathy

Diabetic retinopathy (DR) is a disease that occurs in almost all patients with type 1 diabetes and more than 60% of patients with type 2 diabetes. It can be classified into (i) non-proliferating, when microaneurysms and hemorrhages appear in the retina and (ii) proliferating, when new blood vessels (retinal neovascularization) appear on the surface of the retina or optic disc. These abnormal blood vessels may bleed, leading to vitreous hemorrhage, fibrosis and retinal detachment. DR is frequently associated with diabetic macular edema, characterized by the deposition of hard exudates at the central retina, increased vascular permeability and microaneurysms (Figure 4D) [104,105,106]. DR has been traditionally treated with focal laser photocoagulation, surgical vitrectomy or with administration of corticosteroids with anti-inflammatory and antiangiogenic action (e.g., triamcinolone acetonide). The latter can be administered as intravitreal injections or retinal implants [107]. Following the improved therapeutic results in the treatment of AMD, the anti-VEGF drugs pegaptanib, ranibizumab and bevacizumab are also used in the treatment of DR and diabetic macular edema patients with positive results [105,108,109].

One approach where USMB is used against DR is to enhance the delivery of endostatin (ES). ES is a fragment antibody (MW 20 kDa) known for its inhibitory function in endothelial proliferation, anti-angiogenetic and antitumoral growth action [110]. Xu *et al.* developed cationic microbubbles (CMB) and studied the delivery ES-GFP plasmid to human retinal vascular endothelial cells, aiming to treat DR with inhibiting angiogenesis [111]. The total amount of ES protein was determined in cells, 48 hours post-transfection

(frequency 1 MHz, intensity 1 W/cm², exposure time 1 minute). ES protein level was significantly elevated in cells transfected with CMB + ultrasound, compared to cells treated with neutral nanobubbles (NMB) + ultrasound, or liposomes.

Another approach for the treatment of angiogenic eye diseases such as DR was followed by Kowalczyk *et al.*, who investigated the delivery of genes in the ciliary muscle [112]. As this muscle is located between the anterior and posterior eye segments, it was hypothesized that its transfection may allow for the production of proteins with anti-angiogenic or anti-inflammatory action. Microbubbles were mixed with pDNA encoding for Gaussia luciferase (pCMV-Gluc-1) or GFP (pEGFP-C1) and were injected into the ciliary muscle of rat eyes. Sonications were performed at 1 MHz frequency, 2 W/cm² intensity (0.7 MPa P_{neg}), and 2 minutes exposure time. Analysis of aqueous and vitreous humors samples collected 7 days after treatment showed that luciferase secretion in the pCMV-Gluc-1 + USMB group was 2.6-fold higher compared with the group treated with pCMV-Gluc-1 alone. Enhanced expression of GFP in ciliary muscle cells and around the ciliary body was seen 7 days after treatment with pEGFP-C1 + USMB (Figure 5E). No tissue damage was detected in the ciliary muscle, cornea or retina, showing that USMB treatment was safe at the specific settings. Temperature elevations were monitored in the lens and ciliary muscle during ultrasound exposure. A temperature increase of 3.7 °C and 7.3 °C was seen in the lens and ciliary muscle, respectively, but normal temperature was recovered a few seconds after treatment was completed. No alterations in the transparency of the lens were observed for up to a month later.

In conclusion, there is much less literature compared to AMD and glaucoma, though there are also therapeutic opportunities for USMB in DR.

Proliferative Vitreoretinopathy

Proliferative vitreoretinopathy (PVR) is an abnormal wound-healing process as a result of surgical failure in the treatment of rhegmatogenous retinal detachment. PVR is characterized by fixed retinal folds (Figure 4E), and proliferation and migration of RPE and RGC cells that result in cell collections on the retinal surface and vitreous cavity [113,114]. A pool of growth factors, such as transforming growth factor (TGF-β₂), platelet-derived growth factor (PDGF), and hepatocyte growth factor, are known contributors to the progression of PVR [115,116,117]. PVR is primarily treated with surgical intervention for vitrectomy and membrane peeling [118].

Zheng *et al.* investigated the role of USMB in the enhancement of rAAV-siRNA delivery to inhibit the expression of two of the growth factors (TGF- β 2 and PDGF-B) associated with proliferation of PVR [119]. The study was conducted using a disease animal model for PVR. Three days after induction of PVR, animals were treated with TGF-b2-siRNA, or PDGF-B-siRNA, or a combination of the two siRNAs. In addition, one group received the two siRNAs combined with USMB (frequency 1 MHz, intensity 2 W/cm², exposure time 300 s). Disease progression (proliferation level) was classified on a scale of 0–4, based on the morphological characteristics in the fundus photographs (vitreous haze, retinal folds and epiretinal membrane formation). Fourteen days after treatment, the proliferation level for eyes that received the combination of siRNAs (with and without USMB) was significantly lower than the control groups and the eyes treated with one of the two siRNAs, indicating that combined treatment with USMB decelerated proliferation. On the contrary, 28 days post-treatment, significantly lower proliferation grade was seen in the eyes that received combination of siRNAs + USMB compared with all other treatment groups, with 20% of the eyes in the USMB group showing no further proliferation between days 14 and 28. Twenty-eight days after treatment, the extent of retinal detachment, the number of effector cells (RPE, RGC, fibroblasts and macrophages) and proliferative membrane formation were dramatically reduced in the USMB-treated eyes compared to all other groups. Protein expression levels of TGF- β 2 and PDGF-B in the USMB-treated group were only half of the untreated group (639.85 vs. 1363.15 pg/mL for TGF- β 2, and 66.94 vs. 137.76 pg/mL for PDGF-B), confirming that combined treatment of siRNAs + USMB can limit the expression of TGF- β 2 and PDGF-B, and eventually, delay the progression of PVR.

Retinitis Pigmentosa

Retinitis pigmentosa (RP) is a group of hereditary ocular diseases caused by degeneration of rod and cone photoreceptor and RPE cells in the retina. At early RP stages during adolescence, patients experience difficulties with vision adaptation in darkness and night brightness (due to degeneration of rod photoreceptors), while in young adulthood, mid-peripheral vision is lost, followed by loss of central vision by the age of 60 years (due to degeneration of cone photoreceptors). Typical clinical signs are peripheric retina bone-spicule deposits (Figure 4F). At the progressed disease stages, degeneration of cells in the INL (amacrine, bipolar and horizontal neuron cells) and RGC might occur [120,121]. Currently, no effective treatments are available for RP, though vitamin therapy can be used for the preservation of photoreceptor function. Nutritional supplements aim to provide protection to retinal cells from oxidative damage, optimize key elements

of photoreceptor structure, and maintain the integrity of retinal blood oxygenation network (i.e., retinal blood vessels and choroid). Vitamin A is especially important, as it plays a role in the formation of rhodopsin, a receptor protein with critical function in rod photoreceptors. Supplementation with oral vitamin A is the most widely followed method for slowing photoreceptor degeneration in RP patients [120,122,123].

As previously discussed in the context of the treatment of wet AMD, numerous studies have demonstrated the USMB-mediated enhanced intracellular uptake of macromolecules [82], genes [83,84,85,86,87,88,89] and nanoparticles [90,91] in the neural retina and RPE. A similar USMB approach could also be feasible for treating RP.

Retinoblastoma

Retinoblastoma (RB) (Figure 4G) is an uncommon pediatric cancer, yet it is the primary intraocular malignancy in children. It is caused by a mutation in the RB1 gene and is fatal if untreated [124,125]. Replacement of traditional treatments such as eye enucleation and radiotherapy with chemotherapy has increased the survival rate to nearly 100% [126,127,128,129]. The treatment protocol to be used for RB therapy depends on laterality (tumor diagnosis in one or both eyes) and the International Classification of Retinoblastoma (ICRB) stage. In bilateral tumors, the presence of germline disease, or if optic nerve or choroid invasion is suspected, patients receive intravenous chemotherapy (IVC) to prevent metastases. ICRB classifies unilateral tumors as five subgroups based on tumor size, location and the presence of seeds. Unilateral tumors are treated with cryotherapy or transpupillary thermotherapy if they are small (≤ 3 mm), or larger than 3 mm and in the vicinity of macula and optic nerve. Extensive unilateral tumors and tumors with seeds are treated with intra-arterial chemotherapy (IAC). Usually, systemic toxicity is mild, and no ophthalmic toxicities have been reported as a result of IVC. IAC is more efficacious compared with IVC as the drug dose reaching the eye is increased by 10-fold [130,131]. This results in reduced duration of treatment and systemic toxicity. Despite the tremendous improvement in RB treatment with IVC and IAC, chemoresistant and recurrent tumors do occur often, caused by inadequate drug delivery into the vitreous or subretinal seeds [130,132].

The role of USMB in the enhancement of intracellular uptake of the chemotherapeutic agent doxorubicin (dox) in RB was studied *in vitro* in human RB cells [133]. First, the effect of USMB on cell viability was tested using various ultrasound intensities (0.3–1.0 W/cm²), at frequency of 1 MHz and exposure time of 10 s, in absence of the drug.

Maximum cell viability (97.9% of the untreated cells) was obtained at the lowest intensity. Next, the viability of RB cells after combined treatment with dox and USMB (at 0.3 W/cm²) was studied for 3 days. On the first day after treatment, no significant changes between treated and untreated cells were detected. However, 2 days post-treatment, cells exposed to dox + USMB had significantly reduced viability (34.9%) compared with cells treated with dox only (50.9%). Considering the mechanism of action of dox (i.e., intercalation into DNA and damage to cellular membranes, DNA, and proteins by generation of free radicals), cell apoptosis is not immediately seen after treatment. This might explain why the first induction of cell apoptosis was seen not earlier than 2 days post-treatment.

Eyelid Malignant Melanoma

Eyelid melanoma is an uncommon cutaneous malignancy that results from malignant proliferation of melanocytes in the epidermis of the eyelid skin (Figure 4H) [134,135]. Despite being generally similar to melanomas encountered anywhere on the skin in the head and neck area, eyelid melanoma is associated with sentinel lymph node metastasis due to the unique lymphatic drainage of the periocular skin [136]. Depending on the disease stage, current treatment methods include tumor excision, lymph node dissection and radiotherapy. Although these treatment methods are satisfactory, they are often associated with cosmetic issues.

Considering their superficial location, USMB-mediated treatment of eyelid malignancy could be a non-invasive alternative to surgical excision of the tumor. Sonoda *et al.* studied the uptake of a chemotherapeutic agent (bleomycin) enhanced by USMB in eyelid malignant melanoma *in vitro* and *in vivo* [137]. Mouse melanoma cells were treated with USMB (1 MHz frequency, 1 W/cm² intensity, 60 s exposure time) in combination with bleomycin (50 nm–5 μM concentration). A significant reduction in viability was observed only at the two highest drug concentrations in the cells treated with bleomycin + ultrasound. On the other hand, viability dropped at all bleomycin concentrations in the USMB treated cells, which was more dramatic with increasing drug concentration.

In the *in vivo* study, bleomycin and microbubbles were injected intratumorally and treatment efficacy was assessed by calculating the mean relative tumor weight for up to 8 days after treatment [137]. An ultrasound intensity of 2 W/cm² and exposure time of 240 s were used. Tumors treated with 0.125 mg/mL bleomycin + USMB decreased

in weight 2 days after treatment and continued shrinking until the last measurement. For the same drug concentration and in combination with ultrasound only, tumors grew in size over time and, on the last measurement, the average relative weight had increased by three times. Tumors in the control group were treated with bleomycin only at concentrations 0.25–2 mg/mL, and though these concentrations were higher than those used in the ultrasound and USMB groups, tumor growth was decelerated, but no reduction in size was observed. Furthermore, in the bleomycin + USMB group, for the rest of the drug concentrations tested (0.06 mg/mL, 0.25 mg/mL and 0.5 mg/mL), tumors initially increased in weight (day 2) but later continuously decreased in weight until day 8. Histological assessment of tumor samples revealed that in tumors treated with chemotherapy only, melanoma cells were actively dividing, and cell nuclei were pigmented and heterogeneous. In contrast, in the cases where tumor weight reduction was seen, a small amount of melanoma cells were present in the deepest part of the tumor, while the rest of the tumor area was occupied by necrotic cells. No histologic abnormalities were seen in the tumor peripheral tissue. Consequently, Sonoda *et al.* clearly showed that addition of microbubbles led to a significant decrease in tumor size at all drug concentrations and could enhance treatment efficacy using lower concentrations than the non-USMB treatment groups.

Corneal Opacity

Corneal opacity is the medical condition occurring when corneal clarity is lost. It appears as loss of transparency of the corneal membrane (Figure 4I), which affects the transmission and scattering of light, resulting in reduced visual acuity. Factors that can cause corneal opacity include corneal infection, injury, and edema [138,139]. Depending on the etiology, corneal opacity is treated with antibiotics, corticosteroids, antiviral drugs, or other interventions such as phototherapeutic keratectomy, or in severe cases, with keratoplasty (corneal transplantation) [140,141,142,143,144]. Permeability of cornea after topical administration of drug compounds largely depends on the drug molecule's solubility and polarity: the corneal epithelium and endothelium have a strong lipophilic character and resist penetration of polar molecules, while the corneal stroma is hydrophilic and resists penetration of non-polar molecules [145,146].

USMB-mediated transfection efficiency of pDNA (pEGFP-N2 gene) in the cornea was investigated using rabbit corneal epithelial cells *in vitro* and in rabbit cornea *in vivo* [147]. In the *in vitro* study, cells were exposed to 1 MHz frequency, 15–120 s exposure time and 0.5–2.0 W/cm² ultrasound intensity. An increase in the percentage of GFP-positive

cells was seen at 60 and 120 s exposure times, without a significant reduction in cell viability. Intensity of 0.5 W/cm^2 resulted in the lowest number of GFP-positive cells, and any increase higher than 1.5 W/cm^2 induced cell toxicity. Rabbit eyes that received plasmid alone or pDNA + ultrasound had mild GFP expression on the corneal stroma. In contrast, eyes that received pDNA + USMB (intensity 2 W/cm^2 , intra-corneal injection of microbubbles) showed the highest amount of GFP-positive cell expression, colocalized with the treated area (Figure 5F). It is hypothesized by the authors that because corneal composition consists of multiple cell layers and extracellular matrix, higher ultrasound intensities are required to induce microbubble cavitation bioeffects *in vivo* than *in vitro*, where a single layer of cells is exposed to ultrasound. *In vivo*, ultrasound intensity higher than 3 W/cm^2 caused corneal haziness, which was resolved later without treatment. In the pDNA + USMB group (2 W/cm^2 intensity for 120 s exposure time), GFP-positive cells were detected 1 day after treatment and the highest density was measured 4 days and 8 days after treatment. On day 14 post-treatment, GFP-cell density was significantly lower, and was no longer detected on day 30. Microscopic examination of corneal sections treated with USMB revealed that GFP-positive cells were located inside the corneal stroma, and no GFP-positive cells were detected in untreated corneal tissue, ciliary epithelial cells, trabecular meshwork, lens epithelial cells or retina. Light and electron microscopy performed 48 hours post-treatment revealed no corneal damage. Consequently, this study showed that USMB can enhance gene delivery in the anterior eye without inducing any adverse effects.

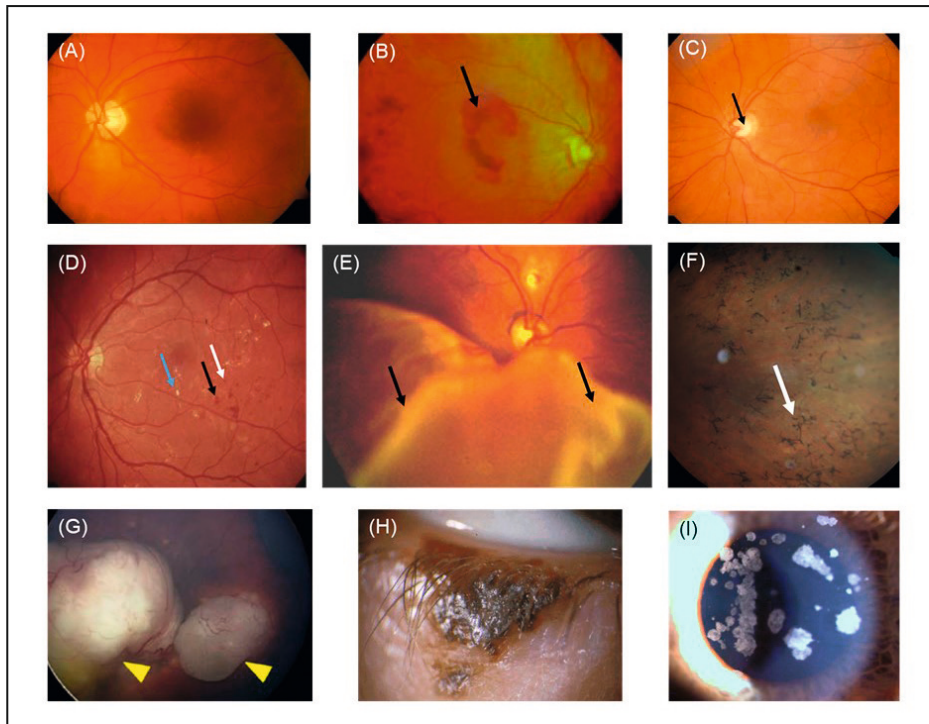


Figure 4. Color fundus photographs of (A) a healthy individual, (B) a patient with wet AMD (black arrow indicates hemorrhage), (C) a patient with glaucoma (black arrow indicates optic disc excavation), (D) a patient with DR (blue, black and white arrows indicate exudation, hemorrhage and microaneurysm, respectively), (E) a patient with retinal detachment (black arrows indicate PVR), (F) a patient with RP (white arrow indicates bone-spicule deposits), (G) a patient with RB (yellow arrowheads indicate tumors) adapted with permission from [148], (H) a patient with eyelid malignant melanoma. (I) Slit lamp image of a granular cornea dystrophy from a patient with corneal opacities. AMD: age-related macular degeneration, DR: diabetic retinopathy, PVR: proliferative vitreoretinopathy, RP: retinitis pigmentosa, RB: retinoblastoma

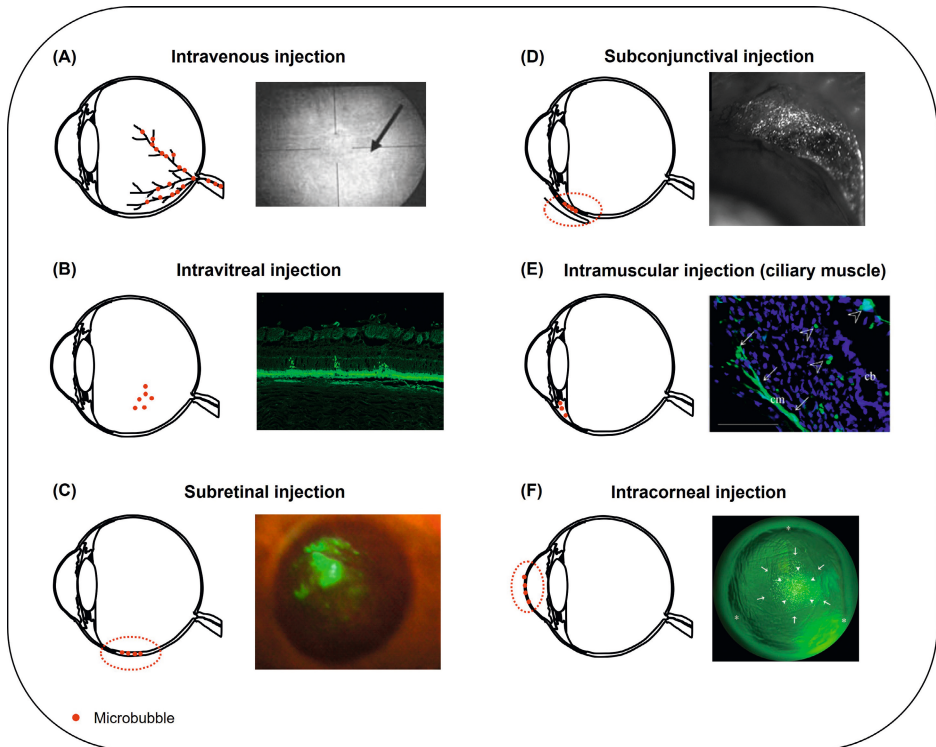


Figure 5. Summary of microbubble injection sites reported in the literature for USMB-mediated ocular drug and gene delivery. **(A)** Following intravenous administration, microbubbles circulate in the retinal blood vessels (left). Microbubble oscillations can induce disruption of the BRB and extravasation of fluorescein from blood retinal vessels (right, arrow). Adapted with permission from [79]. **(B)** The most frequently encountered administration site for microbubbles in ocular drug delivery is intravitreal injection (left). Fluorescence microscopy image of a rabbit retinal section after treatment with bubble liposomes in combination with plasmid GFP and intravitreal ultrasound (right). GFP-positive cells were present in the ONL. Adapted from [85]. **(C)** Schematic illustration of microbubbles injected into the subretinal space (left, dashed line). Fluorescent fundus stereoscopic image of rat retina treated with rAAV2-EGFP and USMB (right). GFP signal covered a large retinal surface area and was visible for 120 days post-treatment. Adapted from [87]. **(D)** Schematic illustration of subconjunctival injection of microbubbles (left, dashed line). Expression of GFP on the conjunctiva of a rat 48 hours after treatment with plasmid-GFP combined with bubble liposomes and ultrasound (right). Adapted with permission from [103]. **(E)** Schematic illustration of microbubbles injected into the ciliary muscle (left). Fluorescence microscopy image of a rat eye after combined treatment with pEGFP-C1 gene, intramuscular microbubbles and ultrasound (right). GFP-positive cells were localized in the ciliary muscle (arrows) and the ciliary body (arrowhead). Adapted with permission from [112]. **(F)** USMB-mediated drug or gene delivery in the cornea can be facilitated upon intracorneal injection of microbubbles (left, dashed line). Fluorescence stereoscopic image of a rabbit cornea, 7 days post-treatment with plasmid GFP and USMB (right). A mixture of microbubbles and plasmid was injected into the center of cornea (arrows), and ultrasound treatment was performed with the ultrasound probe positioned on the corneal surface (arrowheads). GFP-positive cells were colocalized with the area where the ultrasound probe was positioned. Adapted with permission from [147]. Figure not to scale.

Table 1. Summary of the studies investigating the use of USMB in the treatment of ocular diseases.

Study Model	Delivered Compound	Microbubbles and <i>In Vivo</i> Administration Site	Ultrasound Parameters	Efficacy	Safety	Reference
<i>In vivo</i> , (rabbit)	Fluorescein	Definity [®] , intravenous	Frequency 2 MHz, MI 0.2 and 1.7, exposure time 5 minutes	Alteration in the diameter of uveal blood vessels observed in 20% and 80% of eyes treated at low and high MI, respectively. At high MI, vasoconstriction and extravasation of fluorescein were observed, and the mean number of altered segments in blood vessels was higher than at low MI.	No bleeding.	[79]
<i>In vivo</i> , (rat)	Gd	Definity [®] , intravenous	Frequency 0.69 MHz, P _{neg} 0.81, 0.88 and 1.10 MPa (MI 0.98, 1.06, and 1.32, respectively), exposure time 60 seconds	Immediate increase in Gd signal after treatment indicated BRB disruption. For the two lower pressures, Gd signal decreased 3.5 hours post-treatment, revealing reversibility of BRB disruption, but not at P _{neg} 1.10 MPa.	Extravasated erythrocytes in the nuclear layers of the retina with more severe damage at 1.10 MPa.	[80]
<i>In vivo</i> , (rat, mouse)	Evans blue, IgG, IgM	Definity [®] , intravenous	Frequency 1.1 MHz, P _{neg} 0.36–0.84 MPa (MI 0.34–0.80), exposure time 120 seconds	Extravasation of Evans blue, IgG and IgM was observed in the neural retina (INL and RGC) suggesting that the vascular plexi within these layers were permeabilized. No evidence for molecule transfer across the choroid and into the RPE.	Evidence for morphological damage, reactive gliosis, neuroinflammation and presence of erythroid cells. No megakaryocyte infiltration.	[81]
<i>In vitro</i> (RPE, Müller glia, photoreceptors)	IgG	Custom-made NBS with shells made of DPPC/DSPE-PEG(2k)-Ome and PFP inner gaseous phase	Frequency 1 MHz, intensity 0.5 W/cm ² , exposure time 30 seconds	Increase in the intracellular uptake of IgG after treatment with USMB was cell line-dependent. USNB efficacy was highly dependent on ultrasound intensity and exposure time.	N/A	[82]
<i>In vitro</i> (RPE), <i>in vivo</i> (rat)	PEI/pEGFP	SonoVue™, subretinal injection	Frequency 1 MHz, intensity 1–3 W/cm ² , exposure time 1–5 minutes	<i>In vitro</i> : higher exposure time resulted in higher number of GFP-positive cells and decreased cell viability. <i>In vivo</i> : high density EGFP-positive cells were observed in animals treated with PEI/pEGFP + USMB, predominantly distributed in the retina.	No tissue damage.	[83]

Table 1. Continued.

Study Model	Delivered Compound	Microbubbles and <i>In Vivo</i> Administration Site	Ultrasound Parameters	Efficacy	Safety	Reference
<i>In vivo</i> (rat)	pEGFP-N1	SonoVue™, subretinal injection	Frequency 1 MHz, intensity 2 W/cm ² , exposure time 5 minutes	The highest EGFP-positive signal was observed in the PEI/pDNA + USMB group, distributed in neural retina and RPE cells. The same trend was observed in the quantification of EGFP gene copy number and the EGFP mRNA expression level in the RPE and neural retina.	No evidence for corneal or retinal damage, no morphological alterations, no inflammatory cell infiltration.	[84]
<i>In vivo</i> (rabbit)	pEGFP-N2	Custom-made BL Shells made by DSPC/DSPE-PEG (2k)-Ome, inner phase PFP gas, intravitreal injection	Frequency 3 MHz, intensity 0.15 W/cm ² , exposure time 60 seconds	Highest amount of GFP-score in the plasmid and USBL group. GFP-positive cells were colocalized with the areas exposed to ultrasound and were detected in the ONL.	No obvious tissue damage.	[85]
<i>In vitro</i> (human RPE cells), <i>in vivo</i> (rat)	rAAV-EGFP	SonoVue™, subretinal injection	Frequency 1 MHz, intensity 0.5–2 W/cm ² , exposure time 1–5 minutes	<i>In vitro</i> , combined treatment with USMB resulted in the highest transduction efficiency than treatment with ultrasound only. <i>In vivo</i> , quantification of EGFP signal revealed significantly elevated values for the USMB group on the first 35 days post-treatment. EGFP-positive cells in the USMB group were found in neural retina and RPE cells.	No evidence for tissue damage.	[86]
<i>In vitro</i> (rat RPE cells), <i>in vivo</i> (rat)	rAAV2-EGFP	SonoVue™, subretinal injection	Frequency 1 MHz, intensity 0.2–3 W/cm ² , exposure time 15–300 seconds	<i>In vitro</i> : increased rAAV-EGFP transduction of cells observed in groups treated with ultrasound or microbubbles alone, but not their combination. <i>In vivo</i> : USMB resulted in a higher expression of EGFP. An increase in GFP-fluorescence was found until day 35 and reduced up to 120 days post-treatment. GFP signal was found in RPE and neural retina.	<i>In vitro</i> : reduced cell viability at intensity of 3 W/cm ² . <i>In vivo</i> : all retina cell layers were well preserved without photoreceptor loss or inflammation.	[87]

Table 1. Continued.

Study Model	Delivered Compound	Microbubbles and <i>In Vivo</i> Administration Site	Ultrasound Parameters	Efficacy	Safety	Reference
<i>In vivo</i> (rat)	Lipofectamine-formulated fluorescently labelled-siRNA	SonoVue™, intravitreal injection	Frequency 1 MHz, intensity 1–3 W/cm ² , exposure time 300 seconds	The greatest quantity of transduced cells was observed in the group treated with lipofectamine-formulated siRNA combined with USMB. No fluorescence was detected in either the untreated or treated with naked siRNA + ultrasound groups.	No significant cell viability reduction observed 12 h after transfection. Retina cell layers were well preserved without photoreceptor loss, nuclear layer vacuolation, or inflammation.	[88]
<i>In vitro</i> (human RPE cells)	rAAV-EGFP, PEI/pDNA and L/siRNA	SonoVue™	Frequency 1 MHz, intensity 1–3 W/cm ² , exposure time 60–120 seconds	Transfection efficiency of rAAV and PEI/pDNA vectors significantly improved when gene delivery was combined with USMB, in contrast to the L/siRNA efficiency that was benefited by ultrasound alone. Combined treatment with USMB did not cause structural alterations on the pDNA.	N/A	[89]
<i>In vitro</i> (rat RPE cells)	Fluorescently labelled siRNA encapsulated in mPEG-PLGA-PLL nanoparticles	SonoVue™	Frequency 1 MHz, intensity 0.5–2 W/cm ² , exposure time 30–60 seconds	Highest nanoparticle uptake observed in cells treated with ultrasound alone. Combination with USMB did not improve the nanoparticle uptake.	At the settings with the highest nanoparticle uptake, a temperature increase of 1.9 °C was reported with no influence on cell viability.	[90]
<i>In vivo</i> (rat)	Fluorescently labelled PDGF-BB siRNA encapsulated in mPEG-PLGA-PLL nanoparticles	SonoVue™, intravitreal injection	Frequency 1 MHz, intensity 2 W/cm ² , exposure time 5 minutes	The highest transfection efficiency in neural retina was achieved after combined treatment with USMB.	No evidence for tissue damage. All retinal layers were well preserved without photoreceptor loss or inflammation.	[91]

Table 1. Continued.

Study Model	Delivered Compound	Microbubbles and <i>In Vivo</i> Administration Site	Ultrasound Parameters	Efficacy	Safety	Reference
<i>In vivo</i> (rabbit, intraocular hypertension animal model)	mNGF	SonoVue™, intravitreal	Frequency 1 MHz, intensity 0.5 W/cm ² , exposure time 60 seconds	Function of optic nerve myelin and axons was improved in the group that received mNGF + USMB. Retinas treated with mNGF + USMB had clear and orderly arranged cell layers. The thickness of the inner and outer plexiform layers was nearly normal. Rod and cone cells were normally aligned without degeneration, and RGC were normal in structure.	N/A	[100]
<i>In vitro</i> (rat RGC)	pEGFP-N1 and bcl-xl	SonoVue™	Frequency 0.3 MHz, intensity 0.25–1.25 W/cm ² , exposure time 30–120 seconds	Improved transfection efficiency observed in pEGFP-N1 + USMB group. USMB-mediated bcl-xl transfection had a role in protection of RGCs from apoptosis, but did not prevent apoptosis completely.	N/A	[101]
<i>In vivo</i> (rat)	rAAV2-EGFP	Custom-made lipid microbubbles (shell: DSPC, 1,2-DSPA, inner gas: PFP), intravitreal injection	Frequency 0.3 MHz, intensity 0.5–2.5 W/cm ² , exposure time 60 seconds	Greatest EGFP expression was observed in retinas treated with rAAV2-EGFP + USMB. The majority of GFP-positive cells were RGC.	No structural, morphological alterations, no cellular infiltration in the vitreal cavity.	[102]
<i>In vitro</i> (rabbit cornea epithelial cells), <i>In vivo</i> (rat)	pEGFP-N2	Custom-made BL. Shells made by DSPC/DSPA-PEG (2k)-Ome, inner gaseous phase PFP gas, subconjunctival injection.	Frequency 1 MHz, intensity 0.8–1.2 W/cm ² , exposure time 20–60 seconds	<i>In vitro</i> : The ratio of GFP-positive cells treated with USBL was about 2 times higher than the USMB group. <i>In vivo</i> : GFP-positive cell density in eyes treated with USBL was significantly higher than the groups that received plasmid only, plasmid + ultrasound and plasmid + USMB. GFP-positive cells were mostly located beneath the conjunctival epithelium of the area exposed to ultrasound. No significant number of GFP-positive cells was observed in any other part of the eye.	<i>In vitro</i> : no alterations in cell viability. <i>In vivo</i> : the structure of conjunctiva was well preserved. No signs of hemorrhage, edema or inflammation.	[103]

Table 1. Continued.

Study Model	Delivered Compound	Microbubbles and <i>In Vivo</i> Administration Site	Ultrasound Parameters	Efficacy	Safety	Reference
<i>In vitro</i> (human retinal vascular endothelial cells)	ES-GFP	NMB: DPPC/DSPE-PEG2000 and cationic microbubbles CMB: DPPC/DSPE-PEG2000-Biotin/DC-Chol, containing PFP gas	Frequency 1 MHz, intensity 1 W/cm ² , exposure time 1 minute	CMBs had higher plasmid binding compared to NMBs. In cells treated with CMBs, the level of VEGF, Bcl-2, and Bcl-xl mRNA was decreased.	N/A	[111]
<i>In vivo</i> (rat)	pCMV-Gluc-1, pVAX1-LacZ, pEGFP-C1	Artison, intra-muscle injection (ciliary muscle)	Frequency 1 MHz, P _{avg} 0.7 MPa, exposure time 120 seconds	One week after treatment, the group treated with pCMV-Gluc-1 plasmid + USMB had the greatest expression of luciferase. Enhanced expression of β -galactosidase in the ciliary muscle cells and sporadically around the ciliary body was observed. Similar enhancement and localization site of GFP protein observed in the pEGFP-C1 + USMB group.	No apoptotic cells detected in the conjunctiva, retina or cornea. A temperature increase of 3.7 °C in the lens and 7.3 °C in the ciliary muscle measured during ultrasound exposure. Normal temperature was immediately recovered. No alterations in the transparency of the lens for up to a month post-treatment.	[112]
<i>In vivo</i> (rat, proliferative vitreoretinopathy disease model)	rAAV2-TGF- β 2-siRNA and rAAV2-PDGF-B-siRNA	SonoVue™ intravitreal injection	Frequency 1 MHz, intensity 2 W/cm ² , exposure time 300 seconds	In the group treated with siRNAs + USMB, retinal morphologic alterations progressed slower than in control groups. The numbers of effector cells, such as RPE cells, glial cells, fibroblasts and macrophages, and the incidence of retinal detachment, and proliferative membrane formation were significantly less than the eyes treated without USMB.	N/A	[119]

Table 1. Continued.

Study Model	Delivered Compound	Microbubbles and <i>In Vivo</i> Administration Site	Ultrasound Parameters	Efficacy	Safety	Reference
<i>In vitro</i> (human RB cells)	Doxorubicin	Artison	Frequency 1 MHz, intensity 0.3–10 W/cm ² , exposure time 10 seconds	No significant differences in cell viability observed 24 h post-treatment between cells treated with doxorubicin alone and doxorubicin + USMB. Viability of cells exposed to doxorubicin + USMB was significantly lower compared with cells exposed to doxorubicin alone 48 and 72 h, but not 24 h post-treatment.	N/A	[133]
<i>In vitro</i> (mouse melanoma cells), <i>in vivo</i> (mouse)	Bleomycin	Optison™, intratumoral injection	Frequency 1 MHz, intensity 1–2 W/cm ² , exposure time 60–240 seconds	<i>In vitro</i> : Combination of bleomycin and USMB resulted in a significant decrease in cell viability at all concentrations tested. <i>In vivo</i> : in the bleomycin + USMB group, for drug concentrations of 0.06 mg/mL, 0.25 mg/mL and 0.5 mg/mL, tumors initially increased in weight but later had a continuous decrease until day 8. Tumors treated with 0.125 mg/mL bleomycin + USMB responded immediately after the first treatment with a continuous reduction in size. No reduction in tumor size was observed in the group treated with bleomycin alone.	<i>In vivo</i> : temperature inside the tumor increased from 34 °C to 37. The temperature of the ultrasound probe accordingly. No histological abnormalities were seen in other organs (brain, lung, liver, heart).	[137]
<i>In vitro</i> , (rabbit corneal epithelial cells), <i>in vivo</i> (rabbit)	pEGFP-N2	Optison™, intracorneal	Frequency 1 MHz, intensity 0.5–2 W/cm ² , exposure time 15–120 seconds	<i>In vitro</i> : The greatest amount of GFP-positive cells ratio was significantly greater in samples treated with USMB. <i>In vivo</i> : The eyes that received plasmid + USMB showed the highest number of GFP-positive cells. GFP-positive cells appeared one day after treatment. Fluorescence intensity increased the first 8 days, significantly decreased on day 14 and was not measurable on day 30 after treatment. GFP was mainly located inside the corneal stroma.	Immediate corneal stroma haziness appeared at intensity >3 W/cm ² , which was spontaneously resolved immediately after treatment. No corneal damage was observed.	[147]

SAFETY AND TOLERABILITY OF USMB IN OCULAR THERAPEUTIC APPLICATIONS

The safety of USMB is generally reliant on the individual components that play a role during treatment: the microbubbles and the ultrasound settings. The presently commercially available microbubbles (Figure 6) are generally well tolerated by patients [149]. Currently, there are four microbubble products approved for use in ultrasound imaging; these are Optison™ (GE Healthcare, Little Chalfont, UK), SonoVue™ (Bracco, Milan, Italy), Definity® (Lantheus Medical Imaging, North Billerica, MA, USA) and Sonazoid™ (GE Healthcare). Microbubbles are well tolerated, though there are some contraindications related to the microbubble shell-forming agent. For the phospholipid-containing agents (SonoVue™, Definity® and Sonazoid™), a contraindication exists for patients who have a history of hypersensitivity to phospholipids (manifesting, for instance, as an egg allergy). SonoVue™, Definity® and Sonazoid™ contain polyethylene glycol (PEG) as an excipient, as it is present in the microbubble shell. PEG reduces opsonization and interaction with cells, and increases formulation stability [150]. Recently, some case reports were published after anaphylactic reactions to PEG components, indicating the potential for immunoglobulin E-mediated type I hypersensitivity reactions. [151,152]. The FDA MedWatch alert identified 11 anaphylaxis cases, including 2 deaths, over a period of several decades. In 2021, the American Society of Echocardiography published an expert consensus statement with recommendations for laboratory policies on microbubbles containing PEG, stating that SonoVue™ and Definity® are contraindicated in patients with known hypersensitivity to these agents or their components, but also contraindicated in patients with known hypersensitivity to PEG (Sonazoid™ is currently not approved for use in the United States) [153]. The FDA states that Optison™ is an alternative to Definity® and SonoVue™ in patients with hypersensitivity to PEG, as it contains albumin rather PEG [154]. Additionally, a recent animal study on the pharmacokinetics of PEGylated microbubble administration indicated that microbubble blood clearance can be accelerated upon repeated administration. This reduction in microbubble half-life is due to opsonization by IgM and IgG anti-PEG antibodies that are produced by the immune system after the initial microbubble administration [155]. Investigation into the clinical relevance of this effect for microbubbles has yet to be investigated.

Patients with a hypersensitivity to blood products, such as human albumin, are advised against treatment with Optison™ microbubble products. Another parameter in which

the current microbubbles can be categorized is the gas used as disperse phase. For Definity® and Optison™, perflutren gas is used, whereas for Sonazoid™ and SonoVue™, perfluorobutane and sulphur hexafluoride are used, respectively. For all microbubble products, the contained gasses are usually eliminated quickly from the bloodstream, typically without any adverse effect, unless the patient is hypersensitive to the specific gas used [6,156,157].

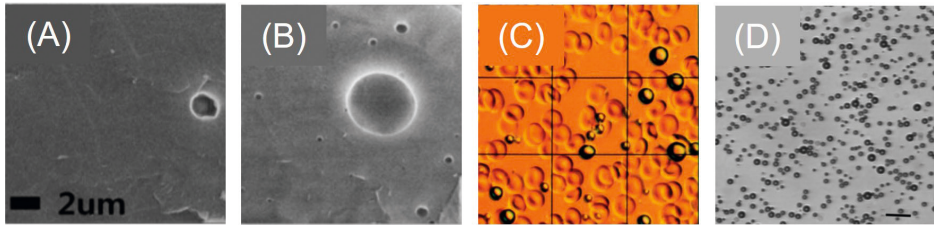


Figure 6. Commercially available microbubbles. Cryo-SEM images of (A) SonoVue™ and (B) Definity® microbubbles. Adapted from [158]. (C) Optison™ microbubbles against a background of red blood cells. Adapted with permission from [159]. (D) Optical microscopy image of Sonazoid™ microbubbles. Adapted with permission from [160].

The induced bioeffects are highly related to the type of cavitation (stable or inertial) microbubbles undergo during USMB treatment. Commercial microbubbles are polydisperse, i.e., there is variation in size within the microbubble population [6,161]. During exposure to ultrasound, microbubbles with different sizes oscillate in a non-uniform manner. Specifically, while some microbubbles with a certain size oscillate in a safe manner, bubbles with different size might simultaneously induce unwanted side effects. As a result, polydispersity is related to a broad spectrum of bioeffects, which makes efficacy and safety more difficult to control. Recently, in order to rectify this safety issue, development of monodisperse microbubbles for imaging and therapy has been gaining momentum [6,31,162].

Prior to clinical translation, a method that will allow the monitoring of the intensity of induced bioeffects in real time is needed. It has been previously reported that acoustic microbubble emissions can be used to monitor the presence, the type, the location and the level of cavitation in the brain, in real-time [163]. The harmonic, subharmonic and ultraharmonic components of microbubble signals can be recorded by a cavitation detector and, using a feedback control algorithm, the acoustic pressure generated can be adjusted [43,164,165]. Touahri *et al.* [81] used the same method as O'Reilly and Hynynen [165] to verify the effect of focused ultrasound on microbubbles when sonicating rat retinas, by monitoring the generation of subharmonic signals. Despite this

monitoring, some evidence for neuroinflammation and the presence of erythroid cells was found in the areas where the BRB was disrupted. In the future, feedback control methods specifically designed to be used in ophthalmic applications are needed in order to avoid irreversible BRB disruption.

Ultrasound settings largely influence the efficacy of the method, as well as the safety. The maximum pressure/intensity of the emitted ultrasound wave is one of the critical safety parameters, as it is one of the determining factors for microbubble cavitation regime and the resulting bioeffects. In ophthalmic ultrasound imaging applications, the FDA limits the maximum MI to 0.23 [166]. Looking at the studies that investigated extravasation of molecules from the retinal vasculature, in all cases with successful BRB disruption, an MI higher than 0.23 was used (assuming that the pressures in [81] were given as P_{neg} , as it was not clear from the paper). However, in all three studies, some type of damage was observed in the retina (vasoconstriction of blood vessels, tissue morphological alterations, neuroinflammation, etc.). The only example where an MI within the FDA's imaging limits was used was from Hirokawa *et al.* but no extravasation of fluorescein was seen [79]. Considering the intracellular uptake of (drug) molecules, most of the studies report ultrasound intensity (in W/cm^2) without specifying to which ultrasound intensity definition this corresponds (e.g., spatial peak–temporal peak, spatial peak–pulse average, etc.). For those studies that used the Sonitron 2000 (Rich-Mar, Inola, OK, USA) system, the MI was calculated based on the calibration of the system performed by Kopechek *et al.* [167]. Sonoda *et al.* [147] reported successful corneal gene delivery in rabbits *in vivo* at MI 0.14–0.21 (intensity 0.5–2 W/cm^2), but when the MI was increased to 0.25 (intensity 3 W/cm^2), corneal stroma haziness was observed. In addition, Yamashita *et al.* [103] treated rat eyes with USMB at MI 0.18 (1.2 W/cm^2) and reported successful gene delivery in conjunctiva without any adverse effects. Overall, it can be concluded that intracellular uptake was successfully enhanced by USMB using MIs within the FDA's safety limit for imaging applications. In contrast, this approach has not been successful for BRB disruption applications so far, and it is to be investigated whether it can be performed without inducing adverse effects in the retina.

In addition to ultrasound intensity and MI, other ultrasound settings, such as the duty cycle (the ratio of the ultrasound pulse duration to the repetition period) and exposure time (the total time ultrasound waves are transmitted to the target site during treatment), are associated with cell damage and safety issues [32]. Indeed, some of the studies discussed above reported increased cell damage with increasing duty cycle,

increasing microbubble concentration and exposure time [83,89,133]. Consequently, a combination of these parameters in addition to the maximum allowed MI is what will likely define the safety limit of USMB in ophthalmology.

Another significant safety aspect is temperature elevation in the eye during ultrasound exposure. Tissue heating depends on the energy of the ultrasound wave and the ability of the tissue to absorb this energy and convert it into heat. Temperature elevation in the lens and cornea can induce the formation of a cataract and alter the expression of a stress protein in corneal epithelial cells, respectively [168]. The regulatory recommendations by the World Federation of Ultrasound in Medicine and Biology (WFUMB) state that tissue temperature increases >1.5 °C above physiological levels should be avoided in the eye [169]. Kowalczyk *et al.* measured a temperature increase of 3.7 °C in rat lens and 7.3 °C in ciliary muscle during sonication (intensity 2 W/cm², exposure time 120 s) using a digital thermocouple needle [112]. Physiological temperature was recovered a few seconds after sonication stopped and no alterations in the transparency of the lens were observed for up to a month post-treatment. Due to the differences in the size between rat and human eyes, heat distribution might differ between the two species. Consequently, the thermal effects of USMB in the human eye are yet to be determined. In clinical practice, temperature-related side effects in the anterior eye could be limited by adjusting the geometry of the ultrasound probe in such a way that exposure of the lens to ultrasound is avoided. An example of a therapeutic device with such geometry is used in the treatment of high IOP with ultrasound cycloplasty (EyeOP1, Eye Tech Care, Lyon, France). The piezoelectric transducers are positioned in a ring on the surface of the eye that allows the ultrasound beam to be focused on the ciliary body without interfering with the lens [170,171]. In addition to transducer geometry, the ultrasound settings that induce a therapeutic effect, but no thermal side effects, need to be investigated.

Finally, an adverse immune reaction to USMB treatment can affect the safety of USMB in ocular drug delivery. In prior studies, USMB-mediated BBB disruption was associated with inflammatory response, presence of albumin in the brain parenchyma and infiltration of macrophages [172,173]. Although moderate gliosis in the retinal Müller cells can be advantageous in the secretion of neurotrophic factors, prolonged disruption of the BRB might induce severe gliosis, which is associated with uncontrolled cell proliferation and depolarization [174]. Furthermore, the presence of fibrinogen and erythrocytes in the retina as a result of BRB disruption is an undesired potential

side effect of USMB treatment. Indeed, some evidence of these adverse effects was observed in earlier BRB-related studies [80,81].

To conclude, *in vitro* and *in vivo* studies in animals indicate that USMB can be used safely to improve drug or gene delivery in the eye. However, long-term toxicity studies are required to determine the exact treatment protocol that permits safe translation of this method to the clinic.

FUTURE DIRECTIONS

In addition to the preclinical studies available in the literature, some patents and patent applications have been published, highlighting the potential of USMB in ocular drug delivery in the clinic. A recent patent application by Carpentier *et al.* describes the technical aspects of an ultrasound device that can be used for targeted drug delivery in the human retina [175]. Another example of microbubble activity against ocular pathologies is the enhancement of blood clot lysis (so-called “sonothrombolysis”). Sonothrombolysis has been investigated *in vitro* and *in vivo* as a method to accelerate recanalization after vascular thrombosis in ischemic stroke and heart disease [176,177,178,179]. Utilizing the same principles, Fawzi *et al.* in 2014 applied for a patent that describes the use of microbubble cavitation against retinal vein occlusions (Figure 7A) [180]. The use of mechanical activity of microbubbles against cataract was described in a recent patent application by Grubbs *et al.* (Figure 7B) [181]. Microbubbles are injected using a thin needle tip into the lens after capsulorhexis and hydrodissection of the lens. By externally applied ultrasound, microbubble cavitation is triggered, which induces cataract fragmentation. A standard irrigation–aspiration device can then be used for aspiration of the cataract fragments.

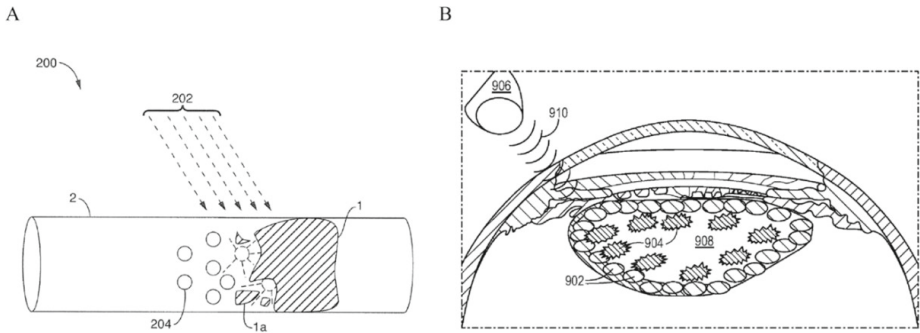


Figure 7. Examples of inventions published as patent applications or patents proposing the use of USMB for the treatment of ocular diseases. **(A)** Sonothrombolysis of a blood clot in a retinal blood vessel. Microbubbles (204) undergo mechanical cavitation when triggered by an externally applied ultrasound beam (202). Oscillations of microbubbles cause the blood clot (1) in the retinal blood vessel (2) to dissolve (1a). Adapted from [180]. **(B)** Fragmentation of cataract using microbubbles. Microbubbles (902) are injected using a thin needle into the lens (908). Ultrasound waves (910) generated by an external source (906) cause the microbubbles to cavitate and fragment the cataracts (904). Adapted from [181].

CONCLUSIONS

Various studies have investigated the use of USMB as a method to improve drug and gene delivery in ophthalmology. Applications include transient and reversible disruption of the BRB, and enhanced intracellular uptake of anticancer drugs, genes and nanoparticles. The studies discussed in this review report limited side effects caused by USMB *in vitro* and *in vivo* in animals. Efficacy and safety are highly dependent on the characteristics of the ultrasound field and the behavior of microbubbles (stable or inertial cavitation) during the treatment. Research into USMB-based permeabilization of the BRB and intracellular delivery of drugs could potentially lead to breakthroughs in the field of ocular therapeutics, allowing for administration of therapeutics in the eye that previously would not be properly delivered and, therefore, suffer from poor efficacy.

REFERENCES

1. Henry Mundt, G.; Hughes, W.F. Ultrasonics in Ocular Diagnosis. *Am. J. Ophthalmol.* 1956, 41, 488–498, doi:10.1016/0002-9394(56)91262-4.
2. B.Rosen, D.; D. Conway, M.; P. Ingram, C.; D. Ross, R.; G. Montilla, L. A Brief Overview of Ophthalmic Ultrasound Imaging. In *Novel Diagnostic Methods in Ophthalmology*; Nowinska, A., Ed.; IntechOpen: London, 2019 ISBN 978-1-83880-311-7, 978-1-83880-312-4.
3. Kendall, C.J.; Prager, T.C.; Cheng, H.; Gombos, D.; Tang, R.A.; Schiffman, J.S. Diagnostic Ophthalmic Ultrasound for Radiologists. *Neuroimaging Clin. N. Am.* 2015, 25, 327–365, doi:10.1016/j.nic.2015.05.001.
4. Silverman, R.H. High-Resolution Ultrasound Imaging of the Eye - a Review. *Clin. Experiment. Ophthalmol.* 2009, 37, 54–67, doi:10.1111/j.1442-9071.2008.01892.x.
5. Gramiak, R.; Shah, P.M. Echocardiography of the Aortic Root: Invest. Radiol. 1968, 3, 356–366, doi:10.1097/00004424-196809000-00011.
6. Frinking, P.; Segers, T.; Luan, Y.; Tranquart, F. Three Decades of Ultrasound Contrast Agents: A Review of the Past, Present and Future Improvements. *Ultrasound Med. Biol.* 2020, 46, 892–908, doi:10.1016/j.ultrasmedbio.2019.12.008.
7. Klibanov, A.L. Ultrasound Contrast: Gas Microbubbles in the Vasculature. *Invest. Radiol.* 2021, 56, 50–61, doi:10.1097/RLI.0000000000000733.
8. Stride, E.; Segers, T.; Lajoinie, G.; Cherkaoui, S.; Bettinger, T.; Versluis, M.; Borden, M. Microbubble Agents: New Directions. *Ultrasound Med. Biol.* 2020, 46, 1326–1343, doi:10.1016/j.ultrasmedbio.2020.01.027.
9. Averkiou, M.A.; Bruce, M.F.; Powers, J.E.; Sheeran, P.S.; Burns, P.N. Imaging Methods for Ultrasound Contrast Agents. *Ultrasound Med. Biol.* 2020, 46, 498–517, doi:10.1016/j.ultrasmedbio.2019.11.004.
10. Cennamo, G.; Rosa, N.; Vallone, G.F.; Smaltino, F. First Experience with a New Echographic Contrast Agent. *Br. J. Ophthalmol.* 1994, 78, 823–826, doi:10.1136/bjo.78.11.823.
11. Lemke, A.-J.; Hosten, N.; Richter, M.; Bechrakis, N.E.; Foerster, P.; Puls, R.; Gutberlet, M.; Felix, R. Contrast-Enhanced Color Doppler Sonography of Uveal Melanomas. *J. Clin. Ultrasound* 2001, 29, 205–211, doi:10.1002/jcu.1021.
12. Forte, R.; Cennamo, G.; Staibano, S.; De Rosa, G. Echographic Examination with New Generation Contrast Agent of Choroidal Malignant Melanomas: *Acta Ophthalmologica Scandinavica* 2005. *Acta Ophthalmol. Scand.* 2005, 83, 347–354, doi:10.1111/j.1600-0420.2005.00428.x.
13. Yan, L.; He, G.; Zhou, X.; Zheng, Y.; Zhu, Y.; Yang, J.; Zhang, M.; Zhou, Y. Contrast-Enhanced Ultrasound in the Diagnosis of Orbital Space-Occupying Lesions. *Clin. Radiol.* 2017, 72, 798.e1–798.e6, doi:10.1016/j.crad.2017.03.026.
14. Bertolotto, M.; Serafini, G.; Sconfienza, L.; Lacelli, F.; Cavallaro, M.; Coslovich, A.; Tognetto, D.; Cova, M. The Use of CEUS in the Diagnosis of Retinal/Choroidal Detachment and Associated Intraocular Masses – Preliminary Investigation in Patients with Equivocal Findings at Conventional Ultrasound. *Ultraschall Med. - Eur. J. Ultrasound* 2013, 35, 173–180, doi:10.1055/s-0032-1330321.

15. Sng, W.J.; Kapur, J.; Sundar, G.; Lian, W.Q.D.; Tan, A.P. Utilization of Contrast-Enhanced Ultrasound in the Evaluation of Craniofacial Osseous Lesions: A Case Report. *Clin. Imaging* 2020, 60, 5–9, doi:10.1016/j.clinimag.2019.10.018.
16. Williamson, T.H.; Harris, A. Color Doppler Ultrasound Imaging of Theeye and Orbit. *Surv. Ophthalmol.* 1996, 40, 255–267, doi:10.1016/S0039-6257(96)82001-7.
17. Skidmore, C.; Saurey, T.; Ferre, R.M.; Rodriguez-Brizuela, R.; Spaulding, J.; Lundgreen Mason, N. A Narrative Review of Common Uses of Ophthalmic Ultrasound in Emergency Medicine. *J. Emerg. Med.* 2021, 60, 80–89, doi:10.1016/j.jemermed.2020.08.003.
18. Sconfienza, L.M.; Lacelli, F.; Ardemagni, A.; Perrone, N.; Bertolotto, M.; Padolecchia, R.; Serafini, G. High-Resolution, Three-Dimensional, and Contrast-Enhanced Ultrasonographic Findings in Diseases of the Eye. *J. Ultrasound* 2010, 13, 143–149, doi:10.1016/j.jus.2010.10.002.
19. Postema, M.; van Wamel, A.; Lancée, C.T.; de Jong, N. Ultrasound-Induced Encapsulated Microbubble Phenomena. *Ultrasound Med. Biol.* 2004, 30, 827–840, doi:10.1016/j.ultrasmedbio.2004.02.010.
20. Postema, M.; van Wamel, A.; ten Cate, F.J.; de Jong, N. High-Speed Photography during Ultrasound Illustrates Potential Therapeutic Applications of Microbubbles: Ultrasonic Microbubbles for Therapy. *Med. Phys.* 2005, 32, 3707–3711, doi:10.1118/1.2133718.
21. Qin, P.; Han, T.; Yu, A.C.H.; Xu, L. Mechanistic Understanding the Bioeffects of Ultrasound-Driven Microbubbles to Enhance Macromolecule Delivery. *J. Controlled Release* 2018, 272, 169–181, doi:10.1016/j.jconrel.2018.01.001.
22. Fan, Z.; Liu, H.; Mayer, M.; Deng, C.X. Spatiotemporally Controlled Single Cell Sonoporation. *Proc. Natl. Acad. Sci.* 2012, 109, 16486–16491, doi:10.1073/pnas.1208198109.
23. Lammertink, B.; Deckers, R.; Storm, G.; Moonen, C.; Bos, C. Duration of Ultrasound-Mediated Enhanced Plasma Membrane Permeability. *Int. J. Pharm.* 2015, 482, 92–98, doi:10.1016/j.ijpharm.2014.12.013.
24. Meijering, B.D.M.; Juffermans, L.J.M.; van Wamel, A.; Henning, R.H.; Zuhorn, I.S.; Emmer, M.; Versteilen, A.M.G.; Paulus, W.J.; van Gilst, W.H.; Kooiman, K.; et al. Ultrasound and Microbubble-Targeted Delivery of Macromolecules Is Regulated by Induction of Endocytosis and Pore Formation. *Circ. Res.* 2009, 104, 679–687, doi:10.1161/CIRCRESAHA.108.183806.
25. Van Wamel, A.; Kooiman, K.; Hartevelde, M.; Emmer, M.; ten Cate, F.J.; Versluis, M.; de Jong, N. Vibrating Microbubbles Poking Individual Cells: Drug Transfer into Cells via Sonoporation. *J. Controlled Release* 2006, 112, 149–155, doi:10.1016/j.jconrel.2006.02.007.
26. Schlicher, R.K.; Radhakrishna, H.; Tolentino, T.P.; Apkarian, R.P.; Zarnitsyn, V.; Prausnitz, M.R. Mechanism of Intracellular Delivery by Acoustic Cavitation. *Ultrasound Med. Biol.* 2006, 32, 915–924, doi:10.1016/j.ultrasmedbio.2006.02.1416.
27. Afadzi, M.; Strand, S.P.; Nilssen, E.A.; Masoy, S.-E.; Johansen, T.F.; Hansen, R.; Angelsen, B.A.; de L Davies, C. Mechanisms of the Ultrasound-Mediated Intracellular Delivery of Liposomes and Dextrans. *IEEE Trans. Ultrason. Ferroelectr. Freq. Control* 2013, 60, doi:10.1109/TUFFC.2013.2534.
28. Paula, D.M.B.; Valero-Lapchik, V.B.; Paredes-Gamero, E.J.; Han, S.W. Therapeutic Ultrasound Promotes Plasmid DNA Uptake by Clathrin-Mediated Endocytosis: Plasmid DNA Endocytosis Induced by Ultrasound. *J. Gene Med.* 2011, 13, 392–401, doi:10.1002/jgm.1586.
29. Wischhusen, J.; Padilla, F. Ultrasound-Targeted Microbubble Destruction (UTMD) for Localized Drug Delivery into Tumor Tissue. *IRBM* 2019, 40, 10–15, doi:10.1016/j.irbm.2018.11.005.

30. Endo-Takahashi, Y.; Negishi, Y. Microbubbles and Nanobubbles with Ultrasound for Systemic Gene Delivery. *Pharmaceutics* 2020, 12, 964, doi:10.3390/pharmaceutics12100964.
31. Deprez, J.; Lajoinie, G.; Engelen, Y.; De Smedt, S.C.; Lentacker, I. Opening Doors with Ultrasound and Microbubbles: Beating Biological Barriers to Promote Drug Delivery. *Adv. Drug Deliv. Rev.* 2021, 172, 9–36, doi:10.1016/j.addr.2021.02.015.
32. Chowdhury, S.M.; Abou-Elkacem, L.; Lee, T.; Dahl, J.; Lutz, A.M. Ultrasound and Microbubble Mediated Therapeutic Delivery: Underlying Mechanisms and Future Outlook. *J. Controlled Release* 2020, 326, 75–90, doi:10.1016/j.jconrel.2020.06.008.
33. Lentacker, I.; De Cock, I.; Deckers, R.; De Smedt, S.C.; Moonen, C.T.W. Understanding Ultrasound Induced Sonoporation: Definitions and Underlying Mechanisms. *Adv. Drug Deliv. Rev.* 2014, 72, 49–64, doi:10.1016/j.addr.2013.11.008.
34. Yang, Y.; Li, Q.; Guo, X.; Tu, J.; Zhang, D. Mechanisms Underlying Sonoporation: Interaction between Microbubbles and Cells. *Ultrason. Sonochem.* 2020, 67, 105096, doi:10.1016/j.ultrasonch.2020.105096.
35. Sheikov, N.; McDannold, N.; Sharma, S.; Hynynen, K. Effect of Focused Ultrasound Applied With an Ultrasound Contrast Agent on the Tight Junctional Integrity of the Brain Microvascular Endothelium. *Ultrasound Med. Biol.* 2008, 34, 1093–1104, doi:10.1016/j.ultrasmedbio.2007.12.015.
36. McMahan, D.; O'Reilly, M.A.; Hynynen, K. Therapeutic Agent Delivery Across the Blood–Brain Barrier Using Focused Ultrasound. *Annu. Rev. Biomed. Eng.* 2021, 23, 89–113, doi:10.1146/annurev-bioeng-062117-121238.
37. Chen, K.-T.; Wei, K.-C.; Liu, H.-L. Focused Ultrasound Combined with Microbubbles in Central Nervous System Applications. *Pharmaceutics* 2021, 13, 1084, doi:10.3390/pharmaceutics13071084.
38. Park, J.; Zhang, Y.; Vykhodtseva, N.; Jolesz, F.A.; McDannold, N.J. The Kinetics of Blood Brain Barrier Permeability and Targeted Doxorubicin Delivery into Brain Induced by Focused Ultrasound. *J. Controlled Release* 2012, 162, 134–142, doi:10.1016/j.jconrel.2012.06.012.
39. Todd, N.; Angolano, C.; Ferran, C.; Devor, A.; Borsook, D.; McDannold, N. Secondary Effects on Brain Physiology Caused by Focused Ultrasound-Mediated Disruption of the Blood–brain Barrier. *J. Controlled Release* 2020, 324, 450–459, doi:10.1016/j.jconrel.2020.05.040.
40. Hynynen, K.; McDannold, N.; Sheikov, N.A.; Jolesz, F.A.; Vykhodtseva, N. Local and Reversible Blood–brain Barrier Disruption by Noninvasive Focused Ultrasound at Frequencies Suitable for Trans-Skull Sonications. *NeuroImage* 2005, 24, 12–20, doi:10.1016/j.neuroimage.2004.06.046.
41. McDannold, N.; Vykhodtseva, N.; Hynynen, K. Effects of Acoustic Parameters and Ultrasound Contrast Agent Dose on Focused-Ultrasound Induced Blood-Brain Barrier Disruption. *Ultrasound Med. Biol.* 2008, 34, 930–937, doi:10.1016/j.ultrasmedbio.2007.11.009.
42. Chen, H.; Konofagou, E.E. The Size of Blood–Brain Barrier Opening Induced by Focused Ultrasound Is Dictated by the Acoustic Pressure. *J. Cereb. Blood Flow Metab.* 2014, 34, 1197–1204, doi:10.1038/jcbfm.2014.71.
43. McDannold, N.; Vykhodtseva, N.; Hynynen, K. Targeted Disruption of the Blood–brain Barrier with Focused Ultrasound: Association with Cavitation Activity. *Phys. Med. Biol.* 2006, 51, 793–807, doi:10.1088/0031-9155/51/4/003.

44. Chen, H.; Brayman, A.A.; Matula, T.J. Microbubble Dynamics in Microvessels: Observations of Microvessel Dilation, Invagination and Rupture.; IEEE, November 2008; pp. 1163–1166.
45. Hwang, J.H.; Tu, J.; Brayman, A.A.; Matula, T.J.; Crum, L.A. Correlation between Inertial Cavitation Dose and Endothelial Cell Damage in Vivo. *Ultrasound Med. Biol.* 2006, 32, 1611–1619, doi:10.1016/j.ultrasmedbio.2006.07.016.
46. Keravnou, C.P.; De Cock, I.; Lentacker, I.; Izamis, M.-L.; Averkiou, M.A. Microvascular Injury and Perfusion Changes Induced by Ultrasound and Microbubbles in a Machine-Perfused Pig Liver. *Ultrasound Med. Biol.* 2016, 42, 2676–2686, doi:10.1016/j.ultrasmedbio.2016.06.025.
47. Keller, S.B.; Suo, D.; Wang, Y.-N.; Kenerson, H.; Yeung, R.S.; Averkiou, M.A. Image-Guided Treatment of Primary Liver Cancer in Mice Leads to Vascular Disruption and Increased Drug Penetration. *Front. Pharmacol.* 2020, 11, doi:10.3389/fphar.2020.584344.
48. Goertz, D.E.; Todorova, M.; Mortazavi, O.; Agache, V.; Chen, B.; Karshafian, R.; Hynynen, K. Antitumor Effects of Combining Docetaxel (Taxotere) with the Antivascular Action of Ultrasound Stimulated Microbubbles. *PLoS ONE* 2012, 7, e52307, doi:10.1371/journal.pone.0052307.
49. Wood, A.K.W.; Ansaloni, S.; Ziemer, L.S.; Lee, W.M.-F.; Feldman, M.D.; Sehgal, C.M. The Antivascular Action of Physiotherapy Ultrasound on Murine Tumors. *Ultrasound Med. Biol.* 2005, 31, 1403–1410, doi:10.1016/j.ultrasmedbio.2005.06.008.
50. D’Souza, J.C.; Sultan, L.R.; Hunt, S.J.; Gade, T.P.; Karmacharya, M.B.; Schultz, S.M.; Brice, A.K.; Wood, A.K.W.; Sehgal, C.M. Microbubble Enhanced Ultrasound for the Antivascular Treatment and Monitoring of Hepatocellular Carcinoma. *Nanotheranostics* 2019, 3, 331–341, doi:10.7150/ntno.39514.
51. He, Y.; Yu, M.; Wang, J.; Xi, F.; Zhong, J.; Yang, Y.; Jin, H.; Liu, J. Improving the Therapeutic Effect of Ultrasound Combined With Microbubbles on Muscular Tumor Xenografts With Appropriate Acoustic Pressure. *Front. Pharmacol.* 2020, 11, doi:10.3389/fphar.2020.01057.
52. Bertuglia, S. Increase in Capillary Perfusion Following Low-Intensity Ultrasound and Microbubbles during Posts ischemic Reperfusion: *Crit. Care Med.* 2005, 33, 2061–2067, doi:10.1097/01.CCM.0000178356.90173.73.
53. Belcik, J.T.; Mott, B.H.; Xie, A.; Zhao, Y.; Kim, S.; Lindner, N.J.; Ammi, A.; Linden, J.M.; Lindner, J.R. Augmentation of Limb Perfusion and Reversal of Tissue Ischemia Produced by Ultrasound-Mediated Microbubble Cavitation. *Circ. Cardiovasc. Imaging* 2015, 8, doi:10.1161/CIRCIMAGING.114.002979.
54. Remington, L.A. *Clinical Anatomy and Physiology of the Visual System*; 3rd ed.; Elsevier/ Butterworth Heinemann: St. Louis, Mo, 2012; ISBN 9781437719260.
55. Ansari, M.W. *Atlas of Ocular Anatomy*; 1st ed. 2016.; Springer International Publishing : Imprint: Springer: Cham, 2016; ISBN 9783319427812.
56. Booi, J.C.; Baas, D.C.; Beisekeeva, J.; Gorgels, T.G.M.F.; Bergen, A.A.B. The Dynamic Nature of Bruch’s Membrane. *Prog. Retin. Eye Res.* 2010, 29, 1–18, doi:10.1016/j.preteyeres.2009.08.003.
57. Maurice, D.M.; Mishima, S. Ocular Pharmacokinetics. In *Pharmacology of the Eye*; Sears, M.L., Ed.; Springer Berlin Heidelberg: Berlin, Heidelberg, 1984; Vol. 69, pp. 19–116 ISBN 978-3-642-69224-6, 978-3-642-69222-2.
58. Del Amo, E.M.; Rimpelä, A.-K.; Heikkinen, E.; Kari, O.K.; Ramsay, E.; Lajunen, T.; Schmitt, M.; Pelkonen, L.; Bhattacharya, M.; Richardson, D.; et al. Pharmacokinetic Aspects of Retinal Drug Delivery. *Prog. Retin. Eye Res.* 2017, 57, 134–185, doi:10.1016/j.preteyeres.2016.12.001.

59. Kidron, H.; del Amo, E.M.; Vellonen, K.-S.; Urtti, A. Prediction of the Vitreal Half-Life of Small Molecular Drug-Like Compounds. *Pharm. Res.* 2012, 29, 3302–3311, doi:10.1007/s11095-012-0822-5.
60. Del Amo, E.M.; Vellonen, K.-S.; Kidron, H.; Urtti, A. Intravitreal Clearance and Volume of Distribution of Compounds in Rabbits: In Silico Prediction and Pharmacokinetic Simulations for Drug Development. *Eur. J. Pharm. Biopharm.* 2015, 95, 215–226, doi:10.1016/j.ejpb.2015.01.003.
61. Kim, H.; Robinson, M.R.; Lizak, M.J.; Tansey, G.; Lutz, R.J.; Yuan, P.; Wang, N.S.; Csaky, K.G. Controlled Drug Release from an Ocular Implant: An Evaluation Using Dynamic Three-Dimensional Magnetic Resonance Imaging. *Investig. Ophthalmology Vis. Sci.* 2004, 45, 2722, doi:10.1167/iovs.04-0091.
62. Jenkins, R.T.; Bell, R.A. Molecular Radii of Probes Used in Studies of Intestinal Permeability. *Gut* 1987, 28, 110–111, doi:10.1136/gut.28.1.110.
63. Ambati, J.; Canakis, C.S.; Miller, J.W.; Gragoudas, E.S.; Edwards, A.; Weissgold, D.J.; Kim, I.; Delori, F.C.; Adamis, A.P. Diffusion of High Molecular Weight Compounds through Sclera. *Invest. Ophthalmol. Vis. Sci.* 2000, 41, 1181–1185.
64. Pitkänen, L.; Ranta, V.-P.; Moilanen, H.; Urtti, A. Permeability of Retinal Pigment Epithelium: Effects of Permeant Molecular Weight and Lipophilicity. *Investig. Ophthalmology Vis. Sci.* 2005, 46, 641, doi:10.1167/iovs.04-1051.
65. Smith, S.J.; Smith, B.D.; Mohney, B.G. Ocular Side Effects Following Intravitreal Injection Therapy for Retinoblastoma: A Systematic Review. *Br. J. Ophthalmol.* 2014, 98, 292–297, doi:10.1136/bjophthalmol-2013-303885.
66. Vo Kim, S.; Fajnkuchen, F.; Sarda, V.; Qu-Knafo, L.; Bodaghi, B.; Giocanti-Aurégan, A. Sustained Intraocular Pressure Elevation in Eyes Treated with Intravitreal Injections of Anti-Vascular Endothelial Growth Factor for Diabetic Macular Edema in a Real-Life Setting. *Graefes Arch. Clin. Exp. Ophthalmol.* 2017, 255, 2165–2171, doi:10.1007/s00417-017-3782-y.
67. Sampat, K.M.; Garg, S.J. Complications of Intravitreal Injections. *Curr. Opin. Ophthalmol.* 2010, 21, 178–183, doi:10.1097/ICU.0b013e328338679a.
68. Urs, R.; Ketterling, J.A.; Yu, A.C.H.; Lloyd, H.O.; Yiu, B.Y.S.; Silverman, R.H. Ultrasound Imaging and Measurement of Choroidal Blood Flow. *Transl. Vis. Sci. Technol.* 2018, 7, 5, doi:10.1167/tvst.7.5.5.
69. Gordiyenko, N.; Campos, M.; Lee, J.W.; Fariss, R.N.; Sztain, J.; Rodriguez, I.R. RPE Cells Internalize Low-Density Lipoprotein (LDL) and Oxidized LDL (oxLDL) in Large Quantities In Vitro and In Vivo. *Investig. Ophthalmology Vis. Sci.* 2004, 45, 2822, doi:10.1167/iovs.04-0074.
70. Farkas, T.G.; Sylvester, V.; Archer, D.; Altona, M. The Histochemistry of Drusen. *Am. J. Ophthalmol.* 1971, 71, 1206–1215, doi:10.1016/0002-9394(71)90964-0.
71. Crabb, J.W.; Miyagi, M.; Gu, X.; Shadrach, K.; West, K.A.; Sakaguchi, H.; Kamei, M.; Hasan, A.; Yan, L.; Rayborn, M.E.; et al. Drusen Proteome Analysis: An Approach to the Etiology of Age-Related Macular Degeneration. *Proc. Natl. Acad. Sci.* 2002, 99, 14682–14687, doi:10.1073/pnas.222551899.
72. Jager, R.D.; Mieler, W.F.; Miller, J.W. Age-Related Macular Degeneration. *N. Engl. J. Med.* 2008, 358, 2606–2617, doi:10.1056/NEJMra0801537.
73. Lim, L.S.; Mitchell, P.; Seddon, J.M.; Holz, F.G.; Wong, T.Y. Age-Related Macular Degeneration. *The Lancet* 2012, 379, 1728–1738, doi:10.1016/S0140-6736(12)60282-7.

74. Dugel, P.U.; Jaffe, G.J.; Sallstig, P.; Warburton, J.; Weichselberger, A.; Wieland, M.; Singerman, L. Brolicizumab Versus Aflibercept in Participants with Neovascular Age-Related Macular Degeneration: A Randomized Trial. *Ophthalmology* 2017, 124, 1296–1304, doi:10.1016/j.ophtha.2017.03.057.
75. Xu, L.; Lu, T.; Tuomi, L.; Jumbe, N.; Lu, J.; Eppler, S.; Kuebler, P.; Damico-Beyer, L.A.; Joshi, A. Pharmacokinetics of Ranibizumab in Patients with Neovascular Age-Related Macular Degeneration: A Population Approach. *Investig. Ophthalmology Vis. Sci.* 2013, 54, 1616, doi:10.1167/iovs.12-10260.
76. Moisseiev, E.; Waisbourd, M.; Ben-Artzi, E.; Levinger, E.; Barak, A.; Daniels, T.; Csaky, K.; Loewenstein, A.; Barequet, I.S. Pharmacokinetics of Bevacizumab after Topical and Intravitreal Administration in Human Eyes. *Graefes Arch. Clin. Exp. Ophthalmol.* 2014, 252, 331–337, doi:10.1007/s00417-013-2495-0.
77. Semeraro, F.; Morescalchi, Duse, S.; Parmeggiani, F.; Gambicorti, Costagliola, C. Aflibercept in Wet AMD: Specific Role and Optimal Use. *Drug Des. Devel. Ther.* 2013, 711, doi:10.2147/DDDT.S40215.
78. Nguyen, Q.D.; Das, A.; Do, D.V.; Dugel, P.U.; Gomes, A.; Holz, F.G.; Koh, A.; Pan, C.K.; Sepah, Y.J.; Patel, N.; et al. Brolicizumab: Evolution through Preclinical and Clinical Studies and the Implications for the Management of Neovascular Age-Related Macular Degeneration. *Ophthalmology* 2020, 127, 963–976, doi:10.1016/j.ophtha.2019.12.031.
79. Hirokawa, T.; Karshafian, R.; Pavlin, C.J.; Burns, P.N. Insonation of the Eye in the Presence of Microbubbles: Preliminary Study of the Duration and Degree of Vascular Bioeffects-Work in Progress. *J. Ultrasound Med.* 2007, 26, 731–738, doi:10.7863/jum.2007.26.6.731.
80. Park, J.; Zhang, Y.; Vykhodtseva, N.; Akula, J.D.; McDannold, N.J. Targeted and Reversible Blood-Retinal Barrier Disruption via Focused Ultrasound and Microbubbles. *PLoS ONE* 2012, 7, e42754, doi:10.1371/journal.pone.0042754.
81. Touahri, Y.; Dixit, R.; Kofoed, R.H.; Miloska, K.; Park, E.; Raeisossadati, R.; Markham-Coultes, K.; David, L.A.; Rijal, H.; Zhao, J.; et al. Focused Ultrasound as a Novel Strategy for Noninvasive Gene Delivery to Retinal Müller Glia. *Theranostics* 2020, 10, 2982–2999, doi:10.7150/thno.42611.
82. Thakur, S.S.; Ward, M.S.; Popat, A.; Flemming, N.B.; Parat, M.-O.; Barnett, N.L.; Parekh, H.S. Stably Engineered Nanobubbles and Ultrasound - An Effective Platform for Enhanced Macromolecular Delivery to Representative Cells of the Retina. *PLOS ONE* 2017, 12, e0178305, doi:10.1371/journal.pone.0178305.
83. Wan, C.; Qian, J.; Li, F.; Li, H. Ultrasound-Targeted Microbubble Destruction Enhances Polyethylenimine-Mediated Gene Transfection in Vitro in Human Retinal Pigment Epithelial Cells and in Vivo in Rat Retina. *Mol. Med. Rep.* 2015, 12, 2835–2841, doi:10.3892/mmr.2015.3703.
84. Li, H.; Qian, J.; Yao, C.; Wan, C.; Li, F. Combined Ultrasound-Targeted Microbubble Destruction and Polyethylenimine-Mediated Plasmid DNA Delivery to the Rat Retina: Enhanced Efficiency and Accelerated Expression: US Assisted PEI/pDNA Delivery in Retina. *J. Gene Med.* 2016, 18, 47–56, doi:10.1002/jgm.2875.
85. Sonoda, S.; Tachibana, K.; Yamashita, T.; Shirasawa, M.; Terasaki, H.; Uchino, E.; Suzuki, R.; Maruyama, K.; Sakamoto, T. Selective Gene Transfer to the Retina Using Intravitreal Ultrasound Irradiation. *J. Ophthalmol.* 2012, 2012, 1–5, doi:10.1155/2012/412752.

86. Li, H.L.; Zheng, X.Z.; Wang, H.P.; Li, F.; Wu, Y.; Du, L.F. Ultrasound-Targeted Microbubble Destruction Enhances AAV-Mediated Gene Transfection in Human RPE Cells in Vitro and Rat Retina in Vivo. *Gene Ther.* 2009, 16, 1146–1153, doi:10.1038/gt.2009.84.
87. Zheng, X.; Li, H.; Du, L.; Wang, H.; Gu, Q. In Vivo and in Vitro Effects of Ultrasound Or/and Microbubbles on Recombinant Adeno-Associated Virus-Mediated Transgene Expression in the Retina. *Asian Biomed.* 2009, 3, 497–506.
88. Zheng, X.; Ji, P.; Hu, J. Sonoporation Using Microbubbles Promotes Lipofectamine -Mediated siRNA Transduction to Rat Retina. *Bosn. J. Basic Med. Sci.* 2011, 11, 147, doi:10.17305/bjbm.2011.2565.
89. Li, H.; Wan, C.; Li, F. Recombinant Adeno-Associated Virus-, Polyethylenimine/plasmid- and Lipofectamine/carboxyfluorescein-Labeled Small Interfering RNA-Based Transfection in Retinal Pigment Epithelial Cells with Ultrasound And/or SonoVue. *Mol. Med. Rep.* 2015, 11, 3609–3614, doi:10.3892/mmr.2015.3219.
90. Du, J.; Shi, Q.S.; Sun, Y.; Liu, P.F.; Zhu, M.J.; Du, L.F.; Duan, Y.R. Enhanced Delivery of Monomethoxypoly(ethylene Glycol)-Poly(lactic-Co-Glycolic Acid)-Poly L-Lysine Nanoparticles Loading Platelet-Derived Growth Factor BB Small Interfering RNA by Ultrasound And/or Microbubbles to Rat Retinal Pigment Epithelium Cells: Enhanced Delivery of NPs Loading siRNA by US And/or MBs. *J. Gene Med.* 2011, 13, 312–323, doi:10.1002/jgm.1574.
91. Du, J.; Sun, Y.; Li, F.-H.; Du, L.-F.; Duan, Y.-R. Enhanced Delivery of Biodegradable mPEG-PLGA-PLL Nanoparticles Loading Cy3-Labelled PDGF-BB siRNA by UTMD to Rat Retina. *J. Biosci.* 2017, 42, 299–309, doi:10.1007/s12038-017-9677-6.
92. Harasymowycz, P.; Birt, C.; Gooi, P.; Heckler, L.; Hutnik, C.; Jinapriya, D.; Shuba, L.; Yan, D.; Day, R. Medical Management of Glaucoma in the 21st Century from a Canadian Perspective. *J. Ophthalmol.* 2016, 2016, 1–22, doi:10.1155/2016/6509809.
93. Allison, K.; Patel, D.; Alabi, O. Epidemiology of Glaucoma: The Past, Present, and Predictions for the Future. *Cureus* 2020, doi:10.7759/cureus.11686.
94. Brooks, A.M.V.; Gillies, W.E. Ocular Beta-Blockers in Glaucoma Management: Clinical Pharmacological Aspects. *Drugs Aging* 1992, 2, 208–221, doi:10.2165/00002512-199202030-00005.
95. Schwartz, K.; Budenz, D. Current Management of Glaucoma. *Curr. Opin. Ophthalmol.* 2004, 15, 119–126, doi:10.1097/00055735-200404000-00011.
96. Apătăchioae, I.; Chiseliță, D. Alpha-2 adrenergic agonists in the treatment of glaucoma. *Oftalmol. Buchar. Rom.* 1990 1999, 47, 35–40.
97. Tang, W.; Zhang, F.; Liu, K.; Duan, X. Efficacy and Safety of Prostaglandin Analogues in Primary Open-Angle Glaucoma or Ocular Hypertension Patients: A Meta-Analysis. *Medicine (Baltimore)* 2019, 98, e16597, doi:10.1097/MD.0000000000016597.
98. Reardon, G.; Kotak; Schwartz, G. Objective Assessment of Compliance and Persistence among Patients Treated for Glaucoma and Ocular Hypertension: A Systematic Review. *Patient Prefer. Adherence* 2011, 441, doi:10.2147/PPA.S23780.
99. Schuster, A.K.; Erb, C.; Hoffmann, E.M.; Dietlein, T.; Pfeiffer, N. The Diagnosis and Treatment of Glaucoma. *Dtsch. Aerzteblatt Online* 2020, doi:10.3238/arztebl.2020.0225.

100. Shen, X.; Huang, L.; Ma, D.; Zhao, J.; Xie, Y.; Li, Q.; Zeng, A.; Zeng, K.; Tian, R.; Wang, T.; et al. Ultrasound Microbubbles Enhance the Neuroprotective Effect of Mouse Nerve Growth Factor on Intraocular Hypertension-Induced Neuroretina Damage in Rabbits. *J. Ophthalmol.* 2016, 2016, 1–9, doi:10.1155/2016/4235923.
101. Li, W.; Liu, S.; Ren, J.; Xiong, H.; Yan, X.; Wang, Z. Gene Transfection to Retinal Ganglion Cells Mediated by Ultrasound Microbubbles in Vitro. *Acad. Radiol.* 2009, 16, 1086–1094, doi:10.1016/j.acra.2009.03.019.
102. Xie, W.; Liu, S.; Su, H.; Wang, Z.; Zheng, Y.; Fu, Y. Ultrasound Microbubbles Enhance Recombinant Adeno-Associated Virus Vector Delivery to Retinal Ganglion Cells In Vivo. *Acad. Radiol.* 2010, 17, 1242–1248, doi:10.1016/j.acra.2010.05.008.
103. Yamashita, T.; Sonoda, S.; Suzuki, R.; Arimura, N.; Tachibana, K.; Maruyama, K.; Sakamoto, T. A Novel Bubble Liposome and Ultrasound-Mediated Gene Transfer to Ocular Surface: RC-1 Cells in Vitro and Conjunctiva in Vivo. *Exp. Eye Res.* 2007, 85, 741–748, doi:10.1016/j.exer.2007.08.006.
104. Fong, D.S.; Aiello, L.; Gardner, T.W.; King, G.L.; Blankenship, G.; Cavallerano, J.D.; Ferris, F.L.; Klein, R. Retinopathy in Diabetes. *Diabetes Care* 2004, 27, S84–S87, doi:10.2337/diacare.27.2007.S84.
105. Mohamed, Q.; Gillies, M.C.; Wong, T.Y. Management of Diabetic Retinopathy: A Systematic Review. *JAMA* 2007, 298, 902, doi:10.1001/jama.298.8.902.
106. Engerman, R.L. Pathogenesis of Diabetic Retinopathy. *Diabetes* 1989, 38, 1203–1206, doi:10.2337/diab.38.10.1203.
107. Chawan-Saad, J.; Wu, M.; Wu, A.; Wu, L. Corticosteroids for Diabetic Macular Edema. *Taiwan J. Ophthalmol.* 2019, 9, 233, doi:10.4103/tjo.tjo_68_19.
108. Stitt, A.W.; Curtis, T.M.; Chen, M.; Medina, R.J.; McKay, G.J.; Jenkins, A.; Gardiner, T.A.; Lyons, T.J.; Hammes, H.-P.; Simó, R.; et al. The Progress in Understanding and Treatment of Diabetic Retinopathy. *Prog. Retin. Eye Res.* 2016, 51, 156–186, doi:10.1016/j.preteyeres.2015.08.001.
109. Mansour, S.E.; Browning, D.J.; Wong, K.; Flynn Jr, H.W.; Bhavsar, A.R. The Evolving Treatment of Diabetic Retinopathy. *Clin. Ophthalmol.* 2020, Volume 14, 653–678, doi:10.2147/OPHT.S236637.
110. Walia, A.; Yang, J.F.; Huang, Y.; Rosenblatt, M.I.; Chang, J.-H.; Azar, D.T. Endostatin's Emerging Roles in Angiogenesis, Lymphangiogenesis, Disease, and Clinical Applications. *Biochim. Biophys. Acta BBA - Gen. Subj.* 2015, 1850, 2422–2438, doi:10.1016/j.bbagen.2015.09.007.
111. Xu, Y.; Xie, Z.; Zhou, Y.; Zhou, X.; Li, P.; Wang, Z.; Zhang, Q. Experimental Endostatin-GFP Gene Transfection into Human Retinal Vascular Endothelial Cells Using Ultrasound-Targeted Cationic Microbubble Destruction. *Mol. Vis.* 2015, 21, 930–938.
112. Kowalczyk, L.; Boudinet, M.; El Sanharawi, M.; Touchard, E.; Naud, M.-C.; Saïed, A.; Jeanny, J.-C.; Behar-Cohen, F.; Laugier, P. In Vivo Gene Transfer into the Ocular Ciliary Muscle Mediated by Ultrasound and Microbubbles. *Ultrasound Med. Biol.* 2011, 37, 1814–1827, doi:10.1016/j.ultrasmedbio.2011.07.010.
113. Campochiaro, P.A. Pathogenic Mechanisms in Proliferative Vitreoretinopathy. *Arch. Ophthalmol.* 1997, 115, 237, doi:10.1001/archophth.1997.01100150239014.
114. Pastor, J.C.; de la Rúa, E.R.; Martín, F. Proliferative Vitreoretinopathy: Risk Factors and Pathobiology. *Prog. Retin. Eye Res.* 2002, 21, 127–144, doi:10.1016/S1350-9462(01)00023-4.

115. Ikuno, Y.; Leong, F.L.; Kazlauskas, A. Attenuation of Experimental Proliferative Vitreoretinopathy by Inhibiting the Platelet-Derived Growth Factor Receptor. *Invest. Ophthalmol. Vis. Sci.* 2000, 41, 3107–3116.
116. Zheng, X.-Z.; Du, L.-F.; Wang, H.-P. A Immunohistochemical Analysis of a Rat Model of Proliferative Vitreoretinopathy and a Comparison of the Expression of Tgf-B and PDGF Among the Induction Methods. *Bosn. J. Basic Med. Sci.* 2010, 10, 204–209, doi:10.17305/bjbm.2010.2686.
117. Nagineni, C.N.; Kutty, V.; Detrick, B.; Hooks, J.J. Expression of PDGF and Their Receptors in Human Retinal Pigment Epithelial Cells and Fibroblasts: Regulation by TGF- β . *J. Cell. Physiol.* 2005, 203, 35–43, doi:10.1002/jcp.20213.
118. Pastor, J.C. Proliferative Vitreoretinopathy. *Surv. Ophthalmol.* 1998, 43, 3–18, doi:10.1016/S0039-6257(98)00023-X.
119. Zheng, X.; Du, L.; Wang, H.; Gu, Q. A Novel Approach to Attenuate Proliferative Vitreoretinopathy Using Ultrasound-Targeted Microbubble Destruction and Recombinant Adeno-Associated Virus-Mediated RNA Interference Targeting Transforming Growth Factor- β 2 and Platelet-Derived Growth Factor-B: Attenuate PVR Using UTMD and RNAi Targeting TGF- β 2 and PDGF-B. *J. Gene Med.* 2012, 14, 339–347, doi:10.1002/jgm.2629.
120. Hartong, D.T.; Berson, E.L.; Dryja, T.P. Retinitis Pigmentosa. *The Lancet* 2006, 368, 1795–1809, doi:10.1016/S0140-6736(06)69740-7.
121. Berson, E.L. Retinitis Pigmentosa. The Friedenwald Lecture. *Invest. Ophthalmol. Vis. Sci.* 1993, 34, 1659–1676.
122. Berson, E.L. A Randomized Trial of Vitamin A and Vitamin E Supplementation for Retinitis Pigmentosa. *Arch. Ophthalmol.* 1993, 111, 761, doi:10.1001/archoph.1993.01090060049022.
123. Sibulesky, L.; Hayes, K.; Pronczuk, A.; Weigel-DiFranco, C.; Rosner, B.; Berson, E.L. Safety of <7500 RE (<25000 IU) Vitamin A Daily in Adults with Retinitis Pigmentosa. *Am. J. Clin. Nutr.* 1999, 69, 656–663, doi:10.1093/ajcn/69.4.656.
124. Knudson, A.G. Mutation and Cancer: Statistical Study of Retinoblastoma. *Proc. Natl. Acad. Sci.* 1971, 68, 820–823, doi:10.1073/pnas.68.4.820.
125. Friend, S.H.; Bernards, R.; Rogelj, S.; Weinberg, R.A.; Rapaport, J.M.; Albert, D.M.; Dryja, T.P. A Human DNA Segment with Properties of the Gene That Predisposes to Retinoblastoma and Osteosarcoma. *Nature* 1986, 323, 643–646, doi:10.1038/323643a0.
126. Global Retinoblastoma Study Group; Fabian, I.D.; Abdallah, E.; Abdullahi, S.U.; Abdulqader, R.A.; Adamou Boubacar, S.; Ademola-Popoola, D.S.; Adio, A.; Afshar, A.R.; Aggarwal, P.; et al. Global Retinoblastoma Presentation and Analysis by National Income Level. *JAMA Oncol.* 2020, 6, 685, doi:10.1001/jamaoncol.2019.6716.
127. MacCarthy, A.; Birch, J.M.; Draper, G.J.; Hungerford, J.L.; Kingston, J.E.; Kroll, M.E.; Stiller, C.A.; Vincent, T.J.; Murphy, M.F.G. Retinoblastoma: Treatment and Survival in Great Britain 1963 to 2002. *Br. J. Ophthalmol.* 2009, 93, 38–39, doi:10.1136/bjo.2008.139626.
128. Munier, F.L.; Mosimann, P.; Puccinelli, F.; Gaillard, M.-C.; Stathopoulos, C.; Houghton, S.; Bergin, C.; Beck-Popovic, M. First-Line Intra-Arterial versus Intravenous Chemotherapy in Unilateral Sporadic Group D Retinoblastoma: Evidence of Better Visual Outcomes, Ocular Survival and Shorter Time to Success with Intra-Arterial Delivery from Retrospective Review of 20 Years of Treatment. *Br. J. Ophthalmol.* 2017, 101, 1086–1093, doi:10.1136/bjophthalmol-2016-309298.

129. Fernandes, A.G.; Pollock, B.D.; Rabito, F.A. Retinoblastoma in the United States: A 40-Year Incidence and Survival Analysis. *J. Pediatr. Ophthalmol. Strabismus* 2018, 55, 182–188, doi:10.3928/01913913-20171116-03.
130. Ancona-Lezama, D.; Dalvin, L.; Shields, C. Modern Treatment of Retinoblastoma: A 2020 Review. *Indian J. Ophthalmol.* 2020, 68, 2356, doi:10.4103/ijo.IJO_721_20.
131. Manjandavida, F.; Stathopoulos, C.; Zhang, J.; Honavar, S.; Shields, C. Intra-Arterial Chemotherapy in Retinoblastoma – A Paradigm Change. *Indian J. Ophthalmol.* 2019, 67, 740, doi:10.4103/ijo.IJO_866_19.
132. Shields, C.L.; Lally, S.E.; Leahey, A.M.; Jabbour, P.M.; Caywood, E.H.; Schwendeman, R.; Shields, J.A. Targeted Retinoblastoma Management: When to Use Intravenous, Intra-Arterial, Periocular, and Intravitreal Chemotherapy. *Curr. Opin. Ophthalmol.* 2014, 25, 374–385, doi:10.1097/ICU.0000000000000091.
133. Lee, N.G.; Berry, J.L.; Lee, T.C.; Wang, A.T.; Honowitz, S.; Murphree, A.L.; Varshney, N.; Hinton, D.R.; Fawzi, A.A. Sonoporation Enhances Chemotherapeutic Efficacy in Retinoblastoma Cells In Vitro. *Investig. Ophthalmology Vis. Sci.* 2011, 52, 3868, doi:10.1167/iovs.10-6501.
134. Giblin, M.E.; Shields, C.L.; Shields, J.A.; Eagle, R.C. Primary Eyelid Malignant Melanoma Associated With Primary Conjunctival Malignant Melanoma. *Aust. N. Z. J. Ophthalmol.* 1988, 16, 127–131, doi:10.1111/j.1442-9071.1988.tb01261.x.
135. Rodriguez-Sains, R.S. Ocular Melanomas. *Dermatol. Clin.* 1985, 3, 297–307, doi:10.1016/S0733-8635(18)30904-5.
136. Bitá Esmaeli Sentinel Lymph Node Mapping for Patients With Cutaneous and Conjunctival Malignant Melanoma: *Ophthalm. Plast. Reconstr. Surg.* 2000, 16, 170–172, doi:10.1097/00002341-200005000-00002.
137. Sonoda, S.; Tachibana, K.; Uchino, E.; Yamashita, T.; Sakoda, K.; Sonoda, K.-H.; Hisatomi, T.; Izumi, Y.; Sakamoto, T. Inhibition of Melanoma by Ultrasound-Microbubble-Aided Drug Delivery Suggests Membrane Permeabilization. *Cancer Biol. Ther.* 2007, 6, 1282–1289, doi:10.4161/cbt.6.8.4485.
138. Dohlman, T.H.; Yin, J.; Dana, R. Methods for Assessing Corneal Opacity. *Semin. Ophthalmol.* 2019, 34, 205–210, doi:10.1080/08820538.2019.1620796.
139. Memarzadeh, F.; Li, Y.; Francis, B.A.; Smith, R.E.; Gutmark, J.; Huang, D. Optical Coherence Tomography of the Anterior Segment in Secondary Glaucoma with Corneal Opacity after Penetrating Keratoplasty. *Br. J. Ophthalmol.* 2007, 91, 189–192, doi:10.1136/bjo.2006.100099.
140. Laibson, P.R. Corneal Infiltrates in Epidemic Keratoconjunctivitis: Response to Double-Blind Corticosteroid Therapy. *Arch. Ophthalmol.* 1970, 84, 36, doi:10.1001/archophth.1970.00990040038010.
141. Macdonald, E.C.A.; Cauchi, P.A.; Azuara-Blanco, A.; Foot, B. Surveillance of Severe Chemical Corneal Injuries in the UK. *Br. J. Ophthalmol.* 2009, 93, 1177–1180, doi:10.1136/bjo.2008.154831.
142. Yamazaki, E.S.; Ferraz, C.A.; Hazarbassanov, R.M.; Allemann, N.; Campos, M. Phototherapeutic Keratectomy for the Treatment of Corneal Opacities After Epidemic Keratoconjunctivitis. *Am. J. Ophthalmol.* 2011, 151, 35–43.e1, doi:10.1016/j.ajo.2010.07.028.
143. Gordon, Y.J. The Evolution of Antiviral Therapy for External Ocular Viral Infections Over Twenty-Five Years: *Cornea* 2000, 19, 673–680, doi:10.1097/00003226-200009000-00012.

144. Tan, D.T.; Dart, J.K.; Holland, E.J.; Kinoshita, S. Corneal Transplantation. *The Lancet* 2012, 379, 1749–1761, doi:10.1016/S0140-6736(12)60437-1.
145. Kupferman, A.; Pratt, M.; Suckewer, K. Topically Applied Steroids in Corneal Disease: III. The Role of Drug Derivative in Stromal Absorption of Dexamethasone. *Arch. Ophthalmol.* 1974, 91, 373, doi:10.1001/archophth.1974.03900060385008.
146. Cox, W.; Allan, K.; Howard, L. Topically Applied Steroids in Corneal Disease: I. The Role of Inflammation in Stromal Absorption of Dexamethasone. *Arch. Ophthalmol.* 1972, 88, 308, doi:10.1001/archophth.1972.01000030310017.
147. Sonoda, S.; Tachibana, K.; Uchino, E.; Okubo, A.; Yamamoto, M.; Sakoda, K.; Hisatomi, T.; Sonoda, K.-H.; Negishi, Y.; Izumi, Y.; et al. Gene Transfer to Corneal Epithelium and Keratocytes Mediated by Ultrasound with Microbubbles. *Investig. Ophthalmology Vis. Sci.* 2006, 47, 558, doi:10.1167/iov.05-0889.
148. Dimaras, H.; Corson, T.W. Retinoblastoma, the Visible CNS Tumor: A Review: DIMARAS and CORSON. *J. Neurosci. Res.* 2019, 97, 29–44, doi:10.1002/jnr.24213.
149. Main, M.L.; Goldman, J.H.; Grayburn, P.A. Thinking Outside the “Box”—The Ultrasound Contrast Controversy. *J. Am. Coll. Cardiol.* 2007, 50, 2434–2437, doi:10.1016/j.jacc.2007.11.006.
150. Fisher, N.G.; Christiansen, J.P.; Klibanov, A.; Taylor, R.P.; Kaul, S.; Lindner, J.R. Influence of Microbubble Surface Charge on Capillary Transit and Myocardial Contrast Enhancement. *J. Am. Coll. Cardiol.* 2002, 40, 811–819, doi:10.1016/S0735-1097(02)02038-7.
151. Oyarzabal, N.A.; Longo Areso, N.; Bernedo Belar, N.; Popolizio, I.G.; Arregui, A.V.; Balza de Vallejo, O.V. Anaphylactic Shock Due to Allergy to Macrogol 4000 Contained in SonoVue<sup>®<sup> Case Rep. *Clin. Med.* 2017, 06, 143–147, doi:10.4236/crcm.2017.66014.
152. Krantz, M.S.; Liu, Y.; Phillips, E.J.; Stone, C.A. Anaphylaxis to PEGylated Liposomal Echocardiogram Contrast in a Patient with IgE-Mediated Macrogol Allergy. *J. Allergy Clin. Immunol. Pract.* 2020, 8, 1416–1419.e3, doi:10.1016/j.jaip.2019.12.041.
153. Lindner, J.R.; Belcik, T.; Main, M.L.; Montanaro, A.; Mulvagh, S.L.; Olson, J.; Olyaei, A.; Porter, T.R.; Senior, R. Expert Consensus Statement from the American Society of Echocardiography on Hypersensitivity Reactions to Ultrasound Enhancing Agents in Patients with Allergy to Polyethylene Glycol. *J. Am. Soc. Echocardiogr.* 2021, 34, 707–708, doi:10.1016/j.echo.2021.05.002.
154. Williams, T.M.; Harvey, R.; Kratzert, W.B.; Fischer, M.A.; Neelankavil, J. Ultrasound-Enhancing Agent Safety: Understanding the New Food and Drug Administration Warning on Polyethylene Glycol. *J. Cardiothorac. Vasc. Anesth.* 2021, doi:10.1053/j.jvca.2021.07.012.
155. Fix, S.M.; Nyankima, A.G.; McSweeney, M.D.; Tsuruta, J.K.; Lai, S.K.; Dayton, P.A. Accelerated Clearance of Ultrasound Contrast Agents Containing Polyethylene Glycol Is Associated with the Generation of Anti-Polyethylene Glycol Antibodies. *Ultrasound Med. Biol.* 2018, 44, 1266–1280, doi:10.1016/j.ultrasmedbio.2018.02.006.
156. Schneider, M.; Arditi, M.; Barrau, M.-B.; Brochot, J.; Broillet, A.; Ventrone, R.; Yan, F. BR1: A New Ultrasonographic Contrast Agent Based on Sulfur Hexafluoride-Filled Microbubbles. *Invest. Radiol.* 1995, 30, 451–457, doi:10.1097/00004424-199508000-00001.
157. Abdelmoneim, S.S.; Mulvagh, S.L. Perflutren Lipid Microsphere Injectable Suspension for Cardiac Ultrasound. *Imaging Med.* 2012, 4, 171–191, doi:10.2217/iim.12.11.

158. Park, J.; Park, D.; Shin, U.; Moon, S.; Kim, C.; Kim, H.; Park, H.; Choi, K.; Jung, B.; Oh, J.; et al. Synthesis of Laboratory Ultrasound Contrast Agents. *Molecules* 2013, 18, 13078–13095, doi:10.3390/molecules181013078.
159. Wilson, S.R.; Burns, P.N. Microbubble-Enhanced US in Body Imaging: What Role? *Radiology* 2010, 257, 24–39, doi:10.1148/radiol.10091210.
160. Sontum, P.C. Physicochemical Characteristics of Sonazoid™, A New Contrast Agent for Ultrasound Imaging. *Ultrasound Med. Biol.* 2008, 34, 824–833, doi:10.1016/j.ultrasmedbio.2007.11.006.
161. Al-Jawadi, S.; Thakur, S.S. Ultrasound-Responsive Lipid Microbubbles for Drug Delivery: A Review of Preparation Techniques to Optimise Formulation Size, Stability and Drug Loading. *Int. J. Pharm.* 2020, 585, 119559, doi:10.1016/j.ijpharm.2020.119559.
162. Van Elburg, B.; Collado-Lara, G.; Bruggert, G.-W.; Segers, T.; Versluis, M.; Lajoinie, G. Feedback-Controlled Microbubble Generator Producing One Million Monodisperse Bubbles per Second. *Rev. Sci. Instrum.* 2021, 92, 035110, doi:10.1063/5.0032140.
163. McMahon, D.; Poon, C.; Hynynen, K. Evaluating the Safety Profile of Focused Ultrasound and Microbubble-Mediated Treatments to Increase Blood-Brain Barrier Permeability. *Expert Opin. Drug Deliv.* 2019, 16, 129–142, doi:10.1080/17425247.2019.1567490.
164. Tung, Y.-S.; Vlachos, F.; Choi, J.J.; Deffieux, T.; Selert, K.; Konofagou, E.E. In Vivo Transcranial Cavitation Threshold Detection during Ultrasound-Induced Blood–brain Barrier Opening in Mice. *Phys. Med. Biol.* 2010, 55, 6141–6155, doi:10.1088/0031-9155/55/20/007.
165. O’Reilly, M.A.; Hynynen, K. Blood-Brain Barrier: Real-Time Feedback-Controlled Focused Ultrasound Disruption by Using an Acoustic Emissions–based Controller. *Radiology* 2012, 263, 96–106, doi:10.1148/radiol.11111417.
166. FDA Guidance for Industry and FDA Staff Information for Manufacturers Seeking Marketing Clearance of Diagnostic Ultrasound Systems and Transducers, June 29, 2019. <https://www.fda.gov/media/71100/download>; 2019;
167. Kopechek, J.A.; Kim, H.; McPherson, D.D.; Holland, C.K. Calibration of the 1-MHz Sonitron Ultrasound System. *Ultrasound Med. Biol.* 2010, 36, 1762–1766, doi:10.1016/j.ultrasmedbio.2010.05.020.
168. Lafond, M.; Aptel, F.; Mestas, J.-L.; Lafon, C. Ultrasound-Mediated Ocular Delivery of Therapeutic Agents: A Review. *Expert Opin. Drug Deliv.* 2017, 14, 539–550, doi:10.1080/17425247.2016.1198766.
169. WFUMB Symposium on Safety and Standardisation in Medical Ultrasound. Issues and Recommendations Regarding Thermal Mechanisms for Biological Effects of Ultrasound. Hornbaek, Denmark, 30 August–1 September 1991. *Ultrasound Med. Biol.* 1992, 18, 731–810.
170. Aptel, F.; Tadjine, M.; Rouland, J.-F. Efficacy and Safety of Repeated Ultrasound Cycloplasty Procedures in Patients With Early or Delayed Failure After a First Procedure: *J. Glaucoma* 2020, 29, 24–30, doi:10.1097/IJG.0000000000001400.
171. Torky, M.A.; Al Zafiri, Y.A.; Hagra, S.M.; Khattab, A.M.; Bassiouny, R.M.; Mokbel, T.H. Safety and Efficacy of Ultrasound Ciliary Plasty as a Primary Intervention in Glaucoma Patients. *Int. J. Ophthalmol.* 2019, 12, 597–602, doi:10.18240/ijo.2019.04.12.
172. Kovacs, Z.I.; Kim, S.; Jikaria, N.; Qureshi, F.; Milo, B.; Lewis, B.K.; Bresler, M.; Burks, S.R.; Frank, J.A. Disrupting the Blood–brain Barrier by Focused Ultrasound Induces Sterile Inflammation. *Proc. Natl. Acad. Sci.* 2017, 114, E75–E84, doi:10.1073/pnas.1614777114.

173. McMahon, D.; Hynynen, K. Acute Inflammatory Response Following Increased Blood-Brain Barrier Permeability Induced by Focused Ultrasound Is Dependent on Microbubble Dose. *Theranostics* 2017, 7, 3989–4000, doi:10.7150/thno.21630.
174. Bringmann, A.; Iandiev, I.; Pannicke, T.; Wurm, A.; Hollborn, M.; Wiedemann, P.; Osborne, N.N.; Reichenbach, A. Cellular Signaling and Factors Involved in Müller Cell Gliosis: Neuroprotective and Detrimental Effects. *Prog. Retin. Eye Res.* 2009, 28, 423–451, doi:10.1016/j.preteyeres.2009.07.001.
175. Carpentier, A. Transient Disruption of the Blood-Retinal Barrier of a Human and Uses Thereof for Treating a Retina Disorder.
176. Nishioka, T.; Luo, H.; Fishbein, M.C.; Cercek, B.; Forrester, J.S.; Kim, C.-J.; Berglund, H.; Siegel, R.J. Dissolution of Thrombotic Arterial Occlusion by High Intensity, Low Frequency Ultrasound and Dodecafluoropentane Emulsion: An In Vitro and In Vivo Study. *J. Am. Coll. Cardiol.* 1997, 30, 561–568, doi:10.1016/S0735-1097(97)00182-4.
177. Mizushige, K.; Kondo, I.; Ohmori, K.; Hirao, K.; Matsuo, H. Enhancement of Ultrasound-Accelerated Thrombolysis by Echo Contrast Agents: Dependence on Microbubble Structure. *Ultrasound Med. Biol.* 1999, 25, 1431–1437, doi:10.1016/S0301-5629(99)00095-2.
178. Culp, W.C.; Porter, T.R.; Xie, F.; Goertzen, T.C.; McCowan, T.C.; Vonk, B.N.; Baxter, B.T. Microbubble Potentiated Ultrasound as a Method of Dec clotting Thrombosed Dialysis Grafts: Experimental Study in Dogs. *Cardiovasc. Intervent. Radiol.* 2001, 24, 407–412, doi:10.1007/s00270-001-0052-4.
179. Janjic, J.; Larsson, M.K.; Bjällmark, A. In-Vitro Sonothrombolysis Using Thick-Shelled Polymer Microbubbles - a Comparison with Thin-Shelled Microbubbles. *Cardiovasc. Ultrasound* 2020, 18, doi:10.1186/s12947-020-00194-2.
180. Fawzi, A.; Ameri, H.; Humayun, M. Ultrasound and Microbubbles in Ocular Diagnostic and Therapies. U.S. Patent 8,764,658, 1 July 2014.
181. Grubbs, R.; Stoller, M.; Han, Y.; Brodie, F. Method for Eye Lens Removal Using Cavitating Microbubbles. U.S. Patent Application 16/733,918, 9 July 2020.

3

The effect of microbubble-assisted ultrasound in molecular permeability across cell barriers

Charis Rousou ^{1,2}, Josanne de Maar ², Boning Qiu ¹, Kim van der Wurff-Jacobs ¹, Marika Ruponen ³, Arto Urtti ^{3,4,5}, Sabrina Oliveira ^{1,6}, Chrit Moonen ², Gert Storm ^{1,7,8}, Enrico Mastrobattista ¹, Roel Deckers ²

¹ Department of Pharmaceutics, Utrecht University, The Netherlands

² Imaging and Oncology Division, University Medical Center Utrecht, The Netherlands

³ School of Pharmacy, University of Eastern Finland, Finland

⁴ Division of Pharmaceutical Biosciences, University of Helsinki, Finland

⁵ Institute of Chemistry, Saint Petersburg State University, Russia

⁶ Cell Biology, Neurobiology and Biophysics, Utrecht University, The Netherlands

⁷ Department of Surgery, National University of Singapore, Singapore

⁸ Department of Biomaterials Science and Technology, University of Twente, The Netherlands

ABSTRACT

The combination of ultrasound and microbubbles (USMB) has been applied to enhance drug permeability across tissue barriers. Most studies focused on only one physicochemical aspect (i.e., molecular weight of the delivered molecule). Using an *in vitro* epithelial (MDCK II) cell barrier, we examined the effects of USMB on the permeability of five molecules varying in molecular weight (182 Da to 20 kDa) and hydrophilicity (LogD at pH 7.4 from 1.5 to highly hydrophilic). Treatment of cells with USMB at increasing ultrasound pressures did not have a significant effect on the permeability of small molecules (molecular weight 259 to 376 Da), despite their differences in hydrophilicity (LogD at pH 7.4 from -3.2 to 1.5). The largest molecules (molecular weight 4 and 20 kDa) showed the highest increase in the epithelial permeability (3-7-fold). Simultaneously, USMB enhanced intracellular accumulation of the same molecules. In the case of the clinically relevant anti-CXC Chemokine Receptor Type 4 (CXCR4) nanobody (molecular weight 15 kDa), USMB enhanced its permeability by two-fold and its increased binding to retinoblastoma cells by five-fold. Consequently, USMB is a potential tool to improve the efficacy and safety of the delivery of drugs to organs protected by tissue barriers, such as the eye and the brain.

INTRODUCTION

The functionality and vitality of tissues depend on a proper regulation of their barriers [1,2,3]. Tissue barriers are formed by layers of epithelial cells that separate organs from their environment, and endothelial cells in the vasculature (separating the bloodstream from the tissues). Examples of tissue barriers include the blood-retina barrier (BRB) in the posterior eye and the blood-brain barrier (BBB). The functions of these cellular barriers are critical for tissue, organ, and organism homeostasis. A factor of prime importance regulating their permeability is the presence of intercellular junctions between the cells [4]. Tight junctions and subjacent adherens junctions control barrier permeability and intercellular interactions. These barriers also hinder the delivery of drug molecules to the diseased tissues (e.g., in retinoblastoma in the eye, glioblastoma in the brain) and limit their therapeutic efficacy. New delivery methods that allow administered drugs to permeate across tissue barriers more efficiently, and in a controlled and safe manner, are therefore needed.

Ultrasound and microbubbles (USMB) have been previously investigated as a method to allow drug molecules to cross epithelial and endothelial barriers [5,6]. Microbubbles are gas-filled spheres with diameters in the range of 0.5–10 μm . They are widely used as vascular contrast agents for diagnostic ultrasound imaging [7]. Microbubbles undergo mechanical oscillations when they are exposed to ultrasound waves. These oscillations are associated with various effects on cells and tissues. Some examples of these effects include (i) increase in the paracellular permeability as a consequence of rearrangement of the intercellular junctions and (ii) enhancement of molecular permeation across cell membranes and intracellular accumulation as a result of pore formation (sonoporation) or enhanced endocytosis [8,9]. These effects have been exploited to increase the permeability of the BRB [10,11,12], the BBB [8,13] (including some clinical trials NCT03119961, NCT04417088, NCT04440358, NCT04528680), the blood-labyrinth barrier in the ear [14,15], and the skin barrier (epidermis) [16,17,18,19] for a variety of materials (small molecule drugs, antibodies, nanoparticles) that otherwise have limited permeation in these barriers. These studies focused on the importance of a single physicochemical feature of a drug; the molecular weight. However, the impact of other drug-related parameters (e.g., hydrophilicity) on USMB-enhanced barrier permeability is still unknown.

This study aimed to investigate the efficacy in the transport of five molecules with different (i) hydrophilicities and (ii) molecular weights across an epithelial cell barrier using USMB. Specifically, the chosen test molecules vary in octanol/water partition coefficient (LogD) at pH 7.4 between 1.5 (i.e., propranolol) and highly hydrophilic (i.e., dextrans), and in molecular weight between 182 Da and 20 kDa. The well-known experimental transwell model was used for studying the transport of the selected molecules across the *in vitro* barrier. Furthermore, the effect of USMB on the permeability of the barrier was investigated using a clinically relevant molecule as a model drug, namely an anti-CXC chemokine receptor type 4 (CXCR4) single domain antibody derived from a heavy chain only camelid antibody (also known as nanobody, molecular weight 15 kDa) [20,21]. To the best of our knowledge, this is the first time that the enhanced permeability of a nanobody across a biological barrier is studied using USMB. In clinical practice, USMB could be used to enhance the distribution of the anti-CXCR4 nanobody in the retina, and improve the efficacy of anti-cancer treatment in retinoblastoma.

MATERIALS AND METHODS

Chemicals

Six-carboxyfluorescein (6-carboxyfluorescein, 8.51072), fluorescent-conjugated dextrans (4400 Da; T1037 and 20,000 Da; 73766), paraformaldehyde (PFA, 158127) and histology mounting medium containing DAPI (Fluoroshield™ with DAPI, F6057) were acquired from Sigma-Aldrich (Steinheim, Germany). Radioactive mannitol (3H-Mannitol, NET101250UC) and propranolol (3H-Propranolol, NET515250UC) were purchased from Perkin Elmer (Waltham, MA, USA). SYTOX™ green (S7020) was obtained by ThermoFisher Scientific (Waltham, MA, USA). Fluorescently labelled anti-CXCR4 nanobody (anti-CXCR4-Hilyte647, molecular weight 15 kDa, Q85c-647) was obtained from QVQuality (Utrecht, The Netherlands).

Cell Culture

Madin-Darby canine kidney (MDCK) II is an epithelial cell line with short doubling time, and when cultured at specific conditions, cells acquire cobblestone morphology, cellular polarity, form microvilli and intercellular junctions (barrier function) [22,23]. MDCK II cells were kindly provided by Prof. Arto Urtti (University of Eastern Finland, Finland) and were maintained in DMEM/F12 medium (Gibco, New York, NY, USA) supplemented with 10% (v/v) FBS and 1% (v/v) L-glutamine (Sigma-Aldrich, Steinheim, Germany). Human

retinoblastoma cells (WERI-RB1) were purchased from ATCC (ATCC, Wesel, Germany) and were cultured in RPMI 1640 medium (Sigma-Andrich) supplemented with 10% (v/v) FBS.

Cells were cultured in standard cell culture flasks in a humidified atmosphere of 5% CO₂ at 37 °C. Epithelial cells were sub-cultured two to three times per week in dilution ratios between 1:5–1:20 and were used up to passage number 32. Sub-culture of epithelial cells involves washing the cells with DPBS, incubation with trypsin/EDTA for 5 minutes at 37 °C and deactivation of trypsin/EDTA with normal culture medium containing all of the supplements. Retinoblastoma cells were sub-cultured one to two times per week and were used up to passage number seven. Sub-culture of retinoblastoma cells (suspension cells) was performed by diluting cells into fresh medium with cell density maintained between 0.1 and 2×10^6 cells/mL.

Differentiation of Epithelial Cells

For the permeability studies, epithelial cells were cultured as tight monolayers on transwell membranes. Cells were seeded to polycarbonate transwell membranes (12 or 24 mm translucent membrane, pore size 0.4 µm, Corning, New York, NY, USA) at the density of 0.16×10^6 cells/cm². Prior to cell seeding, the transwell membranes were equilibrated for 10 minutes with culture medium at room temperature. To maintain equilibrium of hydrostatic pressure between the apical and the basolateral sides of the transwell membrane (Figure 1A), insert medium was added to the recommended final volumes according to the manufacturer (apical/basolateral: 0.5/1.5 mL for 12 mm membranes or 1.5/2.6 mL for 24 mm membranes). Medium containing 1% FBS and 1% antibiotics was used during cell seeding, which was refreshed one, three, and five days after seeding. Cells were cultured for 7 days prior to the experiment to allow for differentiation and development of intercellular junctions, as previously described [22].

USMB Treatment of Epithelial Barriers

The permeability of various test compounds across epithelial monolayers cultured on transwell membranes was studied in the apical-to-basolateral direction (Figure 1A). On the experimental day, fully differentiated epithelial monolayers were washed twice and equilibrated for 10 minutes at 37 °C in Hank's Balanced Salt Solution (HBSS) containing calcium and magnesium without phenol red (ThermoFisher Scientific, Waltham, MA, USA).

Ultrasound experiments were performed using an unfocused, single-element transducer with 20 mm diameter (PA420, Precision Acoustics, Dorchester, UK). The arbitrary wave generator of an oscilloscope (SDS1202X+, Siglent.eu, Helmond, The Netherlands) was used to generate a transistor-transistor logic (TTL) pulse, which was used as an external trigger for an arbitrary wave generator (SDG1032X 30Mhz, Siglent.eu), resulting in an output pulsed sinusoidal signal with central frequency 1.5 MHz, pulse duration 100 μ s, duty cycle 10% and pulse repetition frequency (PRF) 1 kHz. The chosen transducer has a central frequency that falls within the range of resonance frequencies of SonoVue™ [24], which ensures that microbubble oscillations are maximum during USMB treatment. The resulting signal was then amplified (AG1012, T&C Power Conversion Inc., New York, NY, USA) before it was sent to the ultrasound transducer.

A dedicated sonication tank compatible with transwell inserts was used for the USMB experiments (Figure 1B). The ultrasound transducer was positioned at the bottom of the bath and about 250 mL of PBS at 37 °C was added. Subsequently, the transwell insert was immersed in the bath with the transwell membrane covered with cells facing down (Figure 1B) at a fixed axial distance (80 mm) from the ultrasound transducer.

Transwell inserts were randomly assigned to USMB-treated or sham-treated sample groups. Following immersion of USMB-treated samples in the sonication bath, 500 μ L of freshly mixed SonoVue™ microbubbles (Bracco, Milan, Italy) was injected near the cells using a curved-tip 19G needle (Figure 1C). SonoVue™ are lipid-shelled microbubbles with mean diameter of 2.5 μ m, that contain sulfur hexafluoride gas (SF_6) and are approved for clinical use [25]. Microbubbles were allowed to float for 1 minute so that direct contact with the cells was assured. Subsequently, ultrasound was applied for 1 minute with acoustic peak negative pressure (P_{neg}) ranging between 0.3 and 0.7 MPa. Sham-treated samples were treated similar to USMB-treated samples, except for the addition of microbubbles and exposure to ultrasound. Sham-treated samples were immersed in the PBS bath for 2 minutes and served as negative controls (0 MPa). The pressure field maps (Figure 1D) of the transducer were measured with a calibrated hydrophone [26].

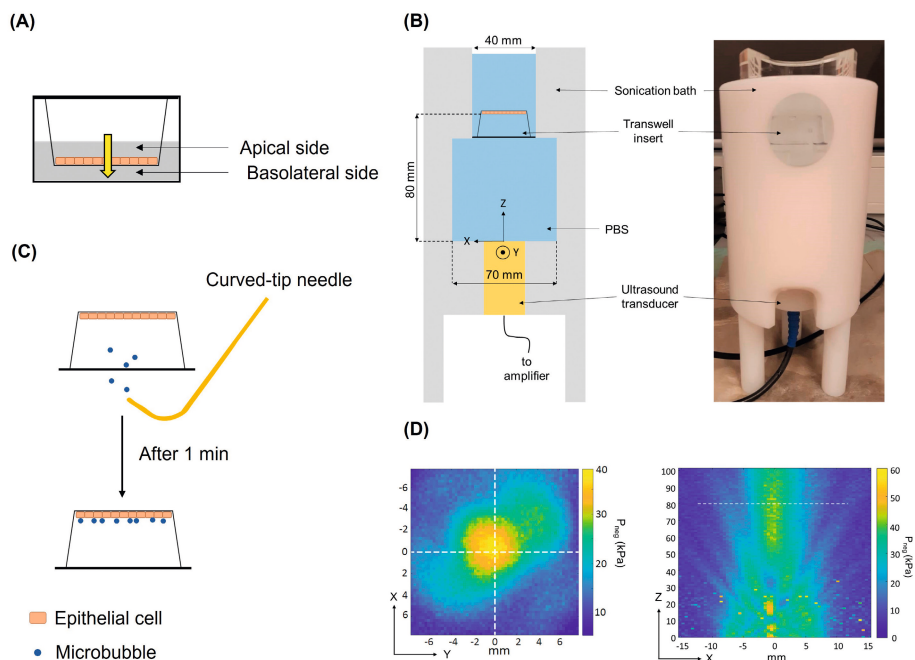


Figure 1. (A) Apical and basolateral sides of transwell insert and direction in which the permeability of model drugs was studied (yellow arrow). (B) Schematic illustration (left) and picture (right) of the custom-made sonication bath, compatible with transwell inserts. The ultrasound transducer is positioned at the bottom of the bath and the transwell insert is immersed upside-down with the cell monolayer fixed at 80 mm from the surface of the transducer. (C) Using a needle with curved tip, microbubbles are injected and allowed to float for 1 minute to ensure cell-microbubble contact. (D) Pressure field maps of ultrasound transducer. Left: transversal plane. Right: axial plane, white dotted line indicates position of transversal plane. Adapted from [26].

Permeability Experiments with an Epithelial Barrier and Model Drugs

Immediately after USMB treatment, transwell inserts were removed from the sonication bath (containing PBS) and were placed in a new six-well plate. The protocol used in the permeability experiments was according to similar studies previously performed by others [22,27]. In short, HBSS was added at the basolateral side followed by addition of test compound dissolved in HBSS (1.5 mL) at the apical side. The initial concentration of test compounds on the apical side was 1 μ Ci/mL for propranolol and mannitol and 200 μ M for 6-carboxyfluorescein and fluorescent dextrans. An overview of the relevant physicochemical characteristics of the test compounds used in the permeability experiments is given in Table 1.

Table 1. Physicochemical properties of compounds used to study the permeability across epithelial barriers.

Compound	Hydrophilic/Lipophilic (LogD)	M _w (Da)	Label
Propranolol	Lipophilic (1.5 [28])	259	Radioactive
Mannitol	Hydrophilic (-3.1 [28])	182	Radioactive
6-carboxyfluorescein	Hydrophilic (-3.2 [29])	376	Fluorescent
4 kDa dextran	Hydrophilic (N/A)	4400	Fluorescent (TRITC)
20 kDa dextran	Hydrophilic (N/A)	20000	Fluorescent (TRITC)

LogD, octanol/water partition coefficient at pH 7.4; N/A, not available; M_w, molecular weight; TRITC, tetramethylrhodamine isothiocyanate.

To determine compound concentration on the basolateral side, samples of 400 μ L were collected at 15, 30, 45, 60, 90 and 120 minutes after treatment with USMB. The volume of removed sample was replaced with fresh HBSS. During the experiment, cells were kept at 37 °C and shaking at 170 rounds per minute. In the experiments where fluorescent compounds were used, samples were protected from light at all times.

The samples containing radioactively-labelled compounds were equilibrated overnight in liquid scintillation cocktail for radiometric detection (Ultima Gold, 6013321, Perkin Elmer, MA, USA) at room temperature. Detection of radioactivity counts was determined by a microplate counter for radiometric counting (MicroBeta, 2450, Perkin Elmer, MA, USA).

Intensity of fluorescence signals was determined by a spectrofluorophotometer (FP 8300, Jasco Benelux BV, Utrecht, The Netherlands). 6-carboxyfluorescein was excited at 492 nm and emission was detected at 517/5 nm (center wavelength/bandwidth) and TRITC-dextran were excited at 550 nm and detected at 575/5 nm. Background radioactivity and fluorescence signal from HBSS were subtracted from the measurements.

Calculation of apparent permeability coefficients (P_{app})

P_{app} values were calculated for each compound:

$$P_{app} = \frac{Q}{(C_0 \times A)} \quad (1)$$

where P_{app} (in cm/s) is the apparent permeability coefficient of the test compound across the barrier. Q is the flux of the test compound (μ g/s), C₀ is the initial concentration of

the test compound at the apical side ($\mu\text{g}/\text{mL}$), and A is the surface area of the transwell membrane (cm^2). In addition to P_{app} , the amount of permeated compound across the cell barrier was calculated as a percentage of the amount of the compound initially added at the apical side (Equation (2)).

$$\% \text{ Permeated amount} = \frac{\text{Amount}_{\text{B}}(t)}{\text{Amount}_{\text{A}}(t=0)} \times 100 \quad (2)$$

where $\text{Amount}_{\text{B}(t)}$ is the amount of the compound at the basolateral side at time t and $\text{Amount}_{\text{A}(t=0)}$ is the amount of the compound added at the apical side at the beginning of the experiment ($t = 0$).

Intracellular Accumulation Study

Epithelial cells were exposed to acoustic pressures of 0 MPa or 0.7 MPa. Directly after USMB treatment, a solution containing 200 μM of 4 kDa or 20 kDa fluorescent dextran and 2 μM of SYTOXTM green was added at the apical side. SYTOXTM green is a small (molecular weight 600 Da) membrane impermeable compound, commonly used as a drug model in studies investigating the effect of USMB on intracellular drug accumulation. Here, we use SYTOXTM green to confirm the action of USMB when investigating the intracellular accumulation of dextrans. As with SYTOXTM green, dextrans are hydrophilic in nature, thus unable to permeate the lipophilic cell membrane as such. When USMB induces cell membrane disruption, these molecules can enter the cytoplasm.

After 30 or 120 minutes of incubation with the test compounds at 37 °C, the transwell membrane was removed from the insert with a scalpel blade. The cells were washed with PBS and fixed with 4% (w/v) PFA in PBS for 10 minutes at room temperature. Subsequently, the transwell membrane was positioned on a glass microscope slide with the cells facing up. A small amount of mounting medium containing DAPI was added on a cover slip, which was used to seal the transwell membrane and the glass microscopy slide. Samples were allowed to dry overnight and were kept at 4 °C until further use.

Fixed cells were imaged using a fluorescence confocal microscope (Leica TCS SP8 X, Leica, Amsterdam, The Netherlands) in three channels (excitation 360 nm; emission 410–480 nm for DAPI, excitation 504 nm; emission 515–546 nm for SYTOXTM green, excitation 550 nm; emission 565–650 nm for TRITC-dextrans). Samples were initially imaged in the DAPI and SYTOXTM green channels at 10 \times magnification (image format:

2048 × 2048 pixels; speed: 100; line average: 4) in order to confirm that USMB acted on cell membranes and to detect the locations where this activity was the most dense (Supplementary Figure S1A). Subsequently, cells at these locations were imaged with a 63× oil immersion objective (image format: 2048 × 2048 pixels, speed: 100, line average: 6) to determine the intracellular accumulation of TRITC-dextran (Supplementary Figure S1B). All imaging settings (laser gain, pinhole size, zoom) remained constant among different samples.

The fluorescence intensity (FI) of cells that showed intracellular accumulation of dextrans was determined with the ImageJ software (National Institutes of Health, Bethesda, MD, USA). A mask was generated by thresholding the original RGB TRITC-dextran image at a fixed pixel intensity. Threshold value was kept the same for all images for each of the two dextrans. Subsequently, holes in the mask were filled automatically using the corresponding software command. The mask was applied to the RGB image to calculate the mean FI of cells within the area of interest. An example of the resulted image for each of the above steps can be found in the supplementary information (Supplementary Figure S2). For each experimental condition images from five different locations were acquired and the average FI intensity per cell with intracellular accumulation was calculated for each experimental group.

USMB-Induced Permeability of Anti-CXCR4 Nanobody across an Epithelial Barrier

Immediately after exposure of epithelial barrier to USMB, 0.5 mL of HBSS containing anti-CXCR4 nanobody (1000 nM) was added to the apical side of the transwell. Hydrostatic equilibrium was maintained with the addition of 1.5 mL of RPMI 1640 medium without phenol red (Gibco, New York, NY, USA) in the basolateral side. The cells were incubated for 120 minutes in a humidified atmosphere of 5% CO₂ at 37 °C, and when incubation was complete, medium from the basolateral side containing the permeated nanobody was collected.

To determine the amount of permeated fluorescent nanobody, 0.5 mL of basolateral medium was measured using a fluorescence plate-reader (FP 8300, Jasco, excitation 650 nm, emission 673/5 nm). Subsequently, 1 mL of the remaining basolateral medium was added to retinoblastoma cells (100,000 cells in Eppendorf tube) allowing for binding of nanobody on CXCR4 receptor for 1 h at 5% CO₂ and 37 °C. Then, the cells were centrifuged (1000× g, 4 minutes) and supernatant was removed. Cell pellets were washed once with PBS and fixed with 4% PFA for 10 minutes at room temperature.

After fixation and removal of PFA, the cell pellets were suspended in PBS, stored at 4 °C and were protected from light until further analysis. Nanobody binding was determined by measuring the fluorescence of cells using the same plate-reader and settings as before, and flow cytometry (excitation 633 nm, emission 780/60 nm, FACSCanto™ II Cell Analyzer, BD Biosciences, Franklin Lakes, NJ, USA). Flow cytometry data were analyzed using FlowLogic™ software (V8, Inivai, Mentone, Victoria, Australia).

Statistical Analysis

Statistical analysis was performed using the GraphPad Prism software (version 8.0.1, GraphPad, San Diego, CA, USA), assuming that the samples follow non-parametric distribution. Statistically significant differences in P_{app} and percentage of permeated amount were calculated between USMB-treated and sham-treated samples (i.e., 0.3–0.7 MPa vs. 0 MPa) using Kruskal-Wallis test. Differences in the normalized IF of intracellular TRITC-dextran accumulation of 0 MPa vs. 0.7 MPa, and permeability and binding of the anti-CXCR4 nanobody were calculated using Mann-Whitney test. Data in the graphs are shown as mean \pm SEM. Statistically significant differences between groups are annotated with asterisks by using * for $p < 0.05$; ** for $p < 0.01$; *** for $p < 0.001$.

RESULTS

Effect of USMB on Molecular Permeability across an Epithelial Barrier

Permeability experiments were conducted using molecules with varying molecular weight and hydrophilicity. In the absence of USMB permeability was highest for propranolol and decreased with increasing molecular weight and decreasing LogD (Figure 2A). More specifically, the total permeated amount was $29.1 \pm 2.2\%$ for lipophilic propranolol, followed by hydrophilic mannitol ($5.6 \pm 1.4\%$), 6-carboxyfluorescein ($4.1 \pm 0.5\%$), 4 kDa dextran ($0.3 \pm 0.1\%$), and 20 kDa dextran ($0.1 \pm <0.1\%$).

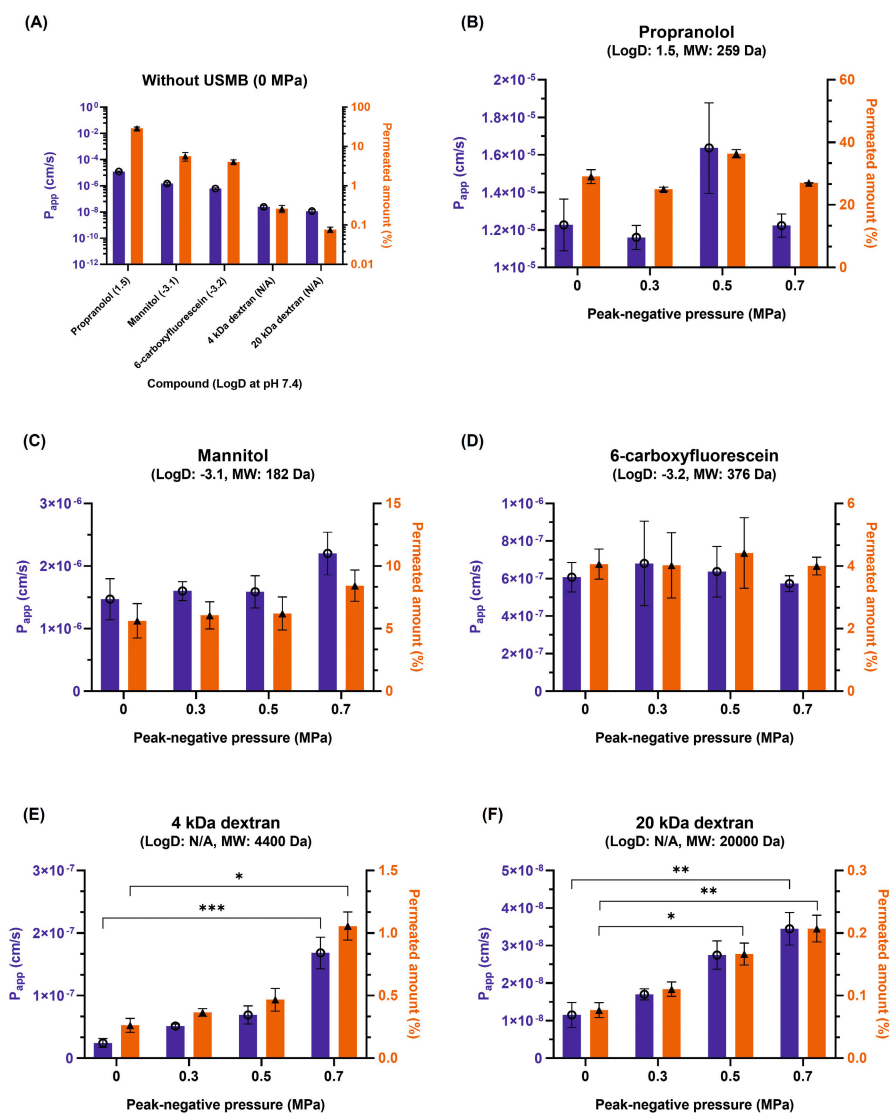


Figure 2. Apparent permeability coefficient (blue bars, ○) and total amount permeated (orange bars, ▲) of five different molecules with varying molecular weight and hydrophilicity across an epithelial barrier **(A)** in the absence of USMB (0 MPa) and **(B–F)** at various ultrasound pressures for **(B)** propranolol, **(C)** mannitol, **(D)** 6-carboxyfluorescein, **(E)** 4 kDa dextran, and **(F)** 20 kDa dextran (n = 5). * for p < 0.05; ** for p < 0.01; *** for p < 0.001

Treatment of cells with USMB at increasing ultrasound pressures did not have a significant effect on the permeability of small molecules (propranolol, mannitol, 6-carboxyfluorescein), despite their differences in hydrophilicity (Figure 2B–D). In contrast, for the large hydrophilic molecules (dextrans), an increase in permeability

was observed with increasing ultrasound pressure (Figure 2E,F). For the 4 kDa dextran, a significant, seven-fold increase in the mean P_{app} was seen at 0.7 MPa ($1.68 \times 10^{-7} \pm 0.25 \times 10^{-7}$ cm/s) compared to 0 MPa ($0.24 \times 10^{-7} \pm 0.07 \times 10^{-7}$ cm/s) (Figure 2E). At the same pressure, the total amount of 4 kDa dextran that permeated the barrier 120 minutes after treatment was four times higher than the sham treatment ($0.3 \pm 0.1\%$ at 0 MPa vs. $1.1 \pm 0.1\%$ at 0.7 MPa). Similarly, a three-fold increase in P_{app} was observed for the 20 kDa dextran ($1.15 \times 10^{-8} \pm 0.33 \times 10^{-8}$ cm/s at 0 MPa vs. $3.44 \times 10^{-8} \pm 0.43 \times 10^{-8}$ cm/s at 0.7 MPa) (Figure 2F). The total amount of 20 kDa dextran that permeated the barrier was increased by two and three times at 0.5 MPa and 0.7 MPa, respectively, compared to 0 MPa ($0.1 \pm <0.1\%$ at 0 MPa, $0.2 \pm <0.1\%$ at 0.5 MPa, $0.2 \pm <0.1\%$ at 0.7 MPa). The results indicate that USMB aided the permeability of the two large hydrophilic molecules, but this effect was absent in the case of small molecules, regardless of their hydrophilicity.

In addition to the permeability experiments using epithelial barriers, similar experiments were performed with an endothelial cell line (HUVEC) (Supplementary Materials). USMB treatment of endothelial barriers at ultrasound pressures of 0.6 and 0.7 MPa led to severe cell detachment and disruption of barrier integrity (Supplementary Figure S6A). Therefore, permeability experiments were only performed at lower ultrasound pressures (0.3 to 0.5 MPa) (Supplementary Figure S6B). Comparison of the permeability coefficients between the MDCK II and HUVEC cells revealed that HUVEC formed a leakier barrier than MDCK II. Specifically, in the absence of USMB, the P_{app} of 6-carboxyfluorescein, 4 kDa, and 20 kDa dextrans was several times higher (~20 times) than the corresponding values from the MDCK II cells.

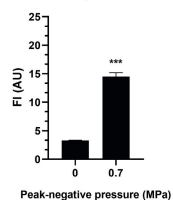
The Effect of USMB on the Intracellular Accumulation of Fluorescent Dextrans in Epithelial Cells

To investigate whether USMB-induced intracellular accumulation occurred in parallel with USMB-enhanced paracellular transport, epithelial barriers were treated with USMB at 0.7 MPa, the ultrasound pressure that was found to increase the paracellular permeability of large hydrophilic molecules (dextrans) across the same barrier. Intracellular accumulation was investigated by incubating cells with the same two fluorescent dextrans (TRITC-dextrans, molecular weight of 4 or 20 kDa). Furthermore, SYTOX™ green was added to confirm that intracellular accumulation of dextrans was induced by USMB. It was observed that all cells with uptake of dextrans had concomitant uptake of SYTOX™ green (Supplementary Figure S1B).

4 kDa TRITC-dextran

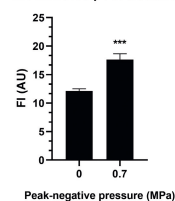
(A)

30 minutes post-treatment

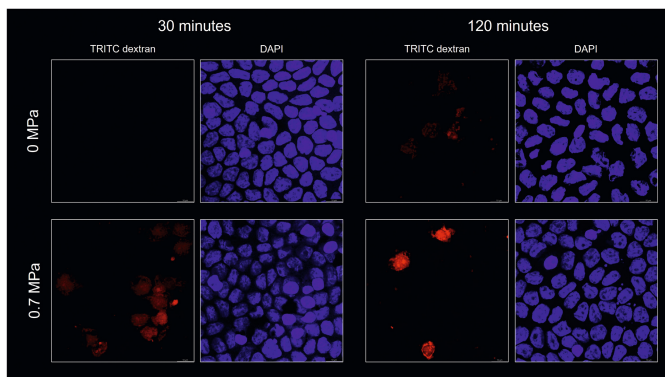


(B)

120 minutes post-treatment



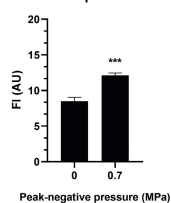
(C)



20 kDa TRITC-dextran

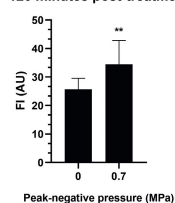
(D)

30 minutes post-treatment



(E)

120 minutes post-treatment



(F)

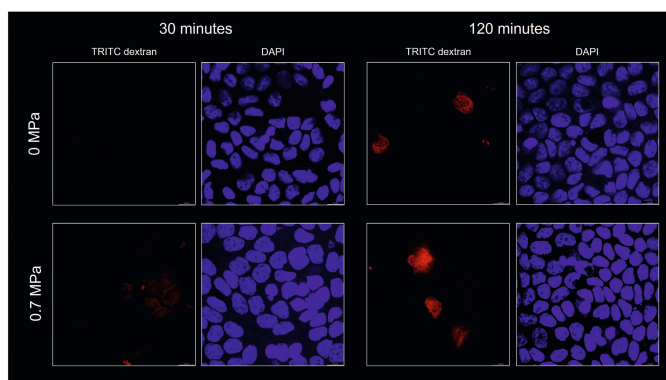


Figure 3. Intracellular accumulation of fluorescent dextrans (4 and 20 kDa) by epithelial barriers after treatment with USMB at acoustic pressure of 0 or 0.7 MPa. Quantification of fluorescence intensity from the intracellular accumulation of a 4 kDa dextran after incubation for (A) 30 minutes and (B) 120 minutes. (C) Representative fluorescence images used for the quantification, scale bar, 10 μm . Quantification of fluorescence intensity from the intracellular accumulation of a 20 kDa dextran after incubation for (D) 30 minutes and (E) 120 minutes. (F) Representative fluorescence images were used for the quantification. Scale bar 10 μm , FI: fluorescence intensity, AU: arbitrary units, (n = 5), ** for $p < 0.01$, *** for $p < 0.001$

Quantification of fluorescent signal revealed that for both dextrans the intracellular accumulation was lowest in the absence of USMB after 30 minutes of incubation (Figure 3A,D). Exposure of cells to USMB significantly increased the uptake of dextrans at both time points. Specifically, 30 minutes after incubation the intracellular accumulation of 4 kDa dextran (4.4 times, Figure 3A) and 20 kDa dextran (1.4 times, Figure 3D) was increased. Two hours after incubation, sham treated cells had intracellular accumulation of dextrans to some extent (Figure 3C,F), yet USMB-induced uptake was significantly higher (1.5 times increase in the uptake of a 4 kDa dextran, 1.3 times increase in the uptake of a 20 kDa dextran).

Effect of USMB on the Permeability of Anti-CXCR4 Nanobody across an Epithelial Barrier

As previously demonstrated, USMB aided paracellular permeability of the hydrophilic dextrans at ultrasound pressure of 0.7 MPa. To demonstrate the clinical relevance of USMB treatment, experiments were performed using a model therapeutic molecule. A nanobody that binds on the CXCR4 was chosen for this purpose [20,21]. CXCR4 is overexpressed in a number of cancer cells including retinoblastoma cells in the eye [30]. Since epithelial cells used in this study did not express CXCR4 receptors (Supplementary Figure S3), any increase in the permeability of the anti-CXCR4 nanobody across the epithelial monolayer is a result of USMB treatment, but not of receptor-mediated transcytosis.

Epithelial monolayers were treated with USMB at 0 MPa or 0.7 MPa, and subsequently the anti-CXCR4 nanobody (fluorescently labelled) was added at the apical side. Exposure of epithelial barrier to USMB increased the amount of permeated nanobody by 1.8 times (FI 15.12 ± 1.65 AU at 0 MPa vs. 27.48 ± 1.72 AU at 0.7 MPa) (Figure 4A). To check that the permeated nanobody retained its ability to bind on the CXCR4 receptor after permeating the barrier, the solution from the basolateral side containing the permeated nanobody was collected and incubated with the retinoblastoma cells. Exposure of epithelial cells to USMB at 0.7 MPa allowed for an increase in the total nanobody binding to retinoblastoma cells of 4.5 times (FI 4.17 ± 0.99 AU at 0 MPa vs. 18.81 ± 1.67 AU at 0.7 MPa) (Figure 4B). This increase in the binding of nanobody was also observed by flow cytometry (Supplementary Figure S4).

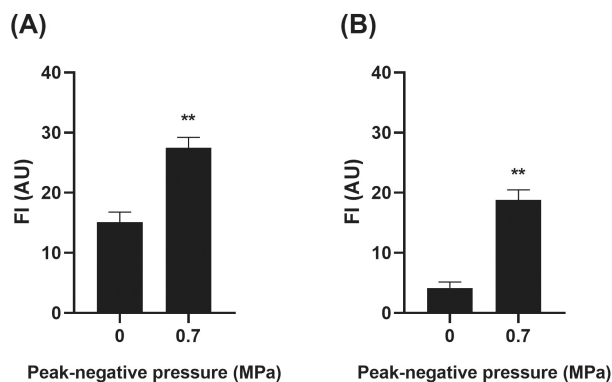


Figure 4. (A) Permeability of anti-CXCR4 nanobody across the epithelial barrier upon USMB treatment at acoustic pressure of 0 or 0.7 MPa and (B) binding of permeated nanobody to retinoblastoma cells. FI: fluorescence intensity, AU: arbitrary units, (n = 5), ** for p < 0.01

DISCUSSION

The objective of this study was to investigate how USMB affects the permeability of molecules with varying physicochemical properties (hydrophilicity and molecular weight) in biological barriers. Permeability of the lipophilic propranolol (molecular weight 259 Da, LogD at pH 7.4 of 1.5) was the highest among the studied molecules and was not changed due to USMB treatment. This is attributed to the lipophilicity of propranolol that allows its high permeation across cellular barriers via transcellular diffusion.

In vitro cell cultures are used as models of *in vivo* biological barriers, which often means that they resemble (but do not perfectly preserve) the characteristics of their *in vivo* counterparts. All *in vitro* epithelial models exhibit some leakiness even for hydrophilic molecules that do not cross the membranes via transcellular diffusion [31]. Small hydrophilic molecules can permeate through the intercellular spaces easier than large molecules. Indeed, in the absence of USMB, P_{app} of mannitol (molecular weight 182 Da, LogD at pH 7.4 of -3.1) in MDCK II monolayer was one order of magnitude higher than the permeability of 6-carboxyfluorescein (molecular weight 376 Da, LogD at pH 7.4 of -3.2) and 4 kDa dextran, and two orders of magnitude higher than the permeability of 20 kDa dextran. The lack of measurable effect on the paracellular permeability of mannitol (molecular radius $\approx 4 \text{ \AA}$ [32]) and 6-carboxyfluorescein is due to this intrinsic permeability that likely overshadowed cell barrier alterations as induced by USMB. On

the contrary, clearly improved permeation of the dextrans (several fold) was achieved with USMB. Presumably, the small size of paracellular pores in the differentiated MDCK II monolayers (radii of pores 5–10 Å; [33]) was increased by USMB thereby facilitating paracellular diffusion of the two dextrans (molecular radius of 4 kDa dextran \approx 11 Å and of 20 kDa dextran \approx 18 Å [34]). It is important to highlight that USMB did not induce any reduction in the viability of epithelial cells or the integrity of the barrier after exposure at this ultrasound pressure (Supplementary Figure S5).

Only few other studies have investigated the effect of USMB on the transport of different molecules through intercellular gaps using the transwell system. In agreement with our findings, Fix *et al.* reported the effect of USMB in the paracellular permeability of a hydrophilic macromolecule (70 kDa dextran) across an epithelial CaCo-2 barrier on transwells [35]. Exposure to ultrasound (frequency 1 MHz, P_{neg} 0.3 MPa, 30 s) combined with phase-change contrast agents (i.e., liquid perfluorocarbon-filled particles of size 100–300 nm that form microbubbles) increased the paracellular permeability of a 70 kDa dextran by 44%. Lelu *et al.* cultured primary porcine brain endothelial cells (PBEC) on transwell inserts as an *in vitro* model for BBB [36]. The barriers were exposed to USMB at 0.1 and 0.8 MPa and permeability of two fluorescent molecules (molecular weight of 0.46 and 67 kDa) was measured across the endothelial barrier. The authors reported a significant increase of P_{app} for both molecules (2.6–5.2 times). Lelu *et al.* [36] reported that immersion of the cells in PBS for USMB treatment affected the tightness of the barrier, which is in agreement with our observations (data not shown). Based on this observation we decided to perform all statistical comparisons in our study with sham treated sample (i.e., cells that were immersed in PBS bath but not exposed to USMB) as a control group rather than completely untreated barriers. This difference between the control group used in our study (sham-treated barriers) versus the study of Lelu *et al.* [36] (untreated barriers), unfortunately makes comparison and interpretation of results difficult.

In addition to increasing the intercellular permeability of hydrophilic molecules across the epithelial barrier, USMB induced intracellular accumulation of SYTOX™ green (molecular weight 600 Da) and two dextrans (molecular weight 4 and 20 kDa) as was already shown by us [26,37] and other groups [38,39,40] before. Quantification of fluorescent signals 30 and 120 minutes after incubation revealed that intracellular accumulation of dextrans was significantly higher in the cells treated with USMB at 0.7 MPa as compared to 0 MPa. Dextrans were distributed homogeneously in the cytosol

of USMB-treated cells, presumably due to cellular access via USMB-induced pores in plasma membrane [40]. Nuclear distribution of 4 kDa dextran was observed as early as 30 minutes after incubation, while the presence of the 20 kDa dextran in the nucleus was only observed after 120 minutes. Meijering *et al.* observed similar distribution of a 4 kDa dextran in the cell nucleus (immediately after treatment with USMB), but not with dextrans larger than 70 kDa [40], which is due to the effective porous radius of the nuclear membrane (macromolecules larger than ~70 kDa do not cross the nuclear pore complex by passive diffusion but rather require energy-dependent processes [41]).

A few studies have reported accumulation of full-length antibodies to the brain aided by USMB [13,42,43]. Nanobodies, which are single-domain antibodies, have been previously coupled to microbubbles and were used to improve ultrasound molecular imaging of atherosclerosis, prostate and renal tumors [44,45,46]. Here, a nanobody (molecular weight 15 kDa) targeting the CXCR4 receptor [20,21] was used as a model molecule to illustrate the potential of USMB in the delivery of pharmaceuticals across epithelial barriers. CXCR4 is a receptor that is highly expressed in over than 20 cancer types and is a major co-receptor for cellular entry of human immunodeficiency virus [47]. It is involved in tumor cell proliferation, survival and metastasis, while it is absent or expressed at very low levels in healthy tissues [48,49]. These characteristics make CXCR4 inhibitors an interesting compound group for the treatment of those malignancies. Recently, results from a phase Ib/II trial using a fully human IgG4 monoclonal anti-CXCR4 antibody (Ulocuplumab, BMS-936564) were published, showing safe and efficacious clinical use of Ulocuplumab against multiple myeloma [50]. Expression of CXCR4 was previously observed in tumor cells isolated from retinoblastoma [30], the most common intraocular malignancy in children. In our study, treatment of epithelial barriers at ultrasound pressure of 0.7 MPa increased the total number of permeated nanobody approximately by 2 times compared with sham-treated barriers, and resulted in 4.5 times higher binding of nanobody to retinoblastoma cells. In clinical practice, USMB could be used to improve the permeability of anti-CXCR4 nanobody across tissue barriers that limit its binding to the target cells. For example, USMB might make it possible to deliver anti-CXCR4 nanobody to retinoblastoma cells, allowing for increased nanobody binding to tumor cells and inhibiting their migration and proliferation. The nanobody could be administered intravenously and USMB is used to temporarily increase the permeability of the BRB or to facilitate nanobody permeation to retinoblastoma cells after intravitreal injection of the nanobody.

In addition to the permeability experiments with the epithelial cells (MDCK II), we performed similar experiments using an endothelial cell line (HUVEC). Comparison of the permeability coefficients between the MDCK II and HUVEC cells revealed that HUVEC formed a leakier barrier than MDCK II. This inherent leakiness of HUVEC explains why no USMB-enhanced permeability was detected when endothelial barriers were treated with USMB. In addition, exposure of HUVEC barriers to acoustic pressures higher than 0.6 MPa resulted in extensive cell detachment from the transwell membrane, making permeability experiments at these pressures practically impossible. Detachment of HUVEC after exposure to USMB was previously reported at similar ultrasound pressures [37]. In conclusion, cell detachment in combination with insufficient barrier tightness [51] make HUVEC not an ideal endothelial barrier model for investigating the effect of USMB on molecular permeability. In future studies, co-culture of HUVEC with other supportive cells, such as pericytes, could improve the tightness of the barrier and provide a more suitable model for permeability studies [52,53].

Our study has some limitations. Our sonication bath set-up did not allow for the integration of cavitation measurements. Real-time monitoring of acoustic emissions from microbubbles could provide additional insights on which mechanisms (i.e., stable vs. inertial cavitation) are responsible for para- and intracellular transport. In this study we only investigated the effect of acoustic pressure on barrier permeability but future studies should focus on the effect of other USMB-related parameters (e.g., microbubble concentration, exposure time, PRF, etc.). Previous *in vivo* studies have shown that increase in the paracellular diffusion of compounds after USMB treatment is on the time scale of several hours [54,55]. This is an interesting aspect to be investigated in future studies using epithelial barriers and the transwell system.

The effect of USMB on the permeability of the BRB has not been yet extensively investigated. Experiments using *ex vivo* eyes or healthy animals could provide further insights on the safety of USMB prior to clinical translation for drug delivery in the posterior eye. A few *in vivo* studies that investigated the extravasation of molecules with different molecular weights as a result of USMB-mediated BRB disruption, are currently available [10,11,12]. New studies using molecules with various hydrophilicities and molecular weights could help to comprehend the potential and limitations of USMB therapy in ocular drug delivery. Ideally, clinically approved microbubbles and a clinical ultrasound system could be used for USMB treatment [26] and to monitor microbubble emissions [56]. Finally, combination of USMB with pharmaceuticals (such as an anti-

CXCR4 nanobody for the treatment of retinoblastoma) could be tested in *in vivo* disease models in order to determine the therapeutic efficacy of the method.

CONCLUSIONS

The role of molecular properties (molecular weight and hydrophilicity) on the intercellular permeation across an epithelial barrier was studied in the presence of USMB. USMB at 0.7 MPa aided the permeability of large hydrophilic molecules and increased their intracellular accumulation, but did not affect the permeability of small molecules regardless of their hydrophilicity. USMB enhanced the permeability of an anti-CXCR4 nanobody and its subsequent binding to retinoblastoma cells. USMB is a potential tool for the delivery of (biological) drugs to protected organs, such as the eye and the brain.

REFERENCES

1. Turner, J.R. Molecular Basis of Epithelial Barrier Regulation. *Am. J. Pathol.* 2006, 169, 1901–1909. <https://doi.org/10.2353/ajpath.2006.060681>.
2. Cunha-Vaz, J. The Blood-Retinal Barrier in the Management of Retinal Disease: EURETINA Award Lecture. *Ophthalmologica* 2017, 237, 1–10. <https://doi.org/10.1159/000455809>.
3. Maiuolo, J.; Gliozzi, M.; Musolino, V.; Carresi, C.; Nucera, S.; Macrì, R.; Scicchitano, M.; Bosco, F.; Scarano, F.; Ruga, S.; et al. The Role of Endothelial Dysfunction in Peripheral Blood Nerve Barrier: Molecular Mechanisms and Pathophysiological Implications. *Int. J. Mol. Sci.* 2019, 20, 3022. <https://doi.org/10.3390/ijms20123022>.
4. González-Mariscal, L.; Nava, P.; Hernández, S. Critical Role of Tight Junctions in Drug Delivery across Epithelial and Endothelial Cell Layers. *J. Membr. Biol.* 2005, 207, 55–68. <https://doi.org/10.1007/s00232-005-0807-y>.
5. McMahan, D.; O'Reilly, M.A.; Hynynen, K. Therapeutic Agent Delivery Across the Blood–Brain Barrier Using Focused Ultrasound. *Annu. Rev. Biomed. Eng.* 2021, 23, 89–113. <https://doi.org/10.1146/annurev-bioeng-062117-121238>.
6. Rousou, C.; Schuurmans, C.C.L.; Urtti, A.; Mastrobattista, E.; Storm, G.; Moonen, C.; Kaarniranta, K.; Deckers, R. Ultrasound and Microbubbles for the Treatment of Ocular Diseases: From Preclinical Research towards Clinical Application. *Pharmaceutics* 2021, 13, 1782. <https://doi.org/10.3390/pharmaceutics13111782>.
7. Averkiou, M.A.; Bruce, M.F.; Powers, J.E.; Sheeran, P.S.; Burns, P.N. Imaging Methods for Ultrasound Contrast Agents. *Ultrasound Med. Biol.* 2020, 46, 498–517. <https://doi.org/10.1016/j.ultrasmedbio.2019.11.004>.
8. Deprez, J.; Lajoinie, G.; Engelen, Y.; De Smedt, S.C.; Lentacker, I. Opening Doors with Ultrasound and Microbubbles: Beating Biological Barriers to Promote Drug Delivery. *Adv. Drug Deliv. Rev.* 2021, 172, 9–36. <https://doi.org/10.1016/j.addr.2021.02.015>.
9. Qin, P.; Han, T.; Yu, A.C.H.; Xu, L. Mechanistic Understanding the Bioeffects of Ultrasound-Driven Microbubbles to Enhance Macromolecule Delivery. *J. Control. Release* 2018, 272, 169–181. <https://doi.org/10.1016/j.jconrel.2018.01.001>.
10. Hirokawa, T.; Karshafian, R.; Pavlin, C.J.; Burns, P.N. Insonation of the Eye in the Presence of Microbubbles: Preliminary Study of the Duration and Degree of Vascular Bioeffects-Work in Progress. *J. Ultrasound Med.* 2007, 26, 731–738. <https://doi.org/10.7863/jum.2007.26.6.731>.
11. Park, J.; Zhang, Y.; Vykhodtseva, N.; Akula, J.D.; McDannold, N.J. Targeted and Reversible Blood-Retinal Barrier Disruption via Focused Ultrasound and Microbubbles. *PLoS ONE* 2012, 7, e42754. <https://doi.org/10.1371/journal.pone.0042754>.
12. Touahri, Y.; Dixit, R.; Kofoed, R.H.; Miloska, K.; Park, E.; Raeisossadati, R.; Markham-Coultes, K.; David, L.A.; Rijal, H.; Zhao, J.; et al. Focused Ultrasound as a Novel Strategy for Noninvasive Gene Delivery to Retinal Müller Glia. *Theranostics* 2020, 10, 2982–2999. <https://doi.org/10.7150/thno.42611>.
13. Meng, Y.; Reilly, R.M.; Pezo, R.C.; Trudeau, M.; Sahgal, A.; Singnurkar, A.; Perry, J.; Myrehaug, S.; Pople, C.B.; Davidson, B.; et al. MR-Guided Focused Ultrasound Enhances Delivery of Trastuzumab to Her2-Positive Brain Metastases. *Sci. Transl. Med.* 2021, 13, eabj4011. <https://doi.org/10.1126/scitranslmed.abj4011>.

14. Lin, Y.-C.; Shih, C.-P.; Chen, H.-C.; Chou, Y.-L.; Sytwu, H.-K.; Fang, M.-C.; Lin, Y.-Y.; Kuo, C.-Y.; Su, H.-H.; Hung, C.-L.; et al. Ultrasound Microbubble–Facilitated Inner Ear Delivery of Gold Nanoparticles Involves Transient Disruption of the Tight Junction Barrier in the Round Window Membrane. *Front. Pharmacol.* 2021, 12, 1623. <https://doi.org/10.3389/fphar.2021.689032>.
15. Zhang, Z.; Li, X.; Zhang, W.; Kohane, D.S. Drug Delivery across Barriers to the Middle and Inner Ear. *Adv. Funct. Mater.* 2020, 31, 2008701. <https://doi.org/10.1002/adfm.202008701>.
16. Wang, R.; Bian, Q.; Xu, Y.; Xu, D.; Gao, J. Recent Advances in Mechanical Force-Assisted Transdermal Delivery of Macromolecular Drugs. *Int. J. Pharm.* 2021, 602, 120598. <https://doi.org/10.1016/j.ijpharm.2021.120598>.
17. Park, D.; Ryu, H.; Kim, H.S.; Kim, Y.; Choi, K.-S.; Park, H.; Seo, J. Sonophoresis Using Ultrasound Contrast Agents for Transdermal Drug Delivery: An In Vivo Experimental Study. *Ultrasound Med. Biol.* 2012, 38, 642–650. <https://doi.org/10.1016/j.ultrasmedbio.2011.12.015>.
18. Park, D.; Yoon, J.; Park, J.; Jung, B.; Park, H.; Seo, J. Transdermal Drug Delivery Aided by an Ultrasound Contrast Agent: An In Vitro Experimental Study. *Open Biomed. Eng. J.* 2010, 4, 56–62. <https://doi.org/10.2174/1874120701004010056>.
19. Liao, A.-H.; Ho, H.-C.; Lin, Y.-C.; Chen, H.-K.; Wang, C.-H. Effects of Microbubble Size on Ultrasound-Induced Transdermal Delivery of High-Molecular-Weight Drugs. *PLoS ONE* 2015, 10, e0138500. <https://doi.org/10.1371/journal.pone.0138500>.
20. Van Hout, A.; Klarenbeek, A.; Bobkov, V.; Doijien, J.; Arimont, M.; Zhao, C.; Heukers, R.; Rimkunas, R.; de Graaf, C.; Verrrips, T.; et al. CXCR4-Targeting Nanobodies Differentially Inhibit CXCR4 Function and HIV Entry. *Biochem. Pharmacol.* 2018, 158, 402–412. <https://doi.org/10.1016/j.bcp.2018.10.015>.
21. Jahnichen, S.; Blanchetot, C.; Maussang, D.; Gonzalez-Pajuelo, M.; Chow, K.Y.; Bosch, L.; De Vrieze, S.; Serruys, B.; Ulrichts, H.; Vandevelde, W.; et al. CXCR4 Nanobodies (VHH-Based Single Variable Domains) Potently Inhibit Chemotaxis and HIV-1 Replication and Mobilize Stem Cells. *Proc. Natl. Acad. Sci. USA* 2010, 107, 20565–20570. <https://doi.org/10.1073/pnas.1012865107>.
22. Hellinen, L.; Pirskanen, L.; Tengvall-Unadike, U.; Urtti, A. and Reinisalo, M. Reinisalo Retinal Pigment Epithelial Cell Line with Fast Differentiation and Improved Barrier Properties. *Pharmaceutics* 2019, 11, 412. <https://doi.org/10.3390/pharmaceutics11080412>.
23. Hellinen, L.; Hongisto, H.; Ramsay, E.; Kaarniranta, K.; Vellonen, K.-S.; Skottman, H.; Ruponen, M. Drug Flux Across RPE Cell Models: The Hunt for An Appropriate Outer Blood–Retinal Barrier Model for Use in Early Drug Discovery. *Pharmaceutics* 2020, 12, 176. <https://doi.org/10.3390/pharmaceutics12020176>.
24. Van der Meer, S.M.; Versluis, M.; Lohse, D.; Chin, C.T.; Bouakaz, A.; Jong, N. d. The Resonance Frequency of SonoVue as Observed by High-Speed Optical Imaging; *IEEE: Piscataway, NJ, USA, 2004; Volume 1, pp. 343–345.*
25. Schneider, M. Characteristics of SonoVue™. *Echocardiography* 1999, 16, 743–746. <https://doi.org/10.1111/j.1540-8175.1999.tb00144.x>.
26. De Maar, J.S.; Rousou, C.; van Elburg, B.; Vos, H.J.; Lajoinie, G.P.R.; Bos, C.; Moonen, C.T.W.; Deckers, R. Ultrasound-Mediated Drug Delivery With a Clinical Ultrasound System: In Vitro Evaluation. *Front. Pharmacol.* 2021, 12, 768436. <https://doi.org/10.3389/fphar.2021.768436>.

27. Pitkänen, L.; Ranta, V.-P.; Moilanen, H.; Urtti, A. Permeability of Retinal Pigment Epithelium: Effects of Permeant Molecular Weight and Lipophilicity. *Investig. Ophthalmology Vis. Sci.* 2005, 46, 641. <https://doi.org/10.1167/iovs.04-1051>.
28. Artursson, P.; Karlsson, J. Correlation between Oral Drug Absorption in Humans and Apparent Drug Permeability Coefficients in Human Intestinal Epithelial (Caco-2) Cells. *Biochem. Biophys. Res. Commun.* 1991, 175, 880–885. [https://doi.org/10.1016/0006-291X\(91\)91647-U](https://doi.org/10.1016/0006-291X(91)91647-U).
29. Grimes, P.A. Carboxyfluorescein: A Probe of the Blood-Ocular Barriers With Lower Membrane Permeability Than Fluorescein. *Arch. Ophthalmol.* 1982, 100, 635. <https://doi.org/10.1001/archophth.1982.01030030637022>.
30. Balla, M.M.S.; Vemuganti, G.K.; Kannabiran, C.; Honavar, S.G.; Murthy, R. Phenotypic Characterization of Retinoblastoma for the Presence of Putative Cancer Stem-like Cell Markers by Flow Cytometry. *Investig. Ophthalmology Vis. Sci.* 2009, 50, 1506. <https://doi.org/10.1167/iovs.08-2356>.
31. Frost, T.S.; Jiang, L.; Lynch, R.M.; Zohar, Y. Permeability of Epithelial/Endothelial Barriers in Transwells and Microfluidic Bilayer Devices. *Micromachines* 2019, 10, 533. <https://doi.org/10.3390/mi10080533>.
32. Fihn, B.; Sjöqvist, A.; Jodal, M. Permeability of the Rat Small Intestinal Epithelium along the Villus-Crypt Axis: Effects of Glucose Transport. *Gastroenterology* 2000, 119, 1029–1036. <https://doi.org/10.1053/gast.2000.18148>.
33. Linnankoski, J.; Mäkelä, J.; Palmgren, J.; Mauriala, T.; Vedin, C.; Ungell, A.; Lazorova, L.; Artursson, P.; Urtti, A.; Yliperttula, M. Paracellular Porosity and Pore Size of the Human Intestinal Epithelium in Tissue and Cell Culture Models. *J. Pharm. Sci.* 2010, 99, 2166–2175. <https://doi.org/10.1002/jps.21961>.
34. Venturoli, D.; Rippe, B. Ficoll and Dextran vs. Globular Proteins as Probes for Testing Glomerular Permselectivity: Effects of Molecular Size, Shape, Charge, and Deformability. *Am. J. Physiol.-Ren. Physiol.* 2005, 288, F605–F613. <https://doi.org/10.1152/ajprenal.00171.2004>.
35. Fix, S.M.; Koppolu, B.P.; Novell, A.; Hopkins, J.; Kierski, T.M.; Zaharoff, D.A.; Dayton, P.A.; Papadopoulou, V. Ultrasound-Stimulated Phase-Change Contrast Agents for Transepithelial Delivery of Macromolecules, Toward Gastrointestinal Drug Delivery. *Ultrasound Med. Biol.* 2019, 45, 1762–1776. <https://doi.org/10.1016/j.ultrasmedbio.2019.02.004>.
36. Lelu, S.; Afadzi, M.; Berg, S.; Aslund, A.K.O.; Torp, S.H.; Sattler, W.; Davies, C.D.L. Primary Porcine Brain Endothelial Cells as In Vitro Model to Study Effects of Ultrasound and Microbubbles on Blood–Brain Barrier Function. *IEEE Trans. Ultrason. Ferroelectr. Freq. Control* 2017, 64, 281–290. <https://doi.org/10.1109/TUFFC.2016.2597004>.
37. Lammertink, B.; Deckers, R.; Storm, G.; Moonen, C.; Bos, C. Duration of Ultrasound-Mediated Enhanced Plasma Membrane Permeability. *Int. J. Pharm.* 2015, 482, 92–98. <https://doi.org/10.1016/j.ijpharm.2014.12.013>.
38. De Cock, I.; Zagato, E.; Braeckmans, K.; Luan, Y.; de Jong, N.; De Smedt, S.C.; Lentacker, I. Ultrasound and Microbubble Mediated Drug Delivery: Acoustic Pressure as Determinant for Uptake via Membrane Pores or Endocytosis. *J. Control. Release* 2015, 197, 20–28. <https://doi.org/10.1016/j.jconrel.2014.10.031>.

39. Afadzi, M.; Strand, S.P.; Nilssen, E.A.; Masoy, S.-E.; Johansen, T.F.; Hansen, R.; Angelsen, B.A.; de L Davies, C. Mechanisms of the Ultrasound-Mediated Intracellular Delivery of Liposomes and Dextrans. *IEEE Trans. Ultrason. Ferroelectr. Freq. Control* 2013, 60, 21–33. <https://doi.org/10.1109/TUFFC.2013.2534>.
40. Meijering, B.D.M.; Juffermans, L.J.M.; van Wamel, A.; Henning, R.H.; Zuhorn, I.S.; Emmer, M.; Versteilen, A.M.G.; Paulus, W.J.; van Gilst, W.H.; Kooiman, K.; et al. Ultrasound and Microbubble-Targeted Delivery of Macromolecules Is Regulated by Induction of Endocytosis and Pore Formation. *Circ. Res.* 2009, 104, 679–687. <https://doi.org/10.1161/CIRCRESAHA.108.183806>.
41. Hicks, G.R.; Raikhel, N.V. Protein Import into the Nucleus: An Integrated View. *Annu. Rev. Cell Dev. Biol.* 1995, 11, 155–188. <https://doi.org/10.1146/annurev.cb.11.110195.001103>.
42. Kinoshita, M.; McDannold, N.; Jolesz, F.A.; Hynynen, K. Noninvasive Localized Delivery of Herceptin to the Mouse Brain by MRI-Guided Focused Ultrasound-Induced Blood-Brain Barrier Disruption. *Proc. Natl. Acad. Sci. USA* 2006, 103, 11719–11723. <https://doi.org/10.1073/pnas.0604318103>.
43. Raymond, S.B.; Treat, L.H.; Dewey, J.D.; McDannold, N.J.; Hynynen, K.; Bacskai, B.J. Ultrasound Enhanced Delivery of Molecular Imaging and Therapeutic Agents in Alzheimer’s Disease Mouse Models. *PLoS ONE* 2008, 3, e2175. <https://doi.org/10.1371/journal.pone.0002175>.
44. Punjabi, M.; Xu, L.; Ochoa-Espinosa, A.; Kosareva, A.; Wolff, T.; Murtaja, A.; Broisat, A.; Devoogdt, N.; Kaufmann, B.A. Ultrasound Molecular Imaging of Atherosclerosis With Nanobodies: Translatable Microbubble Targeting Murine and Human VCAM (Vascular Cell Adhesion Molecule) 1. *Arterioscler. Thromb. Vasc. Biol.* 2019, 39, 2520–2530. <https://doi.org/10.1161/ATVBAHA.119.313088>.
45. Fan, X.; Wang, L.; Guo, Y.; Tu, Z.; Li, L.; Tong, H.; Xu, Y.; Li, R.; Fang, K. Ultrasonic Nanobubbles Carrying Anti-PSMA Nanobody: Construction and Application in Prostate Cancer-Targeted Imaging. *PLoS ONE* 2015, 10, e0127419. <https://doi.org/10.1371/journal.pone.0127419>.
46. Yu, Z.; Hu, M.; Li, Z.; Dan Xu, Zhu, L.; Guo, Y.; Liu, Q.; Lan, W.; Jiang, J.; Wang, L. Anti-G250 Nanobody-Functionalized Nanobubbles Targeting Renal Cell Carcinoma Cells for Ultrasound Molecular Imaging. *Nanotechnology* 2020, 31, 205101. <https://doi.org/10.1088/1361-6528/ab7040>.
47. Murakami, T.; Yamamoto, N. Role of CXCR4 in HIV Infection and Its Potential as a Therapeutic Target. *Future Microbiol.* 2010, 5, 1025–1039. <https://doi.org/10.2217/fmb.10.67>.
48. Shi, Y.; Riese, D.J.; Shen, J. The Role of the CXCL12/CXCR4/CXCR7 Chemokine Axis in Cancer. *Front. Pharmacol.* 2020, 11, 1969. <https://doi.org/10.3389/fphar.2020.574667>.
49. Zhou, W.; Guo, S.; Liu, M.; Burow, M.E.; Wang, G. Targeting CXCL12/CXCR4 Axis in Tumor Immunotherapy. *Curr. Med. Chem.* 2019, 26, 3026–3041. <https://doi.org/10.2174/0929867324666170830111531>.
50. Ghobrial, I.M.; Liu, C.-J.; Redd, R.A.; Perez, R.P.; Baz, R.; Zavidij, O.; Sklavenitis-Pistofidis, R.; Richardson, P.G.; Anderson, K.C.; Laubach, J.; et al. A Phase Ib/II Trial of the First-in-Class Anti-CXCR4 Antibody Ulocuplumab in Combination with Lenalidomide or Bortezomib Plus Dexamethasone in Relapsed Multiple Myeloma. *Clin. Cancer Res.* 2020, 26, 344–353. <https://doi.org/10.1158/1078-0432.CCR-19-0647>.

51. Bischoff, I.; Hornburger, M.C.; Mayer, B.A.; Beyerle, A.; Wegener, J.; Fürst, R. Pitfalls in Assessing Microvascular Endothelial Barrier Function: Impedance-Based Devices versus the Classic Macromolecular Tracer Assay. *Sci. Rep.* 2016, 6, 23671. <https://doi.org/10.1038/srep23671>.
52. Bichsel, C.A.; Hall, S.R.R.; Schmid, R.A.; Guenat, O.T.; Geiser, T. Primary Human Lung Pericytes Support and Stabilize In Vitro Perfusable Microvessels. *Tissue Eng. Part A* 2015, 21, 2166–2176. <https://doi.org/10.1089/ten.tea.2014.0545>.
53. Van Dijk, C.G.M.; Brandt, M.M.; Poulis, N.; Anten, J.; van der Moolen, M.; Kramer, L.; Homburg, E.F.G.A.; Louzao-Martinez, L.; Pei, J.; Krebber, M.M.; et al. A New Microfluidic Model That Allows Monitoring of Complex Vascular Structures and Cell Interactions in a 3D Biological Matrix. *Lab. Chip* 2020, 20, 1827–1844. <https://doi.org/10.1039/D0LC00059K>.
54. Sheikov, N.; McDannold, N.; Sharma, S.; Hynynen, K. Effect of Focused Ultrasound Applied With an Ultrasound Contrast Agent on the Tight Junctional Integrity of the Brain Microvascular Endothelium. *Ultrasound Med. Biol.* 2008, 34, 1093–1104. <https://doi.org/10.1016/j.ultrasmedbio.2007.12.015>.
55. Park, J.; Zhang, Y.; Vykhodtseva, N.; Jolesz, F.A.; McDannold, N.J. The Kinetics of Blood Brain Barrier Permeability and Targeted Doxorubicin Delivery into Brain Induced by Focused Ultrasound. *J. Control. Release* 2012, 162, 134–142. <https://doi.org/10.1016/j.jconrel.2012.06.012>.
56. Keller, S.B.; Sheeran, P.S.; Averkiou, M.A. Cavitation Therapy Monitoring of Commercial Microbubbles With a Clinical Scanner. *IEEE Trans. Ultrason. Ferroelectr. Freq. Control* 2021, 68, 1144–1154. <https://doi.org/10.1109/TUFFC.2020.3034532>.

SUPPLEMENTARY MATERIAL

MATERIALS AND METHODS

Culture of endothelial cells

Human umbilical vein endothelial cells (HUVEC) were acquired from Lonza (Verviers, Belgium) and cultured in Endothelial Basal Medium (EBM-2) supplemented with growth factors (Growth Medium 2 SupplementMix®, PromoCell, Heidelberg, Germany) and 0.1% antibiotics (gentamicin/amphotericin B, Gibco, New York, USA). Cells were sub-cultured 1-2 times per week in dilution ratios between 1:3-1:6 and were used up to passage number 7.

Differentiation of endothelial cells

For the development of endothelial monolayers, polyethylene terephthalate transwell inserts were used (23.1 mm transparent membrane, pore size 0.4 μm , Corning, NY, USA), coated with 2% gelatin (w/v) in sterile PBS. For the coating, 1 mL sterile gelatin solution was added at the apical side of the insert and incubated at 37 $^{\circ}\text{C}$ for 30 minutes. Subsequently, remaining gelatin was removed and membranes were air dried in sterile conditions for 1.5 hours with the well plate lid slightly open. Coated inserts were stored at 4 $^{\circ}\text{C}$ until use but not for longer than 2 weeks. Prior to cell seeding coated inserts were thermally equilibrated with culture medium at room temperature for 15 minutes and cells were added at density of 0.12×10^6 cells/cm². Medium was added at apical and basolateral volumes of 1.5 mL and 2.7 mL, respectively. Cells were cultured for 4 days prior to the experiment and medium was refreshed the first and third day after seeding.

USMB treatment protocol of endothelial cells

In the experiments with endothelial cells HBSS was replaced by EBM-2 medium. As observed in preliminary experiments, HBSS disrupts the integrity of the endothelial monolayer.

Determination of barrier integrity and cell viability after USMB treatment

To determine the effect of USMB on the integrity of endothelial and epithelial barriers, microscopy images of cell monolayers were acquired after USMB treatment. Since endothelial cells were cultured on transparent transwell membranes, brightfield microscopy images were acquired before and after exposure to USMB (P_{neg} 0-0.7 MPa). On the other hand, epithelial cells cultured on translucent transwell membranes were

fixed with 4% PFA in PBS (w/v) for 10 minutes at room temperature after exposure to USMB (P_{neg} 0.5-0.7 MPa), stained with DAPI and imaged with a fluorescent microscope (Leica TCS SP8 X, Leica, Amsterdam, The Netherlands) at 10x and 63x magnification (excitation 360 nm, emission 410-480 nm).

The effect of USMB treatment on the viability of epithelial cells was examined using the alamarBlue™ assay (ThermoFisher Scientific). Cells were exposed to USMB at pressures 0-0.7 MPa. Immediately after USMB treatment, cells at the apical side were exposed to 0.5 mL of 500 μM resazurin sodium salt (Sigma-Aldrich) solution in PBS. Cells were incubated for 120 minutes at 37 °C at low-speed shaking at 170 rounds per minute (Heidolph Titramax 1000 incubator and shaker, Heidolph, Lelystad, The Netherlands). Next, the solution from the apical side was removed and fluorescence intensity was analyzed with a spectrofluorophotometer (FP 8300, Jasco) at excitation and emission wavelengths of 571 nm and 584/5 nm (center wavelength/bandwidth), respectively. Cell viability of each group was calculated as percentage fluorescent signal relative to that of sham treated cells.

Permeability experiments with endothelial cells and model drugs

The protocol followed for the permeability experiments using endothelial cells was the same as with epithelial cells, but culture medium was used instead of HBSS. In preliminary experiments it was observed that HBSS induced detachment of endothelial cells.

RESULTS

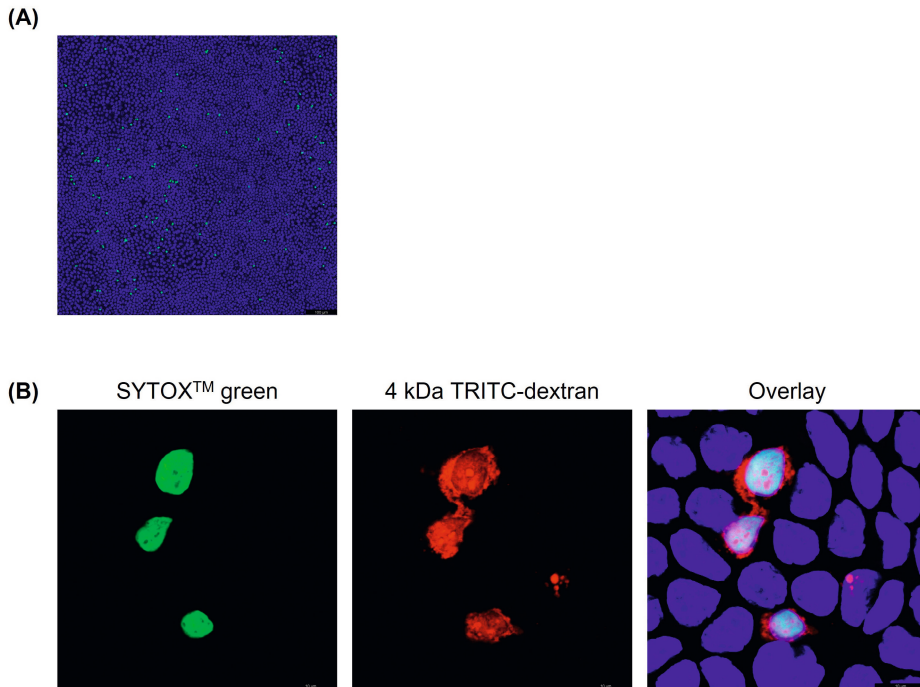


Figure S1. (A) Fluorescence image of epithelial (MDCK II) cells showing an area with intracellular accumulation of SYTOX™ green after treatment with USMB at 0.7 MPa. Cell nuclei stained with DAPI. Scale bar: 100 μm (B) SYTOX™ green positive cells (left) with simultaneous uptake of TRITC-dextran (middle) and overlay with DAPI (right). Scale bar: 10 μm

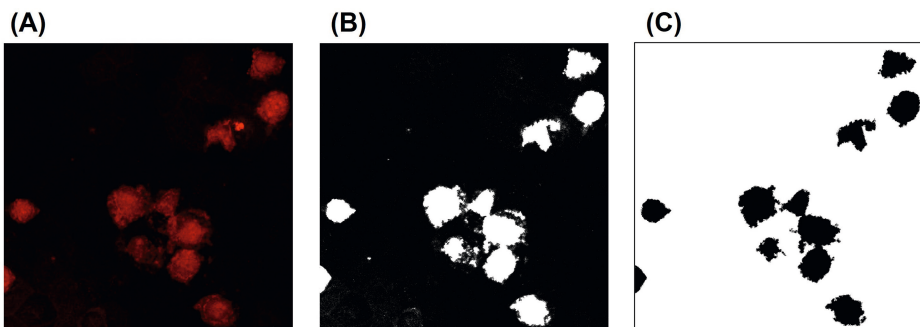


Figure S2. Summary of steps followed for the quantification of intracellular accumulation of TRITC-dextran in epithelial (MDCK II) cells. (A) Raw RGB image used to calculate fluorescence intensity in the regions of interest, (B) Thresholding of RGB image, (C) generation of mask with regions of interest (black areas). Scale bar: 10 μm

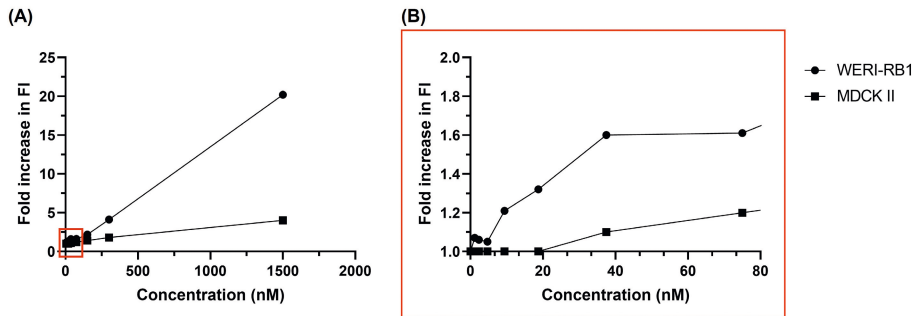


Figure S3. (A) Binding of anti-CXCR4 nanobody to retinoblastoma (WERI-RB1) and epithelial (MDCK II) cells for nanobody concentrations of 0–1500 nM. (B) Magnification of area shown in red box in (A). FI: fluorescence intensity

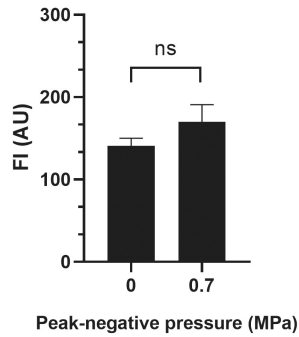


Figure S4. Binding of permeated anti-CXCR4 nanobody in retinoblastoma cells measured with flow cytometry. Nanobody was collected from the basolateral side of epithelial barriers treated with USMB at 0 or 0.7 MPa ($n = 5$). FI: fluorescence intensity, ns: not significant

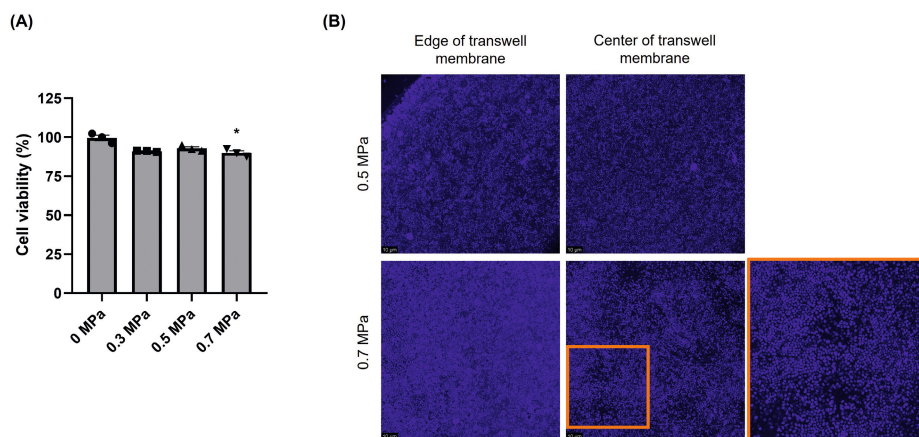


Figure S5. (A) Percentage of viable epithelial cells exposed to USMB at different ultrasound pressures (0.3–0.7 MPa) as compared to sham-treated cells ($n = 3$). Cell viability was studied using the alamarBlue™ assay after incubation of cells with resazurin solution for 120 minutes. **(B)** Fluorescence microscopy images of epithelial cell nuclear staining (DAPI) acquired at the edge (left column) and center (right column) of transwell membranes. No alterations in the integrity of the epithelial barrier were seen at 0.5 or 0.7 MPa. Uniform cell distribution without cell detachment was observed.

The effect of USMB on endothelial barrier integrity and permeability of different molecules

USMB treatment of endothelial cells at acoustic pressures equal to and higher than 0.6 MPa disrupted the endothelial barriers (figure S6, A), and therefore these pressures were excluded from the permeability study.

Unlike the epithelial barrier, USMB did not have any significant effect on the permeability of molecules across the endothelial barrier at any of the ultrasound pressures examined. Overall, comparing the permeability of the endothelial and epithelial barrier at sham treatment (figure 2 vs. supplementary figure S7B, blue bars) revealed that the P_{app} was 22 times higher for the 6-carboxyfluorescein (1.33×10^{-6} cm/s for endothelial barrier; 0.06×10^{-6} cm/s for epithelial barrier), 26 times for the 4 kDa dextran (6.26×10^{-7} cm/s for endothelial barrier, 0.24×10^{-7} cm/s for the epithelial barrier), and 20 times for the 20 kDa dextran (2.31×10^{-7} cm/s for endothelial barrier, 0.12×10^{-7} cm/s for the epithelial barrier). This indicates that endothelial cells form a leakier monolayer than epithelial cells. This is confirmed by the percentage of permeated amount of molecules across the endothelial monolayer. Specifically, 120 minutes after compound injection for the control samples, the average permeated amount of 6-carboxyfluorescein across the endothelial monolayer was almost the same as the epithelial barrier (4.06% vs. 5.14%, figure 2 vs. supplementary figure 7B, orange bars). This difference is 8 times for the 4

kDa dextran (2.05% for endothelial barrier, 0.26% for epithelial barrier) and 10 times for the 20 kDa dextran (0.79% for endothelial barrier, 0.08% for epithelial barrier).

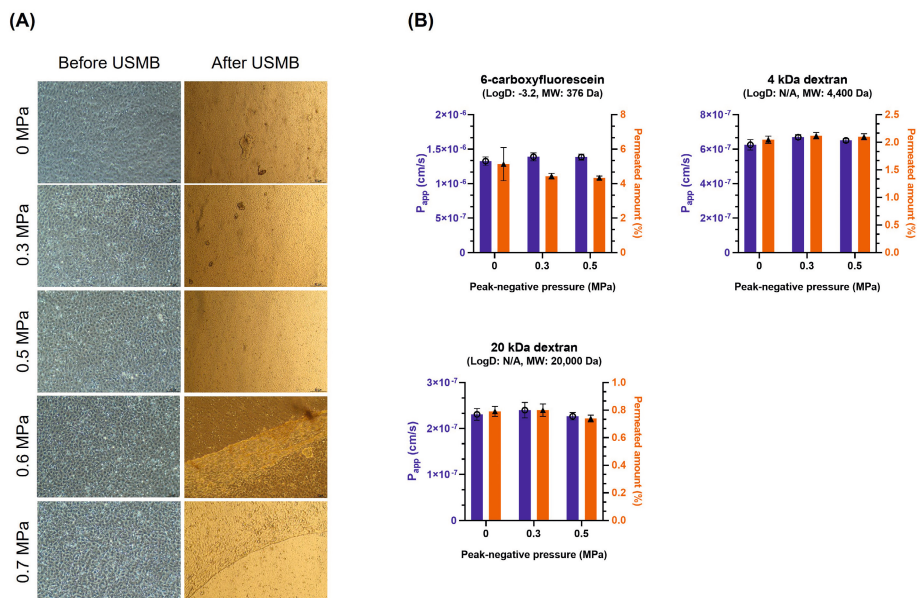


Figure S6. (A) Brightfield microscopy images of endothelial (HUVEC) barriers acquired before (left) after (right) exposure to USMB. Treatment of cells at acoustic pressures of 0.6 and 0.7 MPa resulted in extensive cell detachment and disruption of monolayer integrity. **(B)** Apparent permeability coefficient (blue bars, ○) and total amount permeated 120 minutes post-treatment (orange bars, ▲) of 6-carboxyfluorescein, 4 kDa dextran and 20 kDa dextran after treatment of endothelial cell monolayer with USMB at various acoustic pressures (n = 3).

4

A technical protocol for an experimental *ex vivo* model using arterially perfused porcine eyes

Charis Rousou¹, Piet Hoogenboom², Koen van Overdam³, Gert Storm¹, Netty Dorrestijn⁴, Enrico Mastrobattista¹

¹ Department of Pharmaceutics, Utrecht University, The Netherlands

² The Rotterdam Ophthalmic Institute, Rotterdam, The Netherlands

³ The Rotterdam Eye Hospital, Rotterdam, The Netherlands

⁴ Utrecht Centre for Affordable Biotherapeutics, The Netherlands

ABSTRACT

Ex vivo ocular perfused models have been described in the past and were applied in different mammalian species as platforms to test drug delivery systems and surgical techniques. However, reproduction of those methods is challenging because extensive and precise description of the protocols used is lacking. In this technical paper we provide a detailed description of all the steps to be followed from the enucleation of porcine eyes to cannulation of the ophthalmic artery and perfusion. This model can contribute to the reduction of use of living animals in ophthalmology research, whereas as opposed to *in vitro* models, it preserves tissue complexity and integrity.

INTRODUCTION

The unique anatomy and presence of physical and biological barriers between the different ocular tissues make drug delivery to the posterior segment of the eye one of the greatest challenges in ophthalmology. High elimination rates, tight membrane structures, the high blood flow in the choroid, and immunological responses are some of the factors that clearly indicate the need for the development of novel drug delivery technologies to target the posterior eye segment [1,2].

Efficacy and safety testing of novel drug candidates are mostly performed by using *in vitro* cell models or animal models *in vivo*. *In vitro* testing suffers from over-simplification of the complicated ocular anatomy to only one or a few cell layers and therefore very often does not take into consideration the action of the ocular barriers. Compared to the human eye, posterior ocular physiology might vary between different animal species in terms of vasculature, the cellular anatomy of the retina, the position of the optic nerve head and the area centralis [3]. Despite these anatomic differences, animal models have been extensively used in ophthalmology research because they can provide an advantage over *in vitro* testing: preservation of ocular tissue integration and functionality, which consist important requirements in pharmacokinetic studies.

A strong societal drive for reduction and even elimination of the use of living animals in pharmaceutical testing has recently arisen. In 1992, W. Russel and L. Burch described in their book “The principles of humane experimental techniques” multiple guidelines for more ethical use of animals in experimental research [4]. These principles are also known as “The 3Rs”, which abbreviates the words “Reduction”, “Replacement” and “Refinement”. In order to implement the principles of the 3Rs, various organizations and publications intend to provide advice and description of laboratory methods that can improve the welfare of laboratory animals and make the experiments more reproducible [5,6]. Apart from the ethical aspect, *in vivo* animal testing requires intensive and detailed efforts to prepare documentation for the animal ethics committee and high financial resources. As opposed to animal testing, an alternative that is in line with the principles of the 3Rs and can be particularly applied in ocular drug delivery research, is the use of *ex vivo* eye models. Fresh enucleated eyes can be obtained by animals that are sacrificed for other purposes. These can be either tissues collected after the completion of *in vivo* animal experiments as material that would be otherwise considered as waste, or as slaughterhouse material.

Extracorporeal arterially perfused eye models were introduced in the past and used to study the ocular disposition of dyes and drugs [7–10], and to validate novel instrumentation and surgical techniques [11–13]. For these models, eyes from different mammalian species were used, with feline and bovine eyes being the most frequently encountered. In 1970 Gouras and Hoff developed an extracorporeal perfused system, where retinal function and response of the optic nerve were analyzed using cat eyes [14]. Later, similar *ex vivo* systems were utilized to evaluate the retinal response as a function of perfusate flow rate, and the variation of oxygen tension gradients as a function of the distance from the retinal vessels [15,16]. Furthermore, the feline eye was used as a model to study the effect of administration of pharmaceutical compounds on the retinal function [17,18]. Similarly, electroretinographic activity was measured using *ex vivo* bovine eyes, while the influence of anoxia and hypothermia on the retinal function was studied [19]. De Coo *et al.* examined the response of the extracorporeal bovine eye in normothermic conditions and performed a viability study to determine tissue functionality under continuous perfusion [20]. However, in terms of resemblance of the anatomy of the human eye feline and bovine eyes are not the best choice.

In this report we describe in detail the preparation method of extracorporeally perfused porcine eyes as these show numerous similarities with the human eye with respect to the anatomy of the optic nerve and retinal vasculature, elasticity and size [21–23]. This method is based on cannulation of the ophthalmic artery, which originates from the internal carotid artery. The cannulation point was chosen to be just proximal of the branch of the ophthalmic artery to the anterior and posterior ciliary arteries and the central retinal artery, thus allowing for holistic perfusion of the organ (both the anterior and posterior segments). An essential requirement for successful cannulation is the preservation of the ophthalmic artery attached to the enucleated tissue. Since the ophthalmic artery runs parallel to the optic nerve, a prerequisite is preservation of at least 4 cm of the optic nerve attached to the globe. Therefore, we provide the reader with a step-by-step protocol, images and detailed videos describing how to enucleate, dissect, cannulate the ophthalmic artery and perfuse the porcine eye.

The protocol provided will allow other researchers to reproduce this *ex vivo* model, utilizing it as an experimental platform that can be used for the study of disposition of novel drugs or to validate novel surgical instrumentation/techniques. Particularly in the case of drug delivery testing, perfusion of the entire eye gives the advantage to

this model being not only limited in testing of intravenously administered therapeutics, but also expanded in other routes of administration (e.g., intravitreal, sub-retinal, etc.).

MATERIALS AND SUPPLIES

The name of suppliers and catalogue numbers of the materials and equipment used for the preparation of the system are given in Table 1, including comments on the characteristics and the quantity needed. To ensure more clarity, the materials that require specific characteristics are marked with asterisk (*), and images can be found in the supplementary material (Table S1). The preparation of the model is performed under a binocular operational microscope, with magnification that can vary between eyes from different pigs, but minimum 10×.

Table 1. Names, sources and catalogue numbers of the materials needed for the enucleation and cannulation of the eyes. The materials marked with asterisk require specific characteristics.

Material name	Source	Catalogue number	Comments
Towel forceps (*)	Karl Storz, Germany	796011	Length: 11cm, quantity: 2
Scalpel	Swan-Morton, UK	0934	Stainless steel, handle number 4
Surgical scalpel blades	Swan-Morton, UK	0311	Blade number 24, stainless steel, quantity: 2
Micro preparation forceps (*)	VWR, Netherlands	232-1917	Fine tip, length: 105 mm, quantity: 2
Micro-forceps (*)	Lawton Medizintechnik, Germany	09-0957	Superfine points, length: 11 cm, quantity: 2
Curved forceps	VWR, Netherlands	232-0106	Length: 105 mm, quantity: 2
Microscopy scissors	VWR, Netherlands	233-2123	Length: 100 mm, quantity: 1
Spring scissors (*)	Harvard Apparatus, MA, USA	728503	Vannas micro-dissecting (Eye) scissors, length: 8.5 cm, straight, spring action
Straight/dissecting forceps (*)	VWR, Netherlands	82027-388	Stainless steel, length: 114 mm quantity: 1. The opening distance of the tip should be maximum 1 cm. If it is more than 1 cm, use tape to shorten the distance of the opening.

Table 1. Continued

Material name	Source	Catalogue number	Comments
Suture	Harvard Apparatus, MA, USA	72-3336	Suture material PolyGlycolic undyed brd., length: 70 cm, 5-0. Reverse cutting, C6, length: 19 mm.
Green plastic eye holder (*)	R2Pro, Netherlands	Custom made	Diameter of cup: 2.3 cm outer diameter: 6 cm, height: 2.2 cm, quantity: 1
Black sponge eye holder (*)	R2Pro, Netherlands	Custom made	The bottom side consists by four channels with soft glue. Diameter of the cup: 3.3 cm, diameter of the cannula opening: 1.5 cm, height: 3 cm, size of channels: 7 cm x 2.1 cm, quantity: 1
Cannula (*)	Smiths Medical 800/100/100, Netherlands	02	Fine Bore LDPE (polyethylene) tubing, inner diameter: 0.28 mm, outer diameter: 0.61 mm
Needle 19 G (*)	Any		With bended tip, quantity: 1
Needle 24 G (*)	Any		Cut the sharp tip of the needle and connect with the cannula, quantity: 1
Syringe 1 mL	Any		Quantity: 2
Syringe 50 mL	Any		Quantity: 1
Contact lens (*)	Oculenti BV, Netherlands	PR98080518	Bandage lens, hydrolent 67
Coupling gel (*)	Bausch & Lomb, Belgium	8000000027	EYEFILL high dispersive (H.D.), 2% HPMC in physiological saline solution
Heparin	LEO Pharma, Netherlands	RVG 01372	Heparin natrium, final concentration 5U.I./ mL
Sodium Chloride (Normal saline)	Any		NaCl 0.9%
Tissue adhesive (*)	B. Braun, Germany	1050052	Histoacryl blue topical skin adhesive
Gelofusine	B. Braun, Germany	150347642	Succinylated gelatin 4%
Fluorescein eye drops	Bausch & Lomb, Belgium	02406497	Minims 0.5 mL, fluorescein sodium 2%, eye drops solution
Syringe pump	Fresenius vial, France	17522534	Pilot delta, quantity: 1
Cotton buds	Any		Quantity: minimum 4
Pins	Any		Quantity: minimum 8

DETAILED METHODS

In this section a detailed description of the procedures followed for enucleation, transportation, dissection and cannulation of the ophthalmic artery, and testing of perfusion is given. For more details and visual clarity, videos and images recorded during the implementation of the protocol are included. The videos are entitled as follows:

- Localization and isolation of the ophthalmic artery (Video 1)
- Preparation of the ophthalmic artery and cannulation (Video 2)
- Testing of cannulation and perfusion of the retina (Video 3)

Supplementary videos related to this article can be found at <https://doi.org/10.1016/j.exer.2019.02.003>.

Enucleation and transportation of porcine eyes

Tissue preservation in good conditions requires fast eye enucleation. To avoid blood clotting, it is preferred to enucleate the eyes directly after animal termination, immediately after dissection of the carotid arteries for bleeding. Avoid enucleation of eyes from slaughtered animals that have been exposed to heating or were immersed in a high-temperature water bath for skin cleaning and hair removal purposes, since this can cause heat-induced damage of the tissue. It is recommended that eye enucleation is performed not more than 1 hour after animal termination.

When dissecting the eye, an intact section of adequate length of the optic nerve (≥ 4 cm) should be preserved. To ensure stability and control of the ocular area during enucleation use two towel forceps. Use one of the towel forceps to close the eyelids of the eye that will be enucleated and clamp them together (Figure 1A and B). Use the other towel forceps to fix the ear at the enucleation side together with the neck skin (Figure 1C). This will ensure more free space during enucleation. Incise the skin with a scalpel at the nasal and temporal side of the eye (Figure 1D, solid lines). Use one hand to hold the towel forceps that clamps the eyelids, and the other hand to incise the skin and periocular tissues by moving the scalpel parallel to the orbital rim (Figure 1E, dashed line). At this point, the eyelids are still attached to the anterior part of the eye. Apply moderate pressure on the forceps clamping the eyelids to pull the eye slightly out of the orbital cavity. Locate the optic canal in the sphenoid bone by touch and dissect the optic nerve as deep as possible. This latter step represents the most crucial

of all the enucleation steps, because it must ensure that the length of the optic nerve (distance between the posterior side of the eye and the dissection point) is at least 4 cm. Dissect any other periocular tissues that surround the eye inside the orbital cavity (muscles, connective tissues) and pull the eye entirely out of the orbital cavity. Remove the attached periocular tissues from the anterior part (eyelids, lacrimal gland, etc.). Immerse the eye in heparinized saline (final concentration 5 units/mL) stored at 0 °C (melting ice) to decrease the metabolic activity of the tissues. Repeat the procedure to collect more eyes.

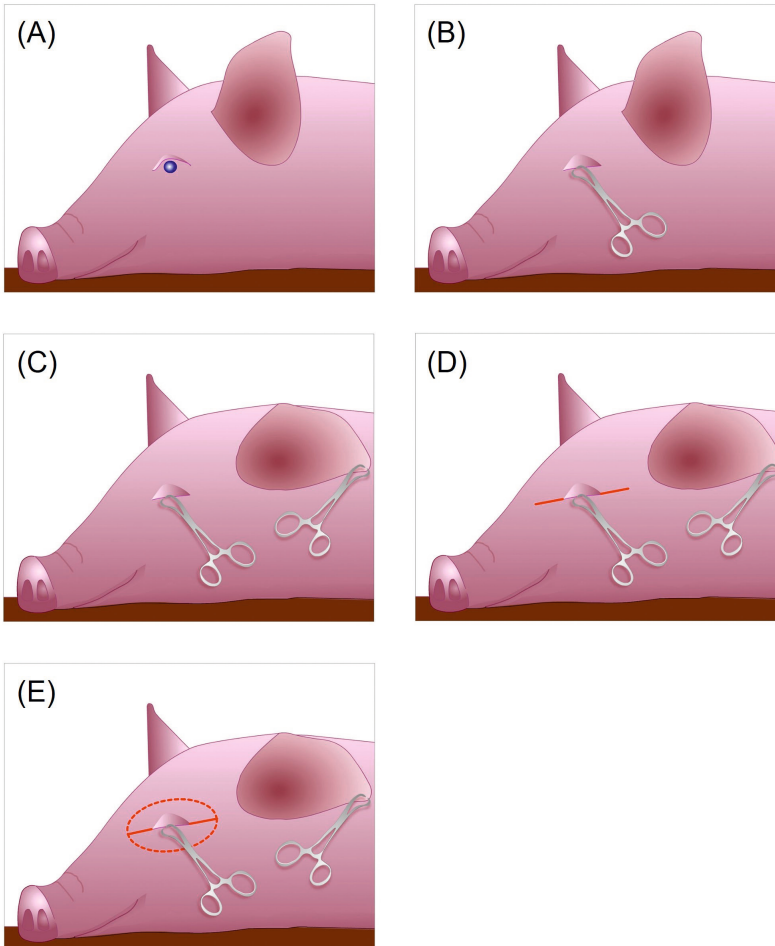


Figure 1. Schematic representation of the incision steps followed for the enucleation of the eye. **(A, B)** Use a towel forceps to close the eyelids and clamp them together. **(C)** Use the second forceps to clamp the ear at the enucleation side with the neck skin to ensure more free space. **(D)** By using a scalpel two incisions are made towards the nasal and temporal side of the eye and **(E)** subsequently the skin and periocular tissues are incised parallel to the orbital rim.

Based on our experience, even if only one eye is required for the experiment, six to eight eyes should be enucleated on the same day. Especially at the first stages of the training on this method, approximately 50% of the eyes collected are damaged and not appropriate for perfusion. More details on how to recognize the eyes that are damaged can be found in Section 4, “Potential pitfalls, trouble shooting and discussion”. The time interval between harvesting and preparation of the *ex vivo* model has to be as short as possible and should never exceed 6 hours.

Transportation of slaughterhouse material to university laboratories in the Netherlands requires yearly registration of a transportation document to the “Netherlands food and consumer product safety authority (NVWA)”. In that document the researcher is obliged to report the type and biosafety level of the animal tissue transported, the average amount of tissue expected to be transported each time, the name and contact details of the transporter, and the address, contact details and license number of the abattoir. This document should always be available for presentation in case of inspection. In addition, records of the number of enucleated eyes obtained each time should be kept. It is important to note that regulations concerning the transportation of slaughterhouse material might vary between different countries.

Dissection and cannulation of the ophthalmic artery

When ready to start the dissection and cannulation procedures, compare all the eyes that have been obtained and start with the one that has a considerable length of the optic nerve preserved, as well as the surrounding connective tissue. Locate the eye into the rigid plastic holder with the anterior part (i.e., cornea) touching the holder cup and the optic nerve facing upwards (Figure 2).



Figure 2. Enucleated porcine eye positioned inside the plastic eye holder with the anterior segment (e.g., cornea) facing downwards. The optic nerve is approximately 4 cm in length. The ophthalmic artery is normally located into the connective tissue indicated by the middle arrow.

Localization and isolation of the ophthalmic artery

A schematic representation of the main arteries within the ocular vascular network is shown in Figure 3. The ophthalmic artery (diameter 0.8 mm) can be cannulated just proximal of the branching point of the short and long posterior ciliary arteries, and the central retinal artery, as shown with the black arrow in Figure 3. Use the two micro-preparation forceps with fine tip to carefully remove the connective and muscle tissues, and isolate the ophthalmic artery (Video 1, 00:08–01:03). The artery wall appears white in color, slightly transparent and usually contains remaining native blood (Video 1, 01:04–01:15). Once the ophthalmic artery is isolated, remove any remaining surrounding tissue with the use of two micro-forceps, until the blood vessel is entirely stripped (Figure 4 and Video 1, 01:16–02:25). To prevent vessel damage due to dryness, moisture the tissue at regular intervals (especially when the artery is stripped) with a cotton bud that is wetted with saline.

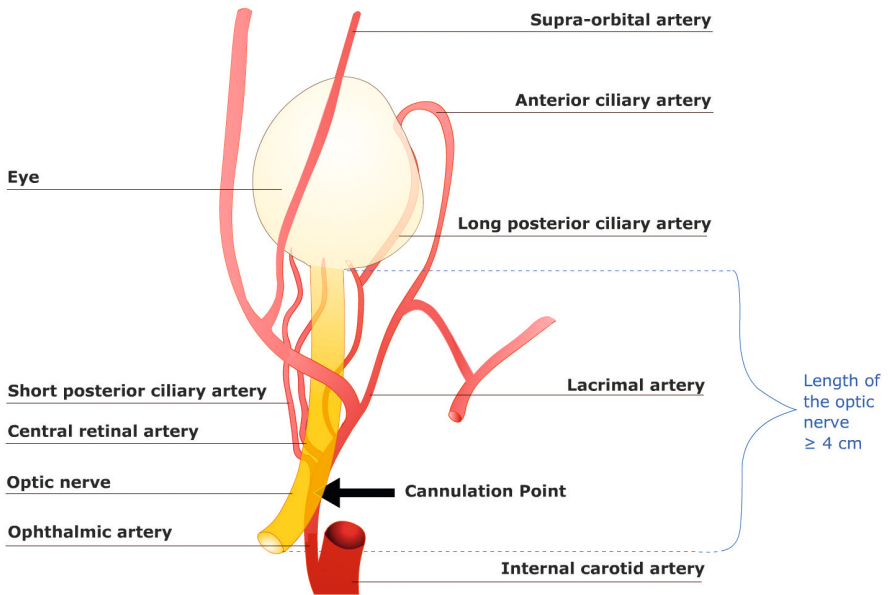


Figure 3. Schematic representation of the ophthalmic artery and its branches originating from the internal carotid artery. The point where dissection and cannulation is performed is just proximal of the branching point of the short and long posterior ciliary arteries, and the central retinal artery (black arrow). Yellow: optic nerve, white: eye, red: arteries

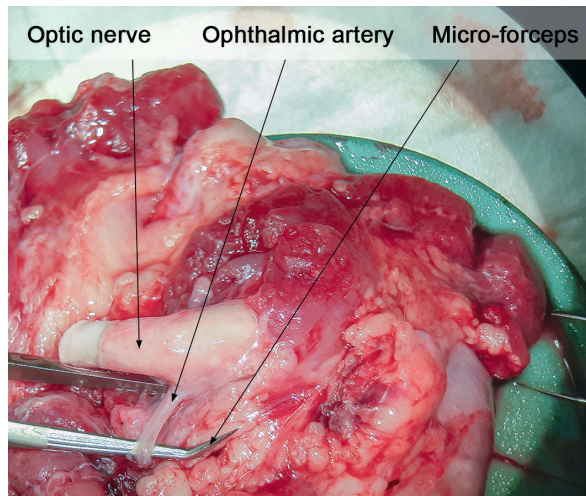


Figure 4. Isolated ophthalmic artery cleaned by the surrounding connective tissue using micro-forceps.

Preparation of the ophthalmic artery and cannulation

Keep the artery stretched without applying excessive tension by using a straight forceps (Figure 5A and Video 2, 00:12–00:27). Make a small incision on the longitudinal axis of the blood vessel using spring scissors (Figure 5B and Video 2, 00:28–00:33), and loosen the incision with the bended-tip needle (19 G), which is connected to a 1 mL empty syringe. If the incision is not large enough for the needle tip to penetrate into the vessel, make the cut larger (Video 2, 00:34–01:20). Subsequently, lift the upper vessel wall by pulling the syringe upwards, loosen the blood vessel wall and gently remove the needle. Fill the second 1 mL syringe with saline, remove air bubbles, and connect it to the cannula. With one hand, using the bended-tip needle, lift the upper wall of the vessel slightly. With the other hand, keep the cannula near the front end with curved forceps, oriented parallel to the artery, and simultaneously insert it into the vessel (Video 2, 01:21–01:27). The tip of the cannula must be pointing towards the direction of the optic nerve that enters the eye (Figure 5C). Using the second curved forceps, gently press the blood vessel walls on the cannula and at the same time insert the cannula tube further in the vessel. The cannula should be placed 0.5–1 cm in the artery (Figure 5C and Video 2, 01:28–01:38). Make a tight, double knot to ensure that the cannula is stably fixed in the blood vessel (Figure 5D and Video 2, 01:39–01:43). Release the vessel from the straight forceps and add 3–4 drops of tissue adhesive (Figure 5E and Video 2, 01:44–01:56). Wait for 1 minute for the tissue adhesive to dry. This will ensure that the connection is tight enough and any leakage during perfusion is prevented.

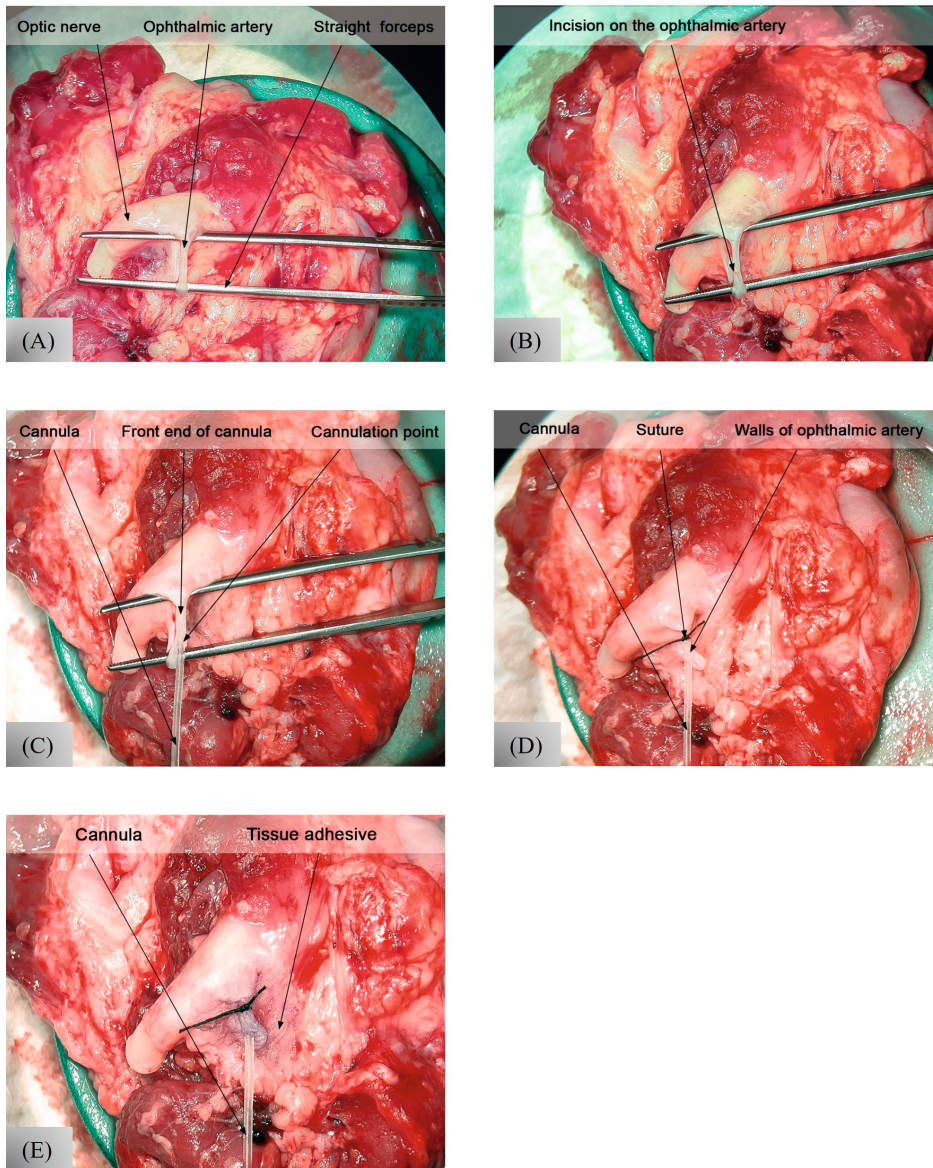


Figure 5. Cannulation steps: **(A)** the ophthalmic artery is kept stretched using straight forceps and **(B)** an incision is made using spring scissors. **(C)** The cannula is subsequently inserted in the artery, with 0.5–1 cm of its front end surrounded by the artery walls. **(D)** Suture is used to fix the cannula and **(E)** 3–4 tissue adhesive drops are added to ensure tight cannulation.

Testing of cannulation and perfusion of the eye

During perfusion the eye should be kept in humid environment e.g., inside a custom-made, sponge eye holder wetted with saline (Figure 6A). Disconnect the cannula from

the syringe, pass it through the holder hole, and place the holder on top of the eye so that the posterior segment of the eye is inside the cup of the holder. After this step the eye is positioned between the two holders (the green plastic holder is below and the black sponge holder is on top). The cannula should be placed parallel to one of the four channels of the holder. Apply slight pressure on the cannula to ensure that it is fixed in the holder channel (Figure 6A). Carefully flip the holder and the eye so that the anterior part is facing upwards (Figure 6B). Insert pins to fix the periocular tissues on the sponge holder, having the cornea aligned in the center of the holder. To further improve the microscopic examination of the retinal blood vessels during perfusion, a contact lens is used to increase the magnification. Add a few drops of coupling gel on top of the cornea and place the contact lens on top of it. Avoid entrapping air bubbles between the gel and the lens. Adjust the microscope focus to have a clear image of the retinal blood vessels and the optic disc (Figure 6B).

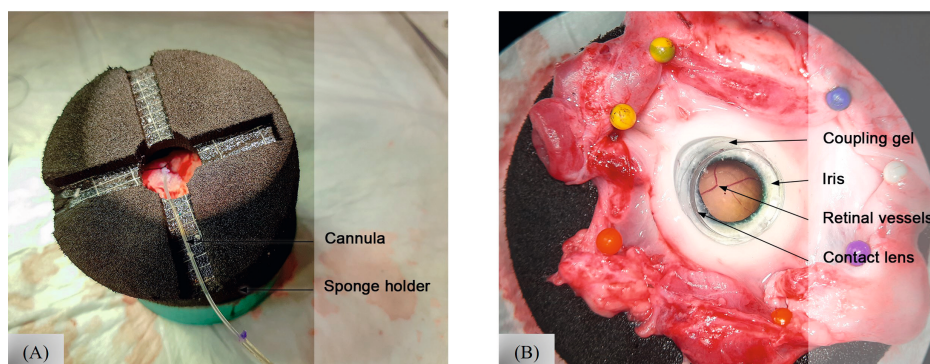


Figure 6. (A) The eye is placed inside the sponge holder, which is wetted with normal saline in order to keep the tissues in physiologic humid conditions. The cannula is fixed in the holder channel that is parallel to the ophthalmic artery. (B) The holder is flipped with the anterior tissues of the eye facing upwards, and pins are used to fix the periocular tissues. The cornea is centrally aligned. Coupling gel is added on the surface of cornea and a contact lens is used to improve the field of view of the retina. The microscope focus is adjusted to have a clear image of the optic disc and the retinal blood vessels before the injection of the perfusion test solution.

Successful cannulation can be confirmed by perfusing the eye with a dye, e.g., fluorescein. To maintain the volume of blood in the blood vessels and prevent the formation of blood clots, a perfusion test solution containing gelofusine and heparin is used. For the preparation of the perfusion test solution add 0.18 mL fluorescein eye drops and 5000 units of heparin in 100 mL of gelofusine. Fill the 50 mL syringe with the test solution, eliminate air bubbles and connect it to the syringe pump. Disconnect the cannula from the 1 mL syringe and connect it to the 50 mL syringe. Connect the

syringe to the pump and initiate perfusion of the test solution at a flow rate of 0.1 mL/minute. After a few seconds the retinal arteries can be seen filled with the dye if the cannulation is successful. While the arteries are filled, move the contact lens and scan the entire retina. A few seconds later, the retinal veins will be filled with the dye too. Check the cannulation point for leakage. If there is no leakage at the cannulated area and the vessels are normally filled with dye, continue perfusing with the test solution, or any other solution that is desired for circulation.

An example of how to test the cannulation and initiate perfusion is given in Video 3. In this example cannulation was initially tested with perfusion with saline. Note that at the start of the injection, first the native blood that is present in the retinal vessels is rinsed out (Video 3, 00:14–00:34). Subsequently, perfusion test solution containing fluorescein was perfused. Note that the dye first arrives in the retinal arteries, which appear smaller in diameter, followed by perfusion of the retinal veins (Video 3, 00:39–00:54).

DISCUSSION, POTENTIAL PITFALLS AND TROUBLESHOOTING

In general, preparation of this system is a process that requires training in many aspects: the correct enucleation of the eyes, isolation of the ophthalmic artery, cleaning the ophthalmic artery from surrounding tissues, and cannulation. The target blood vessel for cannulation is the ophthalmic artery, which emerges from the internal carotid artery, and later branches to the ocular and orbital group of arteries (Figure 3). The ophthalmic artery runs parallel to the optic nerve, and lies proximal of the branching point of the short and long posterior ciliary arteries, and the central retinal artery. Enucleation of eyes should be performed only by a person who has been trained, since a sufficient length of the optic nerve is a crucial prerequisite for preservation of the arterial part that consists the ophthalmic artery.

In the beginning of the training, the cannulation steps can be practiced using eyes that are not necessarily obtained from a slaughterhouse, for instance from laboratory animals that have been euthanized for other research purposes. The eyes used for training can be either fresh or non-fresh, but the tissues must always be at room temperature when the procedure starts. However, perfusion of the test solution most likely will not be successful on freeze-stored eyes because of blood clots that might block the blood vascular network. When the researcher feels comfortable with isolation of the ophthalmic artery on non-fresh eyes, he/she should immediately start practicing

on fresh eyes, since the texture and the color of fresh tissues differ from tissues that underwent freezing and defrost procedures (fresh tissues are softer and color is more reddish since blood is still present). The procedure of enucleation in an abattoir directly after animal termination can be stressful and requires handling in a limited amount of time. Therefore, it is recommended to collect as many eyes as possible, since most likely not all of them will be suitable for cannulation. We recommend to collect at least three times the number of eyes needed for experimentation, especially at the initial training stages.

In the literature there is a discrepancy regarding the duration of time between animal termination and enucleation of the eyes. In the study of Abarca *et al.* porcine eyes were enucleated after animal euthanasia and were cannulated within 15 minutes [7], while in the study of Gouras *et al.* feline eyes were cannulated 3–10 minutes after euthanasia [14]. In two studies where bovine eyes were used [8,20], the authors report blood vessel cannulation 1 hour and 2 hours after animal termination, respectively. However, the time window between animal termination and enucleation is not defined. In the present protocol, enucleation is recommended in animals whose carotid arteries were punctured for bleeding after death. Therefore, the blood is removed from the vascular network and formation of blood clots is limited. In a study where blood samples were obtained from human cadavers 1 hour post mortem, fluid and coagulated blood was found regardless of the cause of death [24]. Thus, if bleeding is not possible to be performed after animal death, the enucleation procedure should be completed as fast as possible after termination, but preferably not later than an hour.

It is useful to check all the enucleated eyes before starting the dissection process and discard those that are not in a proper condition. Some examples are: eyes whose optic nerve is too short, the optic nerve or proximal tissues are damaged, the meningeal sheath is detached from the optic nerve, the cornea is damaged. In addition, in the case that the isolation of the ophthalmic artery takes excessive amount of time, it is a good practice to switch to another eye that is in good condition. Based on our experience, approximately 60% of the enucleated eyes are in proper condition for cannulation, and 70% of the total amount of eyes in good condition is successfully cannulated by a trained person.

Another important point is the distinction of retinal artery from retinal vein, which run alongside the optic nerve. As a general rule, veins have thinner and more elastic walls,

whereas arteries have thicker walls, therefore the remaining, native blood is less visible. In case the artery is isolated but its ending is detached from the optic nerve, make a knot to fix the free ending of the artery on the optic nerve.

If the preserved part of the ophthalmic artery is not long enough for cannulation and it is too proximal to the branching point of the short and long posterior ciliary arteries, and the central retinal artery, cannulation of the branch of the central retinal artery can be an alternative. However, it is recommended to avoid this because the ocular tissues perfused by the lacrimal artery (e.g., conjunctiva) and long and short posterior ciliary arteries (e.g., posterior uveal tract) will not be perfused (Figure 3).

In case the perfusion is tested successfully without leakage in the cannulated area being observed, but nevertheless fluorescein is not visible in the retinal blood vessels, most likely a different vessel rather than the ophthalmic artery or the central retinal artery has been cannulated. Check if fluorescein is visible in other parts of the eye (e.g., if the sclera becomes colored). If that is the case, disconnect the cannula and search for the ophthalmic artery. If not, the presence of blood clot(s) in the ophthalmic artery might be blocking the perfusion. However, using the protocol described above, we have never experienced any perfusion issues due to blood coagulation in the ophthalmic artery.

This system can be further expanded or adapted depending on the intended objectives of the experimental study. Particularly in applications where longer perfusion periods are needed, heparinized porcine blood or physiological buffers enriched with nutrients (e.g., Krebs-Henseleit solution) can be used for perfusion. If gas mixtures are necessary (e.g., O₂, CO₂) then the syringe pump can be replaced by a peristaltic pump. The physiological solution can be mixed and saturated with gases prior to the cannulation point. Adjusting the temperature to physiological conditions can be achieved by pre-heating the tubing of the system using a heat exchanger just prior to the cannulation point. Additionally, the eye can be placed inside a container that is heated at 37 °C.

One limitation of the system described is that it only consists of an inlet (cannulation of the ophthalmic artery), with the venous drainage (outflow) being free. In this case the system is open. As a consequence, the perfused substances are not re-circulated. If a closed system is required (e.g., to evaluate the distribution of pharmaceutical compounds), the eye can be placed in a container in which all outflow fluids will be collected and analyzed. The syringe pump should then be replaced by a peristaltic pump, which will re-circulate the outflow fluids back to the inlet point.

The duration of tissue viability when physiological buffers are perfused can be evaluated over time with various methods, depending on the specific application. Some examples are: (i) activity of lactate dehydrogenase (LDH), (ii) measurement of the blood (or perfused solution) flow using Doppler ultrasonography, (iii) measurement of the intra-ocular pressure (IOP) and (iv) histological evaluation of tissue deterioration. If the system is used to test new surgery equipment, viability of tissues is required normally for shorter periods.

Synergistic or antagonistic interactions between heparine and antibiotics, phenothiazines and anti-inflammatory agents have been previously reported [25]. Therefore, if the system is utilized in pharmaceutical testing, any possible interactions between heparine and the compound under investigation should be examined in advance. No other heparin complications that could affect the functionality of the *ex vivo* system are known.

Hypothermic storage of eyes obtained post-mortem for keratoplasty purposes in humans requires storage of tissue in culture medium at 2–6 °C [26]. At these conditions tissue can be preserved for 7–10 days. Reinhard *et al.* investigated the post-mortem ganglion function using multielectrode arrays in enucleated minipig eyes [27]. According to this study, ganglion activity was maintained for at least 50 hours when the eyes were stored at ischemic and hypothermic conditions (4 °C). To the best of our knowledge, data describing the speed of the post-mortem deterioration of the posterior ocular segment and retinal detachment is lacking from the literature. The maximum time window between enucleation and preparation we tested was 6 hours. During this period no evidence of tissue deterioration was observed. However, a viability study in order to measure the exact time frame for successful hypothermic preservation of porcine eyes in heparinized saline will be performed in the future.

CONCLUSION

In this report a detailed description of the method for enucleation and arterial perfusion of porcine eyes is given, supported by images and videos. This method can open new directions in the field of ophthalmology research by providing an alternative to *in vitro* and *in vivo* animal testing, using a cost- and time-effective protocol, and contributing to the reduction of laboratory animals in experimental research (the principles of the 3Rs).

REFERENCES

1. Díaz-Coránguez, M.; Ramos, C.; Antonetti, D.A. The Inner Blood-Retinal Barrier: Cellular Basis and Development. *Vision Res.* 2017, *139*, 123–137, doi:10.1016/j.visres.2017.05.009.
2. Del Amo, E.M.; Rimpelä, A.-K.; Heikkinen, E.; Kari, O.K.; Ramsay, E.; Lajunen, T.; Schmitt, M.; Pelkonen, L.; Bhattacharya, M.; Richardson, D.; et al. Pharmacokinetic Aspects of Retinal Drug Delivery. *Prog. Retin. Eye Res.* 2017, *57*, 134–185, doi:10.1016/j.preteyeres.2016.12.001.
3. Vézina, M. Comparative Ocular Anatomy in Commonly Used Laboratory Animals. In *Assessing Ocular Toxicology in Laboratory Animals*; Weir, A.B., Collins, M., Eds.; Humana Press: Totowa, NJ, 2012; pp. 1–21 ISBN 978-1-62703-163-9, 978-1-62703-164-6.
4. Russell, W.M.; Burch, R.L. The Principles of Humane Experimental Technique. *Med. J. Aust.* 1960, *1*, 500–500, doi:10.5694/j.1326-5377.1960.tb73127.x.
5. Singh, J. The National Centre for the Replacement, Refinement, and Reduction of Animals in Research. *J. Pharmacol. Pharmacother.* 2012, *3*, 87–89.
6. De Boo, J.; Hendriksen, C. Reduction Strategies in Animal Research: A Review of Scientific Approaches at the Intra-Experimental, Supra-Experimental and Extra-Experimental Levels. *Altern. Lab. Anim.* 2005, *33*, 369–377, doi:10.1177/026119290503300404.
7. Abarca, E.M.; Salmon, J.H.; Gilger, B.C. Effect of Choroidal Perfusion on Ocular Tissue Distribution After Intravitreal or Suprachoroidal Injection in an Arterially Perfused *Ex Vivo* Pig Eye Model. *J. Ocul. Pharmacol. Ther.* 2013, *29*, 715–722, doi:10.1089/jop.2013.0063.
8. Koeberle, M.J.; Hughes, P.M.; Skellern, G.G.; Wilson, C.G. Pharmacokinetics and Disposition of Memantine in the Arterially Perfused Bovine Eye. *Pharm. Res.* 2006, *23*, 2781–2798, doi:10.1007/s11095-006-9106-2.
9. Blue, R. Optical System for Drug Detection in the Anterior Chamber of the Eye.; IEE, 1997; Vol. 1997, pp. 9–9.
10. Niemeyer, G. Retinal Research Using the Perfused Mammalian Eye. *Prog. Retin. Eye Res.* 2001, *20*, 289–318, doi:10.1016/S1350-9462(00)00029-X.
11. Van Overdam, K.A.; Kilic, E.; Verdijk, R.M.; Manning, S. Intra-Ocular Diathermy Forceps. *Acta Ophthalmol. (Copenh.)* 2018, *96*, 420–422, doi:10.1111/aos.13619.
12. Chen, Y.; Wu, W.; Zhang, X.; Fan, W.; Shen, L. Feasibility Study on Retinal Vascular Bypass Surgery in Isolated Arterially Perfused Caprine Eye Model. *Eye* 2011, *25*, 1499–1503, doi:10.1038/eye.2011.197.
13. Townsend, R.; Cringle, S.J.; Morgan, W.H.; Chauhan, B.C.; Yu, D.-Y. Confocal Laser Doppler Flowmeter Measurements in a Controlled Flow Environment in an Isolated Perfused Eye. *Exp. Eye Res.* 2006, *82*, 65–73, doi:10.1016/j.exer.2005.05.003.
14. Gouras, P.; Hoff, M. Retinal Function in an Isolated, Perfused Mammalian Eye. *Invest. Ophthalmol.* 1970, *9*, 388–399.
15. Niemeyer, G. ERG Dependence on Flow Rate in the Isolated and Perfused Mammalian Eye. *Brain Res.* 1973, *57*, 203–207, doi:10.1016/0006-8993(73)90577-5.
16. Alder, V.A.; Niemeyer, G.; Cringle, S.J.; Brown, M.J. Vitreal Oxygen Tension Gradients in the Isolated Perfused Cat Eye. *Curr. Eye Res.* 1986, *5*, 249–256, doi:10.3109/02713688609020050.

17. Sandberg, M.A.; Pawlyk, B.S.; Crane, W.G.; Schmidt, S.Y.; Berson, E.L. Effects of IBMX on the ERG of the Isolated Perfused Cat Eye. *Vision Res.* 1987, *27*, 1421–1430, doi:10.1016/0042-6989(87)90152-0.
18. Thoreson, W.B.; Purple, R.L. Effects of Using the Oxygen-Carrying Fluorocarbon, FC43, on the ERG of the Arterially Perfused Cat Eye. *Curr. Eye Res.* 1989, *8*, 487–498, doi:10.3109/02713688909000029.
19. Tazawa, Y.; Seaman, A.J. The Electroretinogram of the Living Extracorporeal Bovine Eye. The Influence of Anoxia and Hypothermia. *Invest. Ophthalmol.* 1972, *11*, 691–698.
20. De Coo, F.A.M.; Zonnenberg, B.A.; Trap, N.H. Prolonged Normothermic Perfusion of the Isolated Bovine Eye: Initial Results. *Curr. Eye Res.* 1993, *12*, 293–301, doi:10.3109/02713689308999453.
21. Coile, D.C.; O’Keefe, L.P. Schematic Eyes for Domestic Animals. *Ophthalmic Physiol. Opt.* 1988, *8*, 215–219, doi:10.1111/j.1475-1313.1988.tb01040.x.
22. Simoens, P.; De Schaepdrijver, L.; Lauwers, H. Morphologic and Clinical Study of the Retinal Circulation in the Miniature Pig. A: Morphology of the Retinal Microvasculature. *Exp. Eye Res.* 1992, *54*, 965–973, doi:10.1016/0014-4835(92)90161-K.
23. Vestre, W.A. Porcine Ophthalmology. *Vet. Clin. North Am. Large Anim. Pract.* 1984, *6*, 667–676, doi:10.1016/S0196-9846(17)30016-2.
24. Mole, R.H. Fibrinolysin and the Fluidity of the Bloodpost Mortem. *J. Pathol. Bacteriol.* 1948, *60*, 413–427, doi:10.1002/path.1700600308.
25. Colburn, W.A. Pharmacologic Implications of Heparin Interactions with Other Drugs. *Drug Metab. Rev.* 1976, *5*, 281–293, doi:10.3109/03602537609029980.
26. Elisabeth, P.; Hilde, B.; Ilse, C. Eye Bank Issues: II. Preservation Techniques: Warm versus Cold Storage. *Int. Ophthalmol.* 2008, *28*, 155–163, doi:10.1007/s10792-007-9086-1.
27. Reinhard, K.; Mutter, M.; Gustafsson, E.; Gustafsson, L.; Vaegler, M.; Schultheiss, M.; Müller, S.; Yoeruek, E.; Schrader, M.; Münch, T.A. Hypothermia Promotes Survival of Ischemic Retinal Ganglion Cells. *Investig. Ophthalmology Vis. Sci.* 2016, *57*, 658, doi:10.1167/iovs.15-17751.

SUPPLEMENTARY MATERIAL

Table S1. Images of the materials marked with asterisk (*) in Table 1.





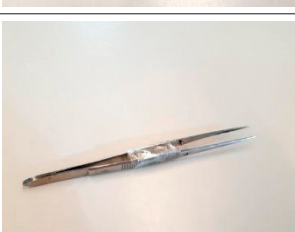
Material name	Picture
Towel forceps	 A pair of large, silver metal towel forceps with long handles and curved tips, resting on a white surface.
Micro preparation forceps	 A pair of small, silver metal micro preparation forceps with long handles and fine, pointed tips, resting on a white surface.
Micro-forceps	 A pair of small, silver metal micro-forceps with long handles and fine, pointed tips, resting on a white surface.
Spring scissors	 A pair of silver metal spring scissors with long handles and curved tips, resting on a white surface.
Straight/dissecting forceps	 A pair of silver metal straight/dissecting forceps with long handles and fine, pointed tips, resting on a white surface.

Table S1. Continued.



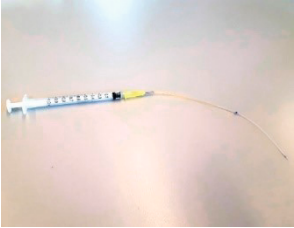

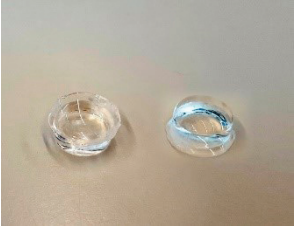


Material name	Picture
Green plastic eye holder	 Three green plastic eye holders, each with a central hole and a small notch on the side, arranged in a row.
Black sponge eye holder	 Two black sponge eye holders, one with a central hole and the other with a cross-shaped hole, arranged side-by-side.
Cannula connected to a 24 G needle. The sharp tip of the needle is removed before connected to the cannula. The needle tip is connected to a 1 ml syringe.	 A cannula connected to a 24 G needle, with the sharp tip removed. The needle tip is connected to a 1 ml syringe.
Needle 19 G with bended tip	 A 19 G needle with a bended tip, connected to a syringe.
Contact lens	 Two contact lenses, one clear and one blue, arranged side-by-side.

Table S1. Continued.

Material name	Picture
Coupling gel	
Tissue adhesive	

5

Microbubble-mediated drug delivery in the retina using a clinical ultrasound system

Charis Rousou ^{1,2}, Nicky van Kronenburg ³, Chrit Moonen ², Gert Storm ^{1,4,5}, Enrico Mastrobattista ¹, Roel Deckers ²

¹ Department of Pharmaceutics, Utrecht University, The Netherlands

² Imaging and Oncology Division, University Medical Center Utrecht, The Netherlands

³ Department of Translational Neuroscience, University Medical Center Utrecht, The Netherlands

⁴ Department of Surgery, National University of Singapore, Singapore

⁵ Department of Biomaterials Science and Technology, University of Twente, The Netherlands

Manuscript in preparation

ABSTRACT

Drug delivery to the retina is one of the major challenges in ophthalmology due to the unique anatomical characteristics of the eye and the biological barriers that protect it from harmful substances in the body. Despite the advancement in ocular therapeutics, there are many unmet needs for the treatment of retinal diseases. Ultrasound and microbubbles (USMB) have been proposed as a minimally invasive method for improving delivery of drugs in the retina from the blood circulation. This study aimed to investigate the efficacy of USMB in the delivery of model drugs (molecular weight varying from 600 Da to 20 kDa) in the retina of *ex vivo* porcine eyes. A clinical ultrasound system in combination with microbubbles approved for clinical ultrasound imaging were used for the treatment. Intracellular accumulation of model drugs was observed in the cells lining blood vessels in the retina and choroid of eyes treated with USMB but not in eyes that received ultrasound only. Specifically, 25.6 ± 2.9 % of cells had intracellular uptake at mechanical index (MI) of 0.2 and 34.5 ± 6.0 % at MI of 0.4. These results demonstrate that USMB can be used as a minimally invasive and targeted means to induce intracellular accumulation of drugs for the treatment of retinal diseases.

INTRODUCTION

Albeit the advancement in ocular therapeutics, retinal drug delivery is yet one of the major challenges in ophthalmology. Retinal diseases such as age-related macular degeneration (AMD) and diabetic retinopathy (DR) are typically treated with intravitreal injection of drugs. This delivery method is unpleasant and is often related to side effects, including retinal detachment, increase of intraocular pressure and retinal hemorrhages [1,2]. Another example of an open challenge is in the treatment of retinoblastoma, which is commonly cured with intravenous or intraarterial injection of chemotherapeutic agents. This therapeutic approach is often associated with inadequate delivery of drugs to the target cells, resulting in the presence of subretinal and vitreous seeds that cause recurrent and chemoresistant tumors [3]. These examples highlight the need for novel and less invasive drug delivery approaches that enable targeted treatment of retinal diseases.

The combination of ultrasound and microbubbles (USMB) has been shown to improve the efficacy and targeting of drug delivery to the retina. Previous studies have shown the potential of USMB to induce transient disruption of the blood-retina barrier (BRB). The *in vivo* animal studies of Hirokawa *et al.* and Park *et al.* focused on the USMB-induced extravasation of small molecules (fluorescein; molecular weight 332 Da, and gadolinium; molecular weight 938 Da) from the retinal blood vessels [4,5]. Park *et al.* reported that BRB disruption was restored within 3.5 hours after USMB treatment, highlighting the reversibility of the effect. Furthermore, USMB-induced extravasation of macromolecules (molecular weight 66-970 kDa) and gene delivery to the retina Müller glial cells was recently shown [6]. While the above studies provided invaluable insights on the activity of USMB on the disruption of the BRB, the effect on intracellular drug delivery is yet to be investigated.

This *ex vivo* study aimed to examine the effect of USMB on the intracellular accumulation of membrane-impermeable fluorescent molecules, both small (SYTOX™ green) and large (4 and 20 kDa dextrans) in the posterior eye. To this end, a clinical ultrasound system (iU22) was used in combination with clinically approved microbubbles (SonoVue™) to perform USMB therapy in arterially perfused porcine eyes.

MATERIALS AND METHODS

Chemicals

Fluorescent-conjugated dextrans (TRITC-dextran 4,400 Da; T1037 and TRITC-dextran 20,000 Da; 73766), histology mounting medium containing DAPI (Fluoroshield™ with DAPI, F6057), paraformaldehyde (PFA, 158127), formaldehyde (100496) and sucrose (S8501) were acquired from Sigma-Aldrich (Steinheim, Germany). SYTOX™ green (S7020) was obtained by ThermoFisher Scientific (Waltham, MA, USA).

Preparation and cannulation of perfused eyes

Enucleation and cannulation of porcine eyes was performed as previously described in Chapter 4. In brief, eyes were dissected directly after animal termination and transported to the laboratory within one hour in heparinized saline (0.9 % NaCl in water) at 0 °C. The ophthalmic artery was localized and cannulated using a 0.61 mm (outer diameter) tube. Subsequently, the ophthalmic artery was perfused with saline using a syringe pump (pump model 33, Harvard Apparatus, MA, USA) at a flow rate of 0.1 mL/minute. Elimination of blood from the retinal blood vessels during perfusion indicated successful cannulation of the ophthalmic artery. Eyes with a successfully cannulated ophthalmic artery were further used for treatment with USMB.

Perfusion of microbubbles and treatment with USMB

SonoVue™ (Bracco International B.V., Amsterdam, Netherlands) was prepared according to the manufacturer's instructions, producing sulfur hexafluoride-filled phospholipid-coated microbubbles with a mean bubble diameter of 2.5 µm and a concentration of 1–5 x10⁸ microbubbles/mL [7]. Microbubbles were kept at 4 °C in between use, resuspended before every use and used within 4 hours after preparation.

Ultrasound imaging and USMB treatment were performed using a clinical system (iU22, Philips Medical Systems Nederland B.V., Best, Netherlands) and the C5-1 probe. Using an articulated arm (MA60103, Noga Engineering & Technology, Israel), the ultrasound probe was fixed on the cornea (Figure 1 A and B) with a small amount of ultrasound gel in between the cornea and the probe to ensure acoustic coupling. Prior to USMB treatment, ocular structures were visualized with B-mode imaging (Figure 2A). Subsequently, eyes were perfused with a solution containing microbubbles (diluted 10-times by volume using PBS), SYTOX™ green (final concentration 2 µM in PBS) and TRITC-dextran (final concentration 0.2 mM in PBS). During perfusion, circulation of

microbubbles in the posterior eye was confirmed by imaging the eye in contrast mode at mechanical index (MI) of 0.05 (Figure 2B). Subsequently, USMB therapy was done in Pulsed Wave (PW) Doppler mode (transmission frequency: 2.25 MHz, Sample Volume: 10 mm, Scale: 6 cm/second). Circulation of microbubbles, SYTOX™ green and TRITC-dextran was continuous during USMB treatment. During USMB treatment the PW Doppler cursor was aligned at the center of the retina and the optic nerve head was used as spatial reference. The acoustic field of the ultrasound probe in PW Doppler mode was measured using a 0.2 mm needle hydrophone (Precision acoustics Ltd., Dorset, United Kingdom) in degassed water [8] (Figure 3). USMB treatment was performed for 2 minutes at two different MIs (MI of 0.2 and 0.4 corresponding to peak-negative pressures of 0.3 and 0.6 MPa, respectively). Contrast images were acquired before and after treatment. Eyes perfused with the same solution but without microbubbles were treated at the same conditions and were used as control samples. Immediately after USMB treatment, eyes were perfused for 30 minutes with a solution containing SYTOX™ green and TRITC-dextran at the same concentrations as above and were subsequently fixed with perfusion of PFA for 1 minute. At the end of the experiment, periorcular tissues were removed, eyeballs were immersed in PFA and preserved at 4 °C for 48 hours until the preparation of flat mounts.

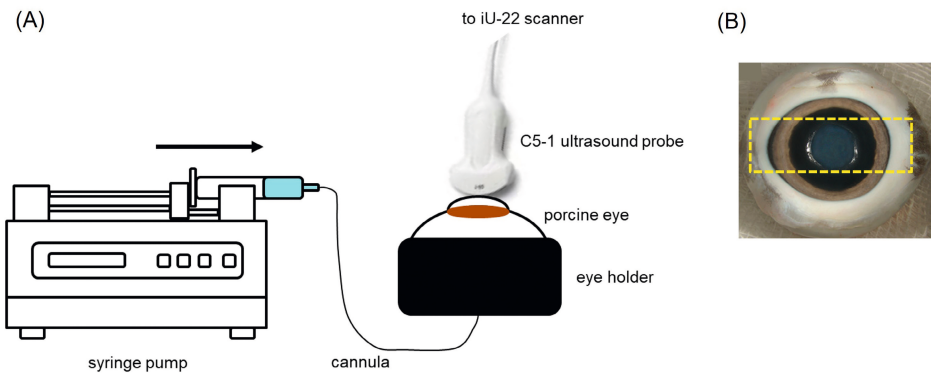


Figure 1. (A) Experimental setup used in USMB experiments. (B) Image of a porcine eye. Yellow rectangle indicates the orientation of the C5-1 probe.

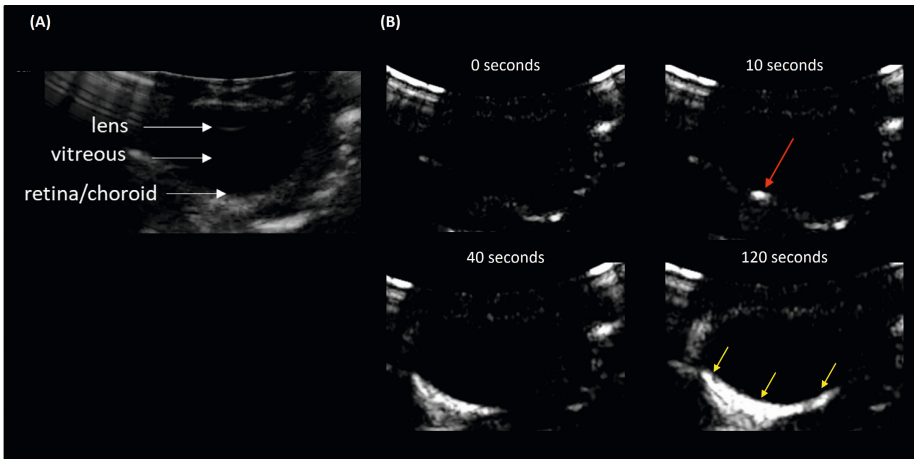


Figure 2. (A) Ocular structures of a porcine eye as imaged in B-mode. (B) Time-lapse contrast images of porcine eye during injection of microbubbles. Ten seconds after injection microbubbles enter the posterior eye in the area of the optic nerve head (red arrow). Two minutes after injection microbubbles circulate in the retina and choroid (yellow arrows).

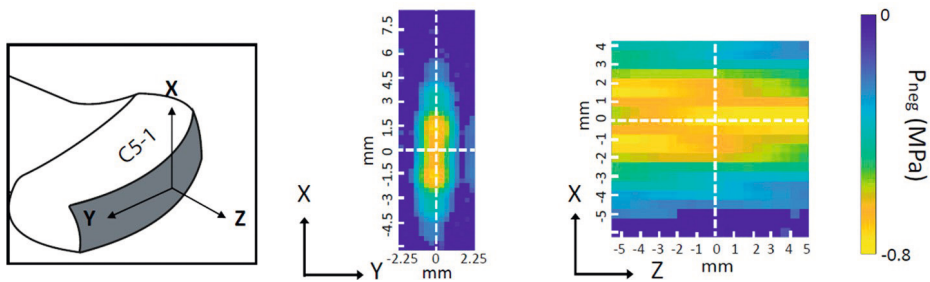


Figure 3. Pressure field maps of the C5-1 probe measured in PW Doppler mode. Middle: transversal plane, right: axial plane. Adapted from [8].

Preparation of flat mounts and cryosectioning

Flat mounts were prepared using fixed eyes. An incision was made in the anterior eye at 2-3 mm from the limbus and anterior ocular structures (cornea, iris, lens) were removed. Four incisions were made radially to the optic nerve head and the vitreous body was removed. Subsequently, flat mounts were illuminated with green fluorescent light (excitation 510-540 nm, NightSea, MA, USA) and macroscopic images were acquired through the viewing shield made of a 600nm longpass filter material. Samples were then preserved in 30 % sucrose in water solution (w/v) at 4 °C overnight. Subsequently, flat mounts were immersed in embedding compound for cryosectioning (OCT) and were preserved at -80 °C until sectioned. Samples were serially sectioned at 10 μm in the sagittal plane (parallel to the direction of ultrasound beam propagation) using a

cryostat (CM1950, Leica, Amsterdam, the Netherlands). Sections were sealed with a coverslip using mounting medium containing DAPI.

Fluorescence microscopy and quantification of the number of cells with intracellular accumulation

Tissue sections were imaged using a fluorescence confocal microscope (Leica TCS SP8X, Leica, Amsterdam, the Netherlands) in four channels (excitation 360 nm; emission 410–480 nm for DAPI, excitation 504 nm; emission 515–546 nm for SYTOX™ green, excitation 550 nm; emission 565–650 nm for TRITC-dextran, and phase contrast, 63x objective, image format 2048 x 2048 pixels; speed: 100; line average: 4)

Quantification of the number of cells with intracellular accumulation as a result of USMB treatment was performed with the ImageJ software (National Institutes of Health, Bethesda, MD, USA). A region of interest (ROI) was drawn in blue channel (DAPI) images surrounding the cells that form the blood vessel lumens. Within this ROI the total number of cells in the blue channel and the number of SYTOX™ green-positive cells in the green channel were automatically determined. Subsequently, the percentage of SYTOX™ green-positive cells over the total number of cells within the ROI was calculated.

Statistical analysis

Statistical analysis was performed using the GraphPad Prism software (version 8.0.1, GraphPad, San Diego, CA, USA), assuming that the samples follow non-parametric distribution. Statistically significant differences in the percentage of cells with intracellular accumulation were calculated between USMB-treated and samples treated only with ultrasound using Mann-Whitney test. Data in the graphs are shown as mean \pm SEM. Statistically significant differences between groups are annotated with asterisks by using * for $p < 0.05$ and ** for $p < 0.005$.

RESULTS

Microbubble circulation in the posterior eye

Microbubble circulation in the retina and choroid was imaged with ultrasound in contrast mode before and after USMB treatment. Figure 4 demonstrates the difference in intensity of microbubble signal for eyes treated at MI 0.2 and 0.4 before and after treatment (green boxes). At MI 0.2 the difference between before and after USMB

treatment was minimal. In contrast, at MI 0.4 contrast signal was dramatically decreased in intensity after USMB treatment at a large area. This area is aligned with the PW Doppler cursor (white cursor), which corresponds to the focus of the probe. This observation is in line with microbubble behavior described in literature: at MI 0.2 microbubbles oscillate but do not collapse (stable cavitation) whilst at MI 0.4, they burst as a result of high acoustic pressure (inertial cavitation) [9].

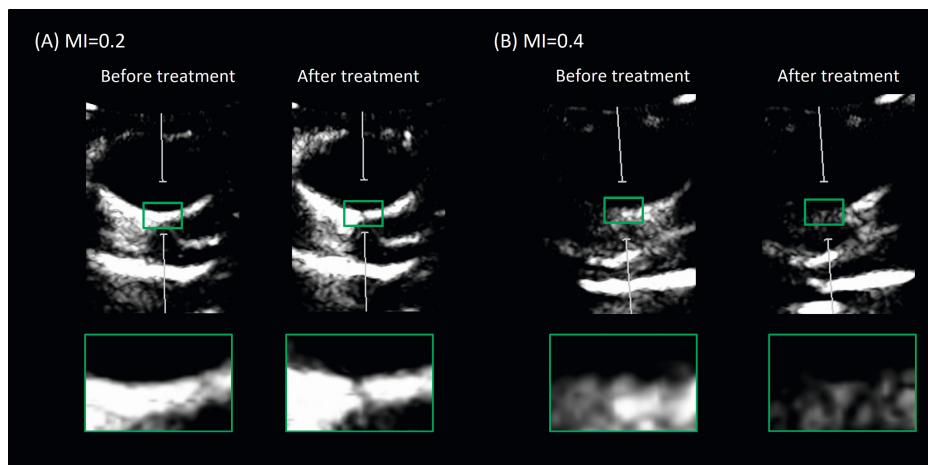


Figure 4. Ultrasound contrast images from porcine eyes treated with USMB at MI (A) 0.2 and (B) 0.4. Green boxes indicate enlargement of the focal area of the probe. Contrast signal was minimally (MI 0.2) and dramatically (MI 0.4) decreased after USMB treatment.

Intracellular accumulation of model drugs in the retina and choroid

During preparation of flat mounts, the retina was macroscopically visualized using green fluorescence light (Figure 5). In 3 out of 5 eyes that were treated with USMB a single, green spot was observed at the center of the retina in close proximity to the optic nerve head (Figure 5, upper row). The location of these spots suggests that they are spatially overlapping with the focus of the ultrasound beam and they likely consist of a group of cells with intracellular uptake of SYTOX™ green. To further examine these areas, the tissue including this spot and the optic nerve was isolated, sectioned and imaged with a fluorescent microscope. These spots were not observed in any of the eyes that were exposed to ultrasound without the presence of microbubbles (Figure 5, bottom row).

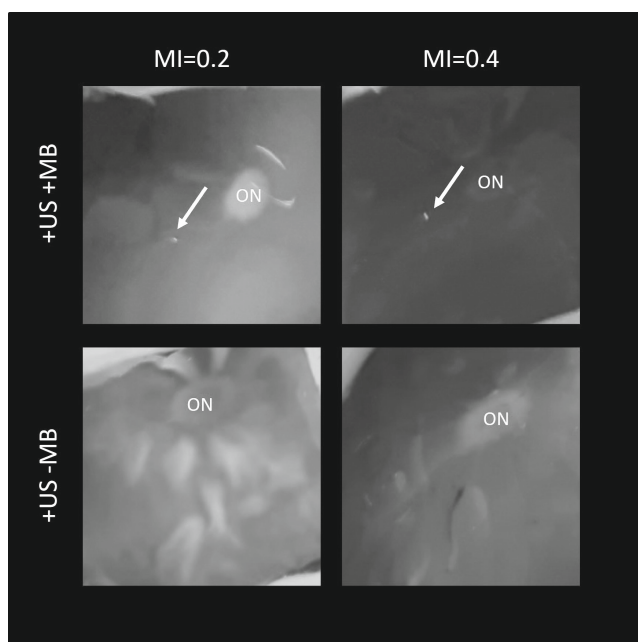


Figure 5. Macroscopic images of retina flat mounts of eyes during excitation with a green fluorescent light. Top: eyes treated with USMB (left: MI 0.2, right: MI 0.4), bottom: eyes exposed to ultrasound but no microbubbles. White arrows indicate the areas where SYTOXTM green-positive cells were present. Retinal detachment is an artefact of the flat mount preparation. ON: optic nerve head

Fluorescence microscopy of tissue sections revealed that USMB induced intracellular uptake of SYTOXTM green and fluorescent dextrans (Figure 6). Microscopic localization of SYTOXTM green and dextrans was observed even in the 2 out of 5 eyes that were treated with USMB but showed no green fluorescent signal macroscopically. In the USMB-treated eyes where a green fluorescent spot was visible macroscopically (3 out of 5 eyes), intracellular accumulation of SYTOXTM green was also seen microscopically in the area of the green spot, with no signs of autofluorescence. Microscopic accumulation of fluorescent molecules was not observed in any of the eyes that were treated with ultrasound without microbubbles.

Intracellular accumulation in USMB-treated eyes was observed in cells lining the lumen of blood vessels in the retina and choroid (Figures 6 and 7). Considering that microbubbles were injected into the ophthalmic artery, the cells lining the blood vessel walls are in contact with microbubbles during treatment and therefore are directly exposed to microbubble oscillations. In all cells with intracellular accumulation, both SYTOXTM green and 4 kDa or 20 kDa dextran were present. SYTOXTM green was localized

only in the cell nucleus whilst dextrans were present both inside the cytosol and the nucleus. No evidence of extravasation of dextrans in the retina or choroid was found.

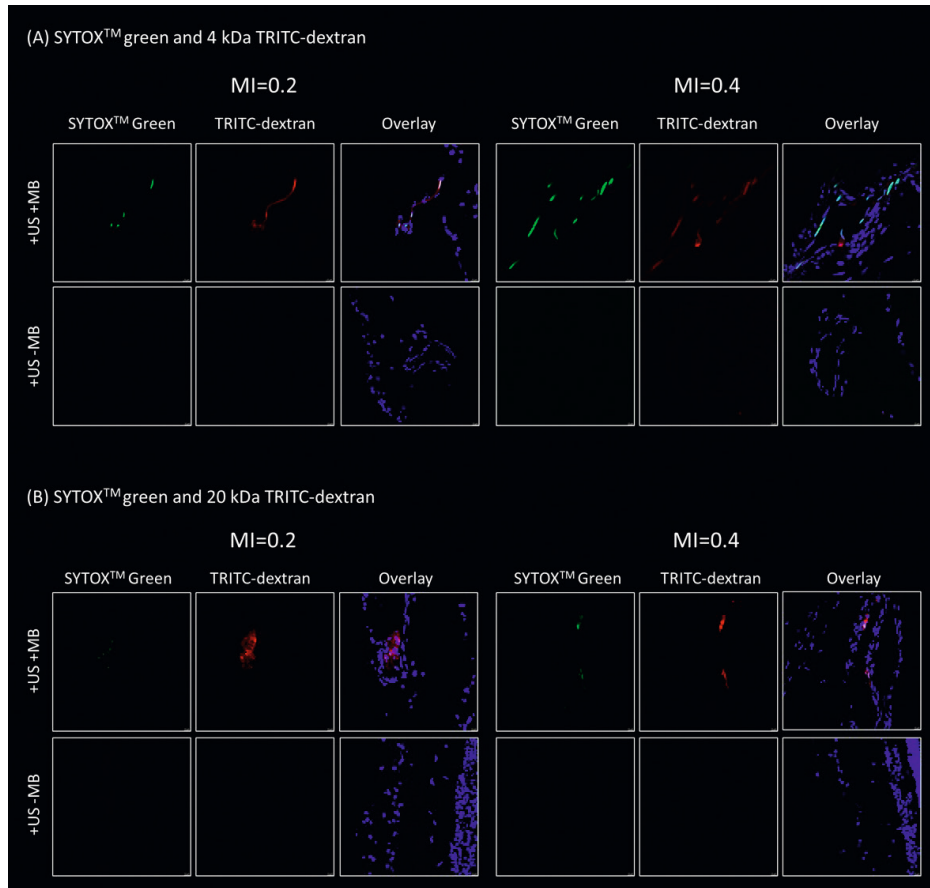


Figure 6. Fluorescence microscopy images showing intracellular accumulation of **(A)** SYTOXTM green and 4 kDa TRITC-dextran and **(B)** SYTOXTM green and 20 kDa TRITC-dextran after exposure to USMB. Blue in overlay images: DAPI, scale bar: 10 μ m

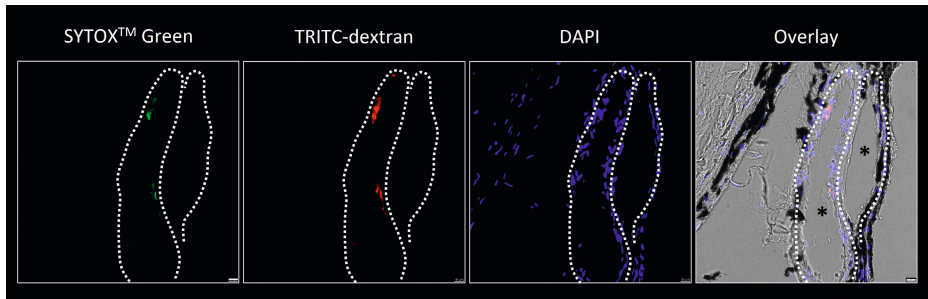


Figure 7. Example of induced intracellular accumulation in cells lining blood vessels in the choroid after treatment with USMB at MI 0.4. Asterisks in the overlay image indicate the lumen of choroidal blood vessels. White dotted line indicates the area of cells lining the blood vessel lumen. Overlay image is a combination of fluorescent and phase contrast images. Scale bar: 10 μm

Quantification of the number of cells with intracellular accumulation as a result of USMB treatment was performed by calculating the number of SYTOX™ green-positive cells over the total number of cells lining the blood vessel, which revealed that USMB induced a significant increase in the intracellular accumulation of this model drug (Figure 8). Specifically, eyes treated at MI 0.2 had on average $25.6 \pm 2.9\%$ of SYTOX™ green-positive cells, and eyes treated at MI 0.4 had $34.5 \pm 6.0\%$ positive cells. The difference between MI 0.2 and 0.4 was, however, not significant. Since no accumulation was observed in the eyes treated with ultrasound only, for the needs of the statistical analysis the number of SYTOX™ green-positive cells for the corresponding groups (i.e., +US-MB) was set to zero. The corresponding number of SYTOX™ green-positive cells in Figure 6A is 25.0 % for MI 0.2 and 38.1 % for MI 0.4, and Figure 6B is 28.6 % for MI 0.2 and 18.8 % for MI 0.4. The number of SYTOX™ green-positive cells in the eyes treated with ultrasound without microbubbles (+US-MB) in figures 6 and 7 was zero.

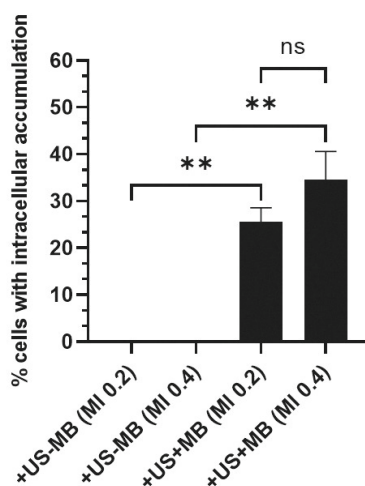


Figure 8. Quantification of the percentage of cells with intracellular accumulation of SYTOXTM green over the total number of cells lining blood vessels (n=5), ** for p<0.005, ns: not significant

DISCUSSION

Targeting the retina from the blood circulation is a less invasive alternative to intravitreal injections; the most frequently encountered drug delivery method in the treatment of retinal degenerative diseases. USMB has been previously proven as a method to transiently disrupt the BRB and allow the extravasation of (model) drugs from the blood circulation [4–6]. In this study, model drugs with molecular weights varying between 600 Da and 20 kDa were used to evaluate the efficacy of USMB using a clinically approved ultrasound system and microbubbles. Intracellular accumulation of SYTOXTM green (molecular weight 600 Da) and fluorescent dextrans (molecular weight 4 kDa and 20 kDa) was simultaneously observed in eyes exposed to MI 0.2 and 0.4, but not in eyes treated with ultrasound only.

The number of cells with SYTOXTM green signal was automatically counted to determine the percentage of cells with intracellular accumulation. The number of cells with intracellular accumulation was significantly increased in eyes treated with USMB at MI 0.2 and 0.4. In contrast to previous studies, no evidence of extravasation of model drugs from the blood vessels was seen as a result of BRB disruption. This difference might be attributed to the lower MIs used in our study. Similar to our observation, Hirokawa *et al.* did not observe any extravasation of fluorescein from retinal blood

vessels after treatment of rabbit eyes with USMB (MI 0.2, frequency 2 MHz, Definity® microbubbles), albeit some alterations in the diameter of uveal blood vessels were detected [4]. However, in their study, uveal endothelial cells were not microscopically examined and therefore no conclusion can be made concerning the intracellular accumulation of fluorescein at this MI. On the other hand, Park *et al.* reported the presence of gadolinium in the vitreous as a result of extravasation from the retina 10 minutes after USMB treatment [5]. However, the ultrasound pressures used in their study were much higher than ours (MI 0.98 to 1.32, frequency 0.7 MHz, Definity® microbubbles). Similarly, Touahri *et al.* observed extravasation of Evans blue in the retina 30 minutes after USMB treatment using MIs between 0.55 and 0.87 (frequency 1 MHz, Definity® microbubbles) [6].

Accumulation of model drugs was seen in cells lining blood vessels in the retina (Figure 6A and Figure 6B; MI 0.2) but also in the choroid (Figure 6B; MI 0.4 and Figure 7). Since microbubbles were circulating in the blood vessels these cells are presumably endothelial cells [10]. However, additional experiments using endothelial cell-specific markers (such as CD31) are needed in order to determine with certainty the exact cell type. Nevertheless, intracellular delivery of drugs in the endothelium of the retina and choroid using USMB could be beneficial for the treatment of certain retinal pathologies. An example is retinal neovascularization as a result of DR. Retinal neovascularization is a condition where abnormal, leaky blood vessels appear on the surface of the retina leading to vitreous hemorrhage and retinal detachment. Endostatin, a C-terminal fragment of collagen XVIII with molecular weight of 20 kDa, could be used in combination with USMB to inhibit endothelial proliferation and angiogenesis [11,12]. Another example of a potential use of USMB is to facilitate the enhancement of intracellular delivery of cisplatin (molecular weight 301 Da) for the treatment of retinoblastoma in children.

In our study, USMB treatment was performed using a clinical ultrasound system in PW Doppler mode. The advantage of this method is that clinical translation can be easier facilitated compared to previous studies that used preclinical ultrasound systems [5,6]. Furthermore, performing USMB treatment using an ultrasound scanner provides the advantage of simultaneous imaging of the ocular structures (in B-mode) and microbubbles (in contrast mode). In a previous study, a clinical ultrasound system (B-mode) was used for USMB treatment [4]. However, the PW Doppler mode used in our study enables to limit microbubble cavitation by focusing the ultrasound beam

in an area of a few millimeters (Figure 3), and therefore have more spatial control of the extent of the treatment. In addition, a larger number of cycles per pulse is more beneficial for therapeutic USMB [8,13], making PW Doppler settings (32 cycles per pulse [8]) more suitable for drug delivery applications over B-mode (typically 4-5 cycles per pulse [14]).

One limitation of our study is that the pressure field map of the ultrasound probe was measured in free field and the interaction of ultrasound waves (e.g., attenuation, refraction) with the anterior ocular tissues, such as the cornea and lens, and vitreous was not taken into account [15–17]. In the future, measurement of the acoustic field in PW Doppler mode in the presence of the anterior eye could accurately determine the acoustic energy the posterior eye is subjected to during USMB treatment. Furthermore, an integrated system for detection of the cavitation regime could be used during treatment in order to provide more insights on the microbubble activity and the safety of USMB in retinal drug delivery. An example of such system is the clinical ultrasound device previously used to induce controlled disruption of the blood-brain barrier and enhance the delivery of carboplatin in a rat glioma model [18]. Another interesting research question that arises from this study is on the bioeffects induced by USMB on the posterior eye; whether disruption of the BRB and extravasation of model drugs occurs along with intracellular accumulation and whether the extend of these bioeffects is driven by the ultrasound pressure.

CONCLUSION

In conclusion, this study has shown that USMB can be used to induce intracellular accumulation of model drugs in the retina and choroid. This technique could provide a minimally invasive method to deliver drugs in the posterior eye, as an alternative to intravitreal injections and enhance the efficacy of intravenous and intraarterial chemotherapy in the retina.

REFERENCES

1. Sampat, K.M.; Garg, S.J. Complications of Intravitreal Injections. *Curr. Opin. Ophthalmol.* 2010, 21, 178–183, doi:10.1097/ICU.0b013e328338679a.
2. Vo Kim, S.; Fajnkuchen, F.; Sarda, V.; Qu-Knafo, L.; Bodaghi, B.; Giocanti-Aurégan, A. Sustained Intraocular Pressure Elevation in Eyes Treated with Intravitreal Injections of Anti-Vascular Endothelial Growth Factor for Diabetic Macular Edema in a Real-Life Setting. *Graefes Arch. Clin. Exp. Ophthalmol.* 2017, 255, 2165–2171, doi:10.1007/s00417-017-3782-y.
3. Shields, C.L.; Bianciotto, C.G.; Jabbour, P.; Griffin, G.C.; Ramasubramanian, A.; Rosenwasser, R.; Shields, J.A. Intra-Arterial Chemotherapy for Retinoblastoma: Report No. 2, Treatment Complications. *Arch. Ophthalmol. Chic. Ill* 1960 2011, 129, 1407–1415, doi:10.1001/archophthalmol.2011.151.
4. Hirokawa, T.; Karshafian, R.; Pavlin, C.J.; Burns, P.N. Insonation of the Eye in the Presence of Microbubbles: Preliminary Study of the Duration and Degree of Vascular Bioeffects-Work in Progress. *J. Ultrasound Med.* 2007, 26, 731–738, doi:10.7863/jum.2007.26.6.731.
5. Park, J.; Zhang, Y.; Vykhodtseva, N.; Akula, J.D.; McDannold, N.J. Targeted and Reversible Blood-Retinal Barrier Disruption via Focused Ultrasound and Microbubbles. *PLoS ONE* 2012, 7, e42754, doi:10.1371/journal.pone.0042754.
6. Touahri, Y.; Dixit, R.; Kofoed, R.H.; Miloska, K.; Park, E.; Raeisossadati, R.; Markham-Coultes, K.; David, L.A.; Rijal, H.; Zhao, J.; et al. Focused Ultrasound as a Novel Strategy for Noninvasive Gene Delivery to Retinal Müller Glia. *Theranostics* 2020, 10, 2982–2999, doi:10.7150/thno.42611.
7. Schneider, M. Characteristics of SonoVue™. *Echocardiography* 1999, 16, 743–746, doi:10.1111/j.1540-8175.1999.tb00144.x.
8. De Maar, J.S.; Rousou, C.; van Elburg, B.; Vos, H.J.; Lajoinie, G.P.R.; Bos, C.; Moonen, C.T.W.; Deckers, R. Ultrasound-Mediated Drug Delivery With a Clinical Ultrasound System: In Vitro Evaluation. *Front. Pharmacol.* 2021, 12, doi:10.3389/fphar.2021.768436.
9. Lin, Y.; Lin, L.; Cheng, M.; Jin, L.; Du, L.; Han, T.; Xu, L.; Yu, A.C.H.; Qin, P. Effect of Acoustic Parameters on the Cavitation Behavior of SonoVue Microbubbles Induced by Pulsed Ultrasound. *Ultrason. Sonochem.* 2017, 35, 176–184, doi:10.1016/j.ultsonch.2016.09.016.
10. Sheikov, N.; McDannold, N.; Vykhodtseva, N.; Jolesz, F.; Hynynen, K. Cellular Mechanisms of the Blood-Brain Barrier Opening Induced by Ultrasound in Presence of Microbubbles. *Ultrasound Med. Biol.* 2004, 30, 979–989, doi:10.1016/j.ultrasmedbio.2004.04.010.
11. O'Reilly, M.S.; Boehm, T.; Shing, Y.; Fukai, N.; Vasios, G.; Lane, W.S.; Flynn, E.; Birkhead, J.R.; Olsen, B.R.; Folkman, J. Endostatin: An Endogenous Inhibitor of Angiogenesis and Tumor Growth. *Cell* 1997, 88, 277–285, doi:10.1016/S0092-8674(00)81848-6.
12. Wu, M.-X.; Zhou, X.-Y.; Xu, Y. Ultrasound-Targeted Cationic Microbubble-Mediated Gene Transfection and Inhibition of Retinal Neovascularization. *Int. J. Ophthalmol.* 2022, 15, 876–885, doi:10.18240/ijo.2022.06.04.
13. Van Rooij, T.; Skachkov, I.; Beekers, I.; Lattwein, K.R.; Voorneveld, J.D.; Kokhuis, T.J.A.; Bera, D.; Luan, Y.; van der Steen, A.F.W.; de Jong, N.; et al. Viability of Endothelial Cells after Ultrasound-Mediated Sonoporation: Influence of Targeting, Oscillation, and Displacement of Microbubbles. *J. Controlled Release* 2016, 238, 197–211, doi:10.1016/j.jconrel.2016.07.037.

14. Kotopoulos, S.; Dimcevski, G.; Helge Gilja, O.; Hoem, D.; Postema, M. Treatment of Human Pancreatic Cancer Using Combined Ultrasound, Microbubbles, and Gemcitabine: A Clinical Case Study: Clinical Sonoporation Setup for Human Pancreatic Cancer. *Med. Phys.* 2013, 40, 072902, doi:10.1118/1.4808149.
15. Thijssen, J.M.; Mol, H.J.M.; Timmer, M.R. Acoustic Parameters of Ocular Tissues. *Ultrasound Med. Biol.* 1985, 11, 157–161, doi:10.1016/0301-5629(85)90018-3.
16. Lafon, C.; Khokhlova, V.A.; Kaczkowski, P.J.; Bailey, M.R.; Sapozhnikov, O.A.; Crum, L.A. Use of a Bovine Eye Lens for Observation of HIFU-Induced Lesions in Real-Time. *Ultrasound Med. Biol.* 2006, 32, 1731–1741, doi:10.1016/j.ultrasmedbio.2006.07.035.
17. Huang, C.-C.; Zhou, Q.; Ameri, H.; Wu, D.W.; Sun, L.; Wang, S.-H.; Humayun, M.S.; Shung, K.K. Determining the Acoustic Properties of the Lens Using A High-Frequency Ultrasonic Needle Transducer. *Ultrasound Med. Biol.* 2007, 33, 1971–1977, doi:10.1016/j.ultrasmedbio.2007.06.004.
18. McDannold, N.; Zhang, Y.; Supko, J.G.; Power, C.; Sun, T.; Peng, C.; Vykhodtseva, N.; Golby, A.J.; Reardon, D.A. Acoustic Feedback Enables Safe and Reliable Carboplatin Delivery across the Blood-Brain Barrier with a Clinical Focused Ultrasound System and Improves Survival in a Rat Glioma Model. *Theranostics* 2019, 9, 6284–6299, doi:10.7150/thno.35892.

6

Summary and general discussion

SUMMARY

The objective of this thesis was to investigate the potential of ultrasound and microbubble (USMB) assisted drug delivery as a means to treat retinal diseases. Retinal diseases such as age-related macular degeneration and diabetic retinopathy are typically treated with intravitreal injection of anti-vascular endothelial growth factor (anti-VEGF) drugs. Owing to fast elimination of drugs from the vitreous humor, intravitreal injections need to be repeated (bi)monthly, which is often related to side effects, namely hemorrhages and in some cases retinal detachment [1,2]. Targeting the retina from the blood circulation could be a less invasive alternative to intravitreal injections. In addition, molecules that are intravenously administered and circulate in the choroid are in closer proximity to the disease site compared to intravitreally administered drugs that need to penetrate through the inner limiting membrane and multiple cell layers in the retina before they reach the target cells. However, intravenously administered drugs need to bypass the blood-retina barrier (BRB) before they have access to the retina [3]. Thus, a method that enables disruption of the BRB in a safe and reversible manner could potentially be combined with intravenously administered drugs.

Another example of a challenge in retinal drug delivery is in the treatment of retinoblastoma. This pediatric ocular malignancy is commonly treated with intravenous or intraarterial injection of chemotherapeutics, which often results in inadequate delivery of drugs to the tumor cells, leading to the presence of subretinal and vitreous seeds that cause recurrent and chemoresistant tumors [4]. A drug delivery method that can enhance the uptake of drug molecules by retinoblastoma cells would improve the efficacy of intravenously and intraarterially administered chemotherapy.

The mechanical oscillations microbubbles undergo when exposed to ultrasound waves are known to induce a number of bioeffects in the cells in their vicinity. These are (i) cellular membrane perforation (also known as sonoporation), (ii) endocytosis and (iii) disruption of intercellular junctions [5,6]. In the case of intravenously administered microbubbles, these bioeffects occur in the cell membranes of endothelial cells or the inter-endothelial junctions [7]. Consequently, intravenously administered microbubbles in combination with externally applied ultrasound, could be used to induce the abovementioned bioeffects at the BRB and facilitate targeted delivery of drugs to the retina.

The potential of USMB to improve ocular drug delivery has been explored worldwide. **Chapter 2** reviews the preclinical studies that examined this. The experimental systems used to date vary from *in vitro* using eye-derived cells to *in vivo* using healthy animals or animal disease models. In *in vivo* studies, microbubbles were administered as intravenous, intravitreal, subretinal, subconjunctival, intracorneal or intramuscular (ciliary muscle) injections, depending on the target side of each application. As delivery molecules various compounds were used namely, fluorescent dyes, nanoparticles, viral vectors, growth factors, small interfering RNA (siRNA) and chemotherapeutic drugs. In the studies that investigated extravasation of molecules from the retinal vasculature, some type of damage was observed in the retina (vasoconstriction of blood vessels, morphological alterations of tissue, neuroinflammation, etc.). In those studies that investigated the intracellular accumulation of compounds, some adverse effects were reported (i.e., haziness of the cornea) when high ultrasound intensities were used (3 W/cm^2). Other parameters that affected the viability of cells in *in vitro* studies were the exposure time, duty cycle and microbubble concentration. Consequently, the safety of USMB in the eye largely depends on the ultrasound settings used during treatment.

The efficacy of USMB in the transport of molecules with different physicochemical characteristics across an epithelial cell barrier was studied in **Chapter 3**. Molecules varied in molecular weight (182 Da to 20 kDa) and hydrophilicity (LogD at pH 7.4 from 1.5 to highly hydrophilic). Molecular permeability was studied using an *in vitro* epithelial (MDCK II) cell barrier. Different ultrasound pressures were used for the USMB treatment (P_{neg} 0.3-0.7 MPa, frequency 1.5 MHz, pulse duration 100 μs , duty cycle 10% and pulse repetition frequency 1 kHz). USMB did not alter the permeability of small molecules (molecular weight 259 to 376 Da) at any of the ultrasound pressures used, despite their differences in hydrophilicity (LogD at pH 7.4 from -3.2 to 1.5). On the contrary, for the two large molecules (molecular weight 4 and 20 kDa) permeability was significantly increased (3-7-fold) at the two highest ultrasound pressures (P_{neg} 0.5-0.7 MPa). At the same time, intracellular accumulation of the same large hydrophilic molecules was facilitated by USMB at P_{neg} of 0.7 MPa. Furthermore, the effect of USMB on the permeability of the barrier was investigated using a clinically relevant molecule (anti-CXCR4 nanobody, molecular weight 15 kDa) as a model drug for the treatment of retinoblastoma. USMB doubled the permeability of nanobody across the cell barrier and increased binding to retinoblastoma cells by five-fold.

To study the efficacy of USMB in a more physiologically representative system than an *in vitro* model, an experimental platform using arterially perfused *ex vivo* porcine eyes was developed. In **Chapter 4** a detailed description of the steps for enucleation of eyes at the abattoir, transportation to the laboratory, localization and cannulation of the ophthalmic artery, and perfusion of the eyes was given. Furthermore, potential pitfalls that might occur during the preparation and troubleshooting were discussed.

Using *ex vivo* eyes that were prepared as described in Chapter 4, the effect of USMB on the porcine retina was investigated in **Chapter 5**. A clinical imaging ultrasound system and commercially available microbubbles were used for the treatment at two different mechanical indexes (MI of 0.2 and 0.4). Intracellular accumulation of model drugs (molecular weight of 0.6-20.0 kDa) was observed in eyes treated with USMB but not in eyes that received ultrasound only. Intracellular accumulation was observed in cells lining the blood vessels in the retina and choroid. More specifically, 25.6 ± 2.9 % of cells had intracellular uptake at MI of 0.2 and 34.5 ± 6.0 % at MI of 0.4.

GENERAL DISCUSSION

USMB as a means to treat retinal diseases

The therapeutic effects of USMB in the anterior and posterior segments of the eye have been explored worldwide and were summarized in this thesis. Different approaches have been investigated in terms of microbubble injection side, the position of the ultrasound source and the delivered compound. From the *in vivo* studies that investigated the bioeffects of USMB in the retina, the majority used intravitreal injection of microbubbles. In the clinical scenario however, this approach will likely suffer from the adverse effects related to intravitreal administration, especially in the case where repeated treatment cycles are required. As a minimally invasive alternative, some other studies proposed treatment of the retina with USMB, using intravenously administered microbubbles [8–10]. Since targeting the retina from the bloodstream requires to bypass the BRB, the above studies focused on the efficacy of USMB in the temporal disruption of this biological barrier. These studies, however, investigated the effect of USMB on the delivery of molecules that varied in one physicochemical property (i.e., molecular weight) and did not examine whether USMB induced intracellular accumulation of the delivered compounds. These two questions were attempted to be answered in this thesis using *in vitro* and *ex vivo* models.

The effects of USMB in the retina: from *in vitro* to *ex vivo* studies

The *in vitro* study presented in this thesis demonstrated that USMB can enhance the permeability of compounds with molecular weight between 4 and 20 kDa. This is in agreement with previous studies that used other endothelial or epithelial cell barriers (Caco-2 and porcine brain endothelial cells) and compounds with various molecular weights (0.46-70 kDa) [11,12]. In addition, our *in vitro* results revealed that USMB enabled the intracellular accumulation of 4 and 20 kDa dextrans, indicating that more than one bioeffect was induced at the same USMB conditions. It was previously shown that multiple cellular mechanisms (cytoplasmic openings and formation of channels, opening of tight junctions and transcytosis) are simultaneously induced as a result of USMB on cells that are in the vicinity of microbubbles [7,13]. In addition, transcytosis appeared to have a significant role in the transport of molecules larger than 500 kDa across the blood-brain barrier (BBB) [14]. In our study intracellular accumulation of molecules was observed at 30 and 120 minutes after USMB treatment. However whether the molecules stay inside the cell or are released on the other side of the barrier as a result of transcellular permeability needs to be further investigated. Future experiments where the transport of molecules is traced over time may provide more insights about the exact cellular mechanisms that facilitated their permeability across the epithelial barrier. High-resolution fluorescence microscopy imaging of dextrans in combination with staining for clathrin and caveolin-1 (two established markers for clathrin- and caveolin-mediated transcytosis, respectively) could provide insights regarding the contribution of transcytosis in the permeability of these molecules across the cell barrier. In addition, independently and simultaneously inhibiting these two transcytosis pathways combined with permeability experiments using transwell inserts could help to comprehend if the permeability of dextrans is due to transcellular transport, opening of intercellular junctions or combination of the two.

The clinical relevance of USMB-induced permeability was demonstrated by examining the delivery of an anti-CXCR-4 nanobody across the epithelial barrier. The results showed a significant increase in the permeated nanobody and a consequent enhancement of its binding on retinoblastoma cells that express the CXCR-4 receptor, which were present on the other side of the cell barrier. To the best of our knowledge, this is the first time nanobody permeability induced by USMB treatment is reported. This positive outcome implies that USMB could be used to enhance the delivery of the anti-CXCR-4 nanobodies to retinoblastoma cells in the eye and enhance the inhibition of tumor cell proliferation and migration.

In contrast to our observations from studying large hydrophilic molecules, no measurable effect of USMB was seen on the permeability of small molecules (molecular weight 182-376 Da) across the MDCK II barrier. This is likely due to the leakiness of the barrier to small molecules, which allows their free permeation through the intercellular space. Indeed, the apparent permeability coefficient measured in our study in the absence of USMB was similar to what was previously reported for the same *in vitro* model ($P_{app} \approx 1.5 \times 10^{-6}$ cm/second) [15], indicating that the permeability of small molecules across the barrier is due to the intrinsic leakiness of the model to small molecules and not due to experimental errors in, for example, the culturing conditions of the cells. As a consequence of the barrier leakiness in small molecules, the increase in their permeability due to USMB treatment was not significant.

In contrast to *in vitro* cell models, the use of intact extracorporeal animal eyes ensures the preservation of tissue integrity and function that are essential when drug delivery applications in a complex organ such as the eye are investigated. Although *ex vivo* perfused animal eyes were used in the past for preclinical research in ophthalmology [16–18], a detailed explanation of the preparation process was not available in the literature. The experimental protocol included in this thesis provided a description of the steps required for the enucleation of porcine eyes at the abattoir and their transportation to the laboratory, the localization and cannulation of the ophthalmic artery and finally, the testing of cannulation in order to ensure successful perfusion of the anterior and posterior eye. In a previous study the viability of *ex vivo* perfused bovine eyes was reported between five and nine days with normothermic arterial perfusion using oxygenated perfusates of various compositions [19]. In future experiments the viability of the *ex vivo* porcine eye model could be determined by evaluating the deterioration of ocular tissues over time or by measuring other parameters such as the electrophysiological activity of the retina and intraocular pressure. Our *ex vivo* porcine eye model offers an attractive alternative to *in vivo* studies as it requires lower financial resources and can have an impact on the replacement of laboratory animals used for research and testing purposes (principle of the 3Rs: replacement, reduction, refinement [20]). The contribution of this work to the scientific community was verified by academic and industrial groups showing interest in the reproduction and use of the model in various applications, including drug delivery in the retina and the validation of a robotic system for the treatment of retinal vein occlusion (unpublished data).

Having the *ex vivo* perfused eye model operating in our laboratory, the next step was to investigate the effects of USMB-assisted drug delivery on the porcine retina. To this end, a clinical ultrasound imaging system and microbubbles approved for ultrasound imaging were used. Microbubbles were injected into the eye via the cannula and were circulating in the ocular blood vessels during USMB treatment, resembling microbubble intravenous administration *in vivo*. Microscopic examination of tissue slices revealed that USMB-assisted drug delivery enabled the intracellular accumulation of model drugs in cells lining the lumens of blood vessels, but not in eyes treated with ultrasound only. Intracellular accumulation in USMB-treated eyes was localized not only in the retina but also in the choroid. No evidence of extravasated molecules from the retinal or choroidal blood vessels was seen. Previous studies that examined the effects of USMB in the posterior eye upon intravenous administration of microbubbles solely reported extravasation of molecules from the retinal blood vessels [8–10]. In those studies intracellular accumulation was either not investigated or evidence was absence. Notably, the MIs used during USMB treatment in previous studies were considerably higher (MI 0.6-1.7) than in our *ex vivo* study (MI 0.2-0.4). However, comparison of the results between different studies should be done carefully as other parameters next to ultrasound pressure (and therefore MI) are pivotal for the bioeffects induced by USMB (e.g., microbubble composition and their resonance frequency, ultrasound frequency, duty cycle, exposure time). Nevertheless, future experiments using *ex vivo* perfused eyes treated with USMB at various ultrasound pressures could provide more insights about the conditions under which permeability and intracellular accumulation of model drugs are induced in the retina and choroid.

The ultrasound pressure field map used in the *ex vivo* experiments in this thesis was measured in free field (i.e., in water). However, anterior eye tissues, such as the lens and cornea, are known to attenuate and refract ultrasound waves [21–23]. Future measurement of the acoustic field in pulsed wave Doppler mode in the presence of the anterior eye would determine more accurately the acoustic energy the retina and choroid are exposed to during USMB treatment.

Therapeutic USMB towards clinical application for the treatment of retinal diseases

Prior to clinical translation of USMB-assisted drug delivery several steps need to be taken in order to further determine its efficacy and safety in the treatment of retinal diseases. The safety aspects discussed below could be tested in the future using

(perfused) post-mortem human eyes in order to have results that better resemble the clinical scenario compared to *in vitro* and *ex vivo* systems that use animal eyes.

Cavitation detection systems have been used in the past to determine *in vivo* the oscillation regime of microbubbles (i.e., stable or inertial cavitation) [24–26]. Using such a system would enable to record the generation of subharmonic, harmonic and ultraharmonic frequencies of cavitating microbubbles in real-time, and acquire information about the induced bioeffects in the retina. Ideally, the therapy system consists of two probes; one used in the USMB-assisted drug delivery and one in cavitation detection. The cavitation detection probe records microbubble signals during therapy and adjusts the ultrasound pressure generated by the USMB-assisted drug delivery probe using a feedback control algorithm. The system is specifically designed for ocular applications (i.e., it takes into account the dimensions of the eyeball and corrects for reflection signals generated by the orbital socket), the two probes are coaxially mounted and can be externally fixed on the eyelid with a small amount of ultrasound gel in between the eyelid and the probes to ensure acoustic coupling.

Microbubble dispersity is another aspect that determines the safety of USMB-assisted drug delivery *in vivo* [5]. To date, all available studies that investigated retinal drug delivery using USMB, used commercially available or home-made polydisperse microbubbles. Future use of monodisperse microbubbles (i.e., microbubble suspension with a unique size) will enable the generation of microbubble oscillations (and their induced bioeffects) that are uniform in terms of intensity and spatial distribution in the retina. Another safety aspect of USMB-assisted drug delivery in the eye is temperature elevation as a result of heat generation in ocular tissues that absorb ultrasound energy (e.g., lens and cornea). Lens hyperthermia (temperature increase to 41–43°C) is known to induce the formation of cataract and alterations in the corneal epithelium [27,28]. Kowalczyk *et al.* recorded a temperature increase of 3.7 °C in the lens and 7.3°C in the ciliary muscle during sonication of rat eyes *in vivo* [29]. Hence, extensive studies in human eyes are needed in order to determine the incidence of temperature elevation in the anterior and posterior ocular tissues during USMB-mediated drug delivery.

Currently available studies that investigated the effect of USMB in the retina using intravenous microbubbles, including the work presented in this thesis, were performed using model drugs in healthy small animals (mouse, rat, rabbit) or *ex vivo* models [8–10]. However, it is apparent that the therapeutic efficacy of USMB in the eye needs to

be further determined using animal models that display the pathological processes observed in human ocular diseases. Using USMB in combination with drugs in disease models for retinoblastoma [30], age-related macular degeneration [31] and diabetic retinopathy [32] would aid the understanding of the efficacy and the limitations of this treatment approach, which is essential prior to clinical trials.

Finally, some evidence of immunoreactivity has been previously reported as a result of BBB disruption with USMB [33]. In the eye, fibrinogen and erythrocytes were observed in the rat retina upon USMB-mediated disruption of the BRB, particularly at high ultrasound pressures [9,10]. Future studies are therefore needed to determine whether the intracellular accumulation observed in our study could lead to immunoactivation, other irreversible damage or adverse effects.

CONCLUSION

The work presented in this thesis aimed to investigate the potential of USMB-mediated drug delivery as a means to treat retinal diseases. The effects of USMB in the permeability of compounds with various molecular weights, including a nanobody that can be used in the treatment of retinoblastoma, were investigated *in vitro*. Furthermore, a clinical imaging ultrasound system in combination with commercially available microbubbles were tested in *ex vivo* perfused eyes validating the potential of USMB in retinal drug delivery. The encouraging results obtained in these studies showed a first promising step towards implementation of USMB-assisted drug delivery in the clinic to improve the cure of retinopathies.

REFERENCES

1. Sampat, K.M.; Garg, S.J. Complications of Intravitreal Injections. *Curr. Opin. Ophthalmol.* 2010, 21, 178–183, doi:10.1097/ICU.0b013e328338679a.
2. Vo Kim, S.; Fajnkuchen, F.; Sarda, V.; Qu-Knafo, L.; Bodaghi, B.; Giocanti-Aurégan, A. Sustained Intraocular Pressure Elevation in Eyes Treated with Intravitreal Injections of Anti-Vascular Endothelial Growth Factor for Diabetic Macular Edema in a Real-Life Setting. *Graefes Arch. Clin. Exp. Ophthalmol.* 2017, 255, 2165–2171, doi:10.1007/s00417-017-3782-y.
3. O’Leary, F.; Campbell, M. The Blood–retina Barrier in Health and Disease. *FEBS J.* 2021, doi:10.1111/febs.16330.
4. Shields, C.L.; Bianciotto, C.G.; Jabbour, P.; Griffin, G.C.; Ramasubramanian, A.; Rosenwasser, R.; Shields, J.A. Intra-Arterial Chemotherapy for Retinoblastoma: Report No. 2, Treatment Complications. *Arch. Ophthalmol. Chic. Ill* 1960 2011, 129, 1407–1415, doi:10.1001/archophthalmol.2011.151.
5. Deprez, J.; Lajoinie, G.; Engelen, Y.; De Smedt, S.C.; Lentacker, I. Opening Doors with Ultrasound and Microbubbles: Beating Biological Barriers to Promote Drug Delivery. *Adv. Drug Deliv. Rev.* 2021, 172, 9–36, doi:10.1016/j.addr.2021.02.015.
6. Qin, P.; Han, T.; Yu, A.C.H.; Xu, L. Mechanistic Understanding the Bioeffects of Ultrasound-Driven Microbubbles to Enhance Macromolecule Delivery. *J. Controlled Release* 2018, 272, 169–181, doi:10.1016/j.jconrel.2018.01.001.
7. Sheikov, N.; McDannold, N.; Vykhodtseva, N.; Jolesz, F.; Hynynen, K. Cellular Mechanisms of the Blood-Brain Barrier Opening Induced by Ultrasound in Presence of Microbubbles. *Ultrasound Med. Biol.* 2004, 30, 979–989, doi:10.1016/j.ultrasmedbio.2004.04.010.
8. Hirokawa, T.; Karshafian, R.; Pavlin, C.J.; Burns, P.N. Insonation of the Eye in the Presence of Microbubbles: Preliminary Study of the Duration and Degree of Vascular Bioeffects-Work in Progress. *J. Ultrasound Med.* 2007, 26, 731–738, doi:10.7863/jum.2007.26.6.731.
9. Park, J.; Zhang, Y.; Vykhodtseva, N.; Akula, J.D.; McDannold, N.J. Targeted and Reversible Blood-Retinal Barrier Disruption via Focused Ultrasound and Microbubbles. *PLoS ONE* 2012, 7, e42754, doi:10.1371/journal.pone.0042754.
10. Touahri, Y.; Dixit, R.; Kofoed, R.H.; Miloska, K.; Park, E.; Raeisossadati, R.; Markham-Coutles, K.; David, L.A.; Rijal, H.; Zhao, J.; et al. Focused Ultrasound as a Novel Strategy for Noninvasive Gene Delivery to Retinal Müller Glia. *Theranostics* 2020, 10, 2982–2999, doi:10.7150/thno.42611.
11. Fix, S.M.; Koppolu, B.P.; Novell, A.; Hopkins, J.; Kierski, T.M.; Zaharoff, D.A.; Dayton, P.A.; Papadopoulou, V. Ultrasound-Stimulated Phase-Change Contrast Agents for Transepithelial Delivery of Macromolecules, Toward Gastrointestinal Drug Delivery. *Ultrasound Med. Biol.* 2019, 45, 1762–1776, doi:10.1016/j.ultrasmedbio.2019.02.004.
12. Lelu, S.; Afadzi, M.; Berg, S.; Aslund, A.K.O.; Torp, S.H.; Sattler, W.; de L. Davies, C. Primary Porcine Brain Endothelial Cells as In Vitro Model to Study Effects of Ultrasound and Microbubbles on Blood–Brain Barrier Function. *IEEE Trans. Ultrason. Ferroelectr. Freq. Control* 2017, 64, 281–290, doi:10.1109/TUFFC.2016.2597004.

13. Beekers, I.; Langeveld, S.A.G.; Meijlink, B.; van der Steen, A.F.W.; de Jong, N.; Verweij, M.D.; Kooiman, K. Internalization of Targeted Microbubbles by Endothelial Cells and Drug Delivery by Pores and Tunnels. *J. Controlled Release* 2022, 347, 460–475, doi:10.1016/j.jconrel.2022.05.008.
14. Pandit, R.; Koh, W.K.; Sullivan, R.K.P.; Palliyaguru, T.; Parton, R.G.; Götz, J. Role for Caveolin-Mediated Transcytosis in Facilitating Transport of Large Cargoes into the Brain via Ultrasound. *J. Controlled Release* 2020, 327, 667–675, doi:10.1016/j.jconrel.2020.09.015.
15. Hellinen; Pirskanen; Tengvall-Unadike; Urtti; Reinisalo Retinal Pigment Epithelial Cell Line with Fast Differentiation and Improved Barrier Properties. *Pharmaceutics* 2019, 11, 412, doi:10.3390/pharmaceutics11080412.
16. Niemeyer, G. Retinal Research Using the Perfused Mammalian Eye. *Prog. Retin. Eye Res.* 2001, 20, 289–318, doi:10.1016/S1350-9462(00)00029-X.
17. Abarca, E.M.; Salmon, J.H.; Gilger, B.C. Effect of Choroidal Perfusion on Ocular Tissue Distribution After Intravitreal or Suprachoroidal Injection in an Arterially Perfused Ex Vivo Pig Eye Model. *J. Ocul. Pharmacol. Ther.* 2013, 29, 715–722, doi:10.1089/jop.2013.0063.
18. Koeberle, M.J.; Hughes, P.M.; Skellern, G.G.; Wilson, C.G. Pharmacokinetics and Disposition of Memantine in the Arterially Perfused Bovine Eye. *Pharm. Res.* 2006, 23, 2781–2798, doi:10.1007/s11095-006-9106-2.
19. De Coo, F.A.M.; Zonnenberg, B.A.; Trap, N.H. Prolonged Normothermic Perfusion of the Isolated Bovine Eye: Initial Results. *Curr. Eye Res.* 1993, 12, 293–301, doi:10.3109/02713689308999453.
20. Russell, W.M.; Burch, R.L. The Principles of Humane Experimental Technique. *Med. J. Aust.* 1960, 1, 500–500, doi:10.5694/j.1326-5377.1960.tb73127.x.
21. Lafon, C.; Khokhlova, V.A.; Kaczkowski, P.J.; Bailey, M.R.; Sapozhnikov, O.A.; Crum, L.A. Use of a Bovine Eye Lens for Observation of HIFU-Induced Lesions in Real-Time. *Ultrasound Med. Biol.* 2006, 32, 1731–1741, doi:10.1016/j.ultrasmedbio.2006.07.035.
22. Huang, C.-C.; Zhou, Q.; Ameri, H.; Wu, D.W.; Sun, L.; Wang, S.-H.; Humayun, M.S.; Shung, K.K. Determining the Acoustic Properties of the Lens Using A High-Frequency Ultrasonic Needle Transducer. *Ultrasound Med. Biol.* 2007, 33, 1971–1977, doi:10.1016/j.ultrasmedbio.2007.06.004.
23. Thijssen, J.M.; Mol, H.J.M.; Timmer, M.R. Acoustic Parameters of Ocular Tissues. *Ultrasound Med. Biol.* 1985, 11, 157–161, doi:10.1016/0301-5629(85)90018-3.
24. Ji, R.; Karakatsani, M.E.; Burgess, M.; Smith, M.; Murillo, M.F.; Konofagou, E.E. Cavitation-Modulated Inflammatory Response Following Focused Ultrasound Blood-Brain Barrier Opening. *J. Controlled Release* 2021, 337, 458–471, doi:10.1016/j.jconrel.2021.07.042.
25. Tung, Y.-S.; Vlachos, F.; Choi, J.J.; Deffieux, T.; Selert, K.; Konofagou, E.E. In Vivo Transcranial Cavitation Threshold Detection during Ultrasound-Induced Blood-brain Barrier Opening in Mice. *Phys. Med. Biol.* 2010, 55, 6141–6155, doi:10.1088/0031-9155/55/20/007.
26. McDannold, N.; Vykhodtseva, N.; Hynynen, K. Targeted Disruption of the Blood-brain Barrier with Focused Ultrasound: Association with Cavitation Activity. *Phys. Med. Biol.* 2006, 51, 793–807, doi:10.1088/0031-9155/51/4/003.

27. Lafond, M.; Aptel, F.; Mestas, J.-L.; Lafon, C. Ultrasound-Mediated Ocular Delivery of Therapeutic Agents: A Review. *Expert Opin. Drug Deliv.* 2017, 14, 539–550, doi:10.1080/17425247.2016.1198766.
28. Yamaguchi, K.; Barbe, M.F.; Brown, I.R.; Tytell, M. Induction of Stress (heat Shock) Protein 70 and Its mRNA in Rat Corneal Epithelium by Hyperthermia. *Curr. Eye Res.* 1990, 9, 913–918, doi:10.3109/02713689008999563.
29. Kowalczyk, L.; Boudinet, M.; El Sanharawi, M.; Touchard, E.; Naud, M.-C.; Saïed, A.; Jeanny, J.-C.; Behar-Cohen, F.; Laugier, P. In Vivo Gene Transfer into the Ocular Ciliary Muscle Mediated by Ultrasound and Microbubbles. *Ultrasound Med. Biol.* 2011, 37, 1814–1827, doi:10.1016/j.ultrasmedbio.2011.07.010.
30. Chévez-Barrios, P.; Hurwitz, M.Y.; Louie, K.; Marcus, K.T.; Holcombe, V.N.; Schafer, P.; Aguilar-Cordova, C.E.; Hurwitz, R.L. Metastatic and Nonmetastatic Models of Retinoblastoma. *Am. J. Pathol.* 2000, 157, 1405–1412, doi:10.1016/S0002-9440(10)64653-6.
31. Purevjav, E.; Pierre, J.F.; Lu *Preclinical Animal Modeling in Medicine*; 2022; ISBN 9781839688041 1839688041.
32. Quiroz, J.; Yazdanyar, A. Animal Models of Diabetic Retinopathy. *Ann. Transl. Med.* 2021, 9, 1272–1272, doi:10.21037/atm-20-6737.
33. McMahon, D.; Poon, C.; Hynynen, K. Evaluating the Safety Profile of Focused Ultrasound and Microbubble-Mediated Treatments to Increase Blood-Brain Barrier Permeability. *Expert Opin. Drug Deliv.* 2019, 16, 129–142, doi:10.1080/17425247.2019.1567490.

LIST OF ABBREVIATIONS

AMD	age-related macular degeneration
BBB	blood–brain barrier
BLs	bubble liposomes
BRB	blood–retina barrier
CEUS	contrast-enhanced ultrasound
CMB	cationic microbubbles
DPPC	1,2-dipalmitoyl-sn-glycero-3-phosphocholine
DSPA	1,2-distearoyl-snglycero-phosphoacid
DSPC	1,2-distearoyl-sn-glycero-phosphatidylcholine
DSPE-PEG(2k)-OMe	1,2-distearoyl-sn-glycero-3-phosphoethanolamine-N-[methoxy(polyethylene glycol)-2000]
DR	diabetic retinopathy
EGFP	enhanced green fluorescent protein
ES	endostatin
FDA	Food and Drug Administration
F-VEP	flash visual evoked potential
Gd	gadolinium
GFAP	glial fibrillary acidic protein
GFP	green fluorescence protein
H&E	hematoxylin and eosin
iBRB	inner blood–retina barrier
IgG	immunoglobulin G
IgM	immunoglobulin M
ILM	inner limiting membrane
INL	inner nuclear layer
IOP	intraocular pressure
L/siRNA	lipofectamine-formulated siRNA
MFI	mean fluorescence intensity
MI	mechanical index

mNGF	mouse neuron growth factor
mRNA	messenger RNA
mPEG-PLGA-PLL	monomethoxypoly(ethylene glycol)-poly(lactic-co-glycolic acid)-poly L-lysine
M_w	molecular weight
NMB	neutral microbubbles
NBs	nanobubbles
oBRB	outer blood–retina barrier
OLM	outer limiting membrane
ONL	outer nuclear layer
PDGF	platelet-derived growth factor
pDNA	plasmid DNA
pEGFP	plasmid enhanced green fluorescence protein
P_{app}	apparent permeability coefficient
PEI	polyethylenimine
PFP	perfluoropropane
P_{neg}	peak-negative pressure
PVR	proliferative vitreoretinopathy
rAAV	recombinant adeno-associated virus
RB	retinoblastoma
RGC	retinal ganglion cells
RP	retinitis pigmentosa
RPE	retina pigment epithelium
siRNA	small interfering RNA
TGF- β 2	transforming growth factor- β 2
UBM	ultrasound biomicroscopy
USMB	ultrasound and microbubbles
USNB	ultrasound and nanobubbles
USBL	ultrasound and bubble liposomes
VEGF	vascular endothelial growth factor
WFUMB	World Federation of Ultrasound in Medicine and Biology



Appendices

Nederlandse samenvatting

List of publications

Acknowledgements

About the author

NEDERLANDSE SAMENVATTING

Het doel van dit proefschrift was om de potentie van ultrageluid en microbellen (USMB) geassisteerde medicijnafgifte te onderzoeken als middel om netvliesandoeningen te behandelen. Netvliesandoeningen zoals leeftijdsgebonden maculaire degeneratie en diabetische retinopathie worden typisch behandeld met intravitreale injecties van anti-vasculaire endotheliale groeifactor (anti-VEGF) medicijnen. Vanwege de snelle eliminatie van medicijnen uit het glasvocht, moeten intravitreale injecties (twee) maandelijks worden herhaald, wat vaak verband houdt met bijwerkingen. De meest ernstige bijwerkingen zijn bloedingen en in sommige gevallen zelfs netvliesloslating. Het toedienen van medicatie in het netvlies vanuit de bloedcirculatie zou een minder ingrijpend alternatief kunnen zijn voor intravitreale injecties. Bovendien bevinden moleculen die intraveneus worden toegediend en circuleren in het vaatvlies zich dichterbij de ziektezijde in vergelijking met intravitreaal toegediende geneesmiddelen die door het binnenste beperkende membraan en meerdere cellagen in het netvlies moeten penetreren voordat ze de doelcellen bereiken. Intraveneus toegediende geneesmiddelen moeten echter wel de bloed-retinabarière (BRB) passeren voordat ze toegang hebben tot het netvlies. De USMB methode die verstoring van de BRB op een veilige en tijdelijke manier mogelijk maakt, zou dus mogelijk kunnen worden gecombineerd met intraveneus toegediende medicijnen, zodat deze beter het netvlies kunnen bereiken.

Een ander voorbeeld van de bestaande uitdagingen bij de toediening van geneesmiddelen aan het netvlies is de behandeling van retinoblastoom. Deze pediatrische oculaire maligniteit wordt gewoonlijk genezen met intraveneuze of intra-arteriële injectie van chemotherapeutica, wat vaak resulteert in onvoldoende afgifte van medicijnen aan de tumorcellen, wat leidt tot het onvolledig verwijderen van tumorcellen in het glasvocht en de subretinale ruimte. Deze overgebleven tumorcellen kunnen terugkerende en chemoresistente tumoren veroorzaken. Een medicijnafgiftemethode die de opname van medicijnmoleculen door retinoblastoomcellen kan verbeteren, zou de werkzaamheid van intraveneus en intra-arterieel toegediende chemotherapie kunnen verbeteren.

Het is bekend dat de mechanische oscillaties die microbellen ondergaan wanneer ze worden blootgesteld aan ultrageluid golven, een aantal bio-effecten veroorzaken in de cellen in hun directe omgeving. Dit zijn (i) celmembraanperforatie (ook bekend als sonoporatie), (ii) endocytose en (iii) verstoring van intercellulaire verbindingen. In

het geval van intraveneus toegediende microbellen treden deze bio-effecten op in de celmembranen van endotheelcellen of de inter-endotheelverbindingen. Bijgevolg zouden intraveneus toegediende microbellen in combinatie met extern aangebrachte ultrageluid kunnen worden gebruikt om de bovengenoemde bio-effecten op de BRB te induceren en gerichte toediening van medicijnen aan het netvlies te vergemakkelijken.

Het idee dat USMB oculaire medicijnafgifte kan verbeteren, is wereldwijd onderzocht. Hoofdstuk 2 geeft een overzicht van de preklinische studies die dit hebben onderzocht. De tot nu toe gebruikte experimentele systemen variëren van in vitro met behulp van cellen die hun oorsprong vinden in het oog tot in vivo met behulp van gezonde dieren of dierziektmodellen. In in vivo studies werden microbellen toegediend als intraveneuze, intravitreale, subretinale, subconjunctivale, intracorneale of intramusculaire (ciliaire spier) injecties, afhankelijk van de specifieke, te bereiken locatie in het oog van elke toepassing. Als afgiftemoleculen werden verschillende stoffen gebruikt, namelijk fluorescerende kleurstoffen, nanodeeltjes, virale vectoren, groeifactoren, klein interfererend RNA en chemotherapeutische geneesmiddelen. In de onderzoeken die de extravasatie van moleculen uit het vaatstelsel van het netvlies onderzochten, werd beschadiging van het netvlies waargenomen (vasoconstrictie van bloedvaten, morfologische veranderingen van het weefsel, neuro-inflammatie, enz.). In de onderzoeken die de intracellulaire accumulatie van bepaalde stoffen onderzochten, werden enkele nadelige effecten gemeld (bijv. troebelheid van het hoornvlies) wanneer hoge ultrageluid intensiteiten werden gebruikt (3 W/cm²). Andere parameters die de levensvatbaarheid van cellen in in vitro-onderzoeken beïnvloedden, waren de blootstellingstijd, de arbeidscyclus en de concentratie van microbellen. Bijgevolg hangt de veiligheid van USMB in het oog grotendeels af van de ultrageluid instellingen die tijdens de behandeling worden gebruikt.

De effectiviteit van USMB in het verbeteren van het transport van moleculen met verschillende fysisch-chemische eigenschappen door een epitheelcelbarrière werd bestudeerd in Hoofdstuk 3. Moleculen met variërende molecuulgewicht (182 Da tot 20 kDa) en hydrofiliciteit (LogD bij pH 7.4 van 1.5 tot zeer hydrofiel). Moleculaire permeabiliteit werd bestudeerd met behulp van een in vitro epitheliale (MDCK II) celbarrière. Voor de USMB-behandeling werden verschillende ultrageluid drukwaarden gebruikt (Pneg 0.3-0.7 MPa). USMB veranderde de permeabiliteit van kleine moleculen (molecuulgewicht 259 tot 376 Da) bij geen van de gebruikte ultrageluid drukken, ondanks hun verschillen in hydrofiliciteit (LogD bij pH 7.4 van -3.2 tot 1.5). Voor de

twee grote moleculen (molecuulgewicht 4 en 20 kDa) was de permeabiliteit significant verhoogd (3-7 maal) bij de twee hoogste ultrageluid drukken (Pneg 0.5 en 0.7 MPa). Tegelijkertijd werd intracellulaire accumulatie van dezelfde grote hydrofiele moleculen vergemakkelijkt door USMB bij Pneg van 0.7 MPa. Verder werd het effect van USMB op de permeabiliteit van de barrière onderzocht met behulp van een klinisch relevant molecuul (anti-CXCR4 nanobody, molecuulgewicht 15 kDa) als modelgeneesmiddel voor de behandeling van retinoblastoom. USMB verdubbelde de permeabiliteit van nanobody over de celbarrière en verhoogde de binding aan retinoblastoomcellen met een factor vijf.

Om de werkzaamheid van USMB te bestuderen in een meer fysiologisch representatief systeem dan een in vitro model, werd een experimenteel platform ontwikkeld met arterieel geperfuseerde ex vivo varkensogen. In Hoofdstuk 4 wordt een gedetailleerde beschrijving gegeven van de stappen voor het verwijderen van de ogen in het slachthuis, het transport naar het laboratorium, het lokaliseren en canuleren van de oogslagader en perfusie van de ogen. Verder werden mogelijke valkuilen besproken die kunnen optreden tijdens de voorbereiding en het oplossen van mogelijke problemen.

Met behulp van ex vivo ogen die waren geprepareerd zoals beschreven in Hoofdstuk 4, werd het effect van USMB op het netvlies van varkens onderzocht in Hoofdstuk 5. Een klinisch beeldvormend echografiesysteem en commercieel verkrijgbare microbellen werden gebruikt voor de behandeling bij twee verschillende mechanische indexen (MI van 0.2 en 0.4). Intracellulaire accumulatie van modelgeneesmiddelen (molecuulgewicht van 0.6-20.0 kDa) werd waargenomen in ogen die waren behandeld met USMB, maar niet in ogen die alleen ultrageluid ontvingen. Intracellulaire accumulatie werd waargenomen in cellen langs de bloedvaten in het netvlies en de choroidea. Specifiek had 25.6 ± 2.9 % van de cellen intracellulaire opname bij een MI van 0.2 en 34.5 ± 6.0 % bij een MI van 0.4.

De bemoedigende resultaten die in deze onderzoeken werden verkregen, tonen een eerste, veelbelovende stap in de richting van implementatie van door USMB ondersteunde medicijnafgifte in de kliniek om de genezing van retinopathieën te bevorderen.

LIST OF PUBLICATIONS

Rousou, C.; Schuurmans, C.C.L.; Urtti, A.; Mastrobattista, E.; Storm, G.; Moonen, C.; Kaarniranta, K.; Deckers, R. Ultrasound and Microbubbles for the Treatment of Ocular Diseases: From Preclinical Research towards Clinical Application. *Pharmaceutics* 2021, 13, 1782

Rousou, C.; de Maar, J.; Qiu, B.; van der Wurff-Jacobs, K.; Ruponen, M.; Urtti, A.; Oliveira, S.; Moonen, C.; Storm, G.; Mastrobattista, E.; et al. The Effect of Microbubble-Assisted Ultrasound on Molecular Permeability across Cell Barriers. *Pharmaceutics* 2022, 14, 494

Rousou, C.; Hoogenboom, P.; van Overdam, K.A.; Storm, G.; Dorrestijn, J.; Mastrobattista, E. A Technical Protocol for an Experimental Ex Vivo Model Using Arterially Perfused Porcine. *Eyes. Exp. Eye Res.* 2019, 181, 171–177

Rousou, C.; van Kronenburg, N.; Moonen, C.; Storm, G.; Mastrobattista, E.; Deckers, R. Microbubble-mediated drug delivery in the retina using a clinical ultrasound system. Manuscript in preparation

De Maar, J.S.; **Rousou, C.**; van Elburg, B.; Vos, H.J.; Lajoinie, G.P.R.; Bos, C.; Moonen, C.T.W.; Deckers, R. Ultrasound-Mediated Drug Delivery With a Clinical Ultrasound System: In Vitro Evaluation. *Front. Pharmacol.* 2021, 12

Ilochonwu, B.C.; Mihajlovic, M.; Maas-Bakker, R.F.; **Rousou, C.**; Tang, M.; Chen, M.; Hennink, W.E.; Vermonden, T. Hyaluronic Acid-PEG-Based Diels–Alder In Situ Forming Hydrogels for Sustained Intraocular Delivery of Bevacizumab. *Biomacromolecules* 2022, 23, 2914–2929

ACKNOWLEDGEMENTS

During the past five years I was fortunate to meet and collaborate with a lot of people that helped me to develop both professionally and personally. I would like to thank the colleagues, family and friends that made it possible for me to complete this journey but most importantly, made me enjoy along the way.

I would like to express my deepest gratitude to **Enrico**. You have been a great advisor; you always trusted my capabilities, even those days that I had my doubts. You encouraged me to take the lead in my research and independently make decisions about the next steps. You were always willing to answer my questions, even when your schedule was very tight. Thanks for the tips about integration into Dutch society back in 2017, for practicing Dutch and for all the parenting-related advice. I deeply appreciate your honesty, fairness and your ability to create a feeling of safeness and togetherness within a group of people. Pharmaceutics is very lucky to have you as a leader!

I also appreciate the input of **Gert** during our meetings. Your pragmatic and structured way of thinking, helped me to materialize my research and develop a view point for the long term. I also learned a lot from you about scientific writing; your feedback has been invaluable.

Chrit, when I met you in Cyprus, back in 2015, I could tell right away that you are a person overflowing with kindness. Thank you for the support you provided already before the beginning of my PhD journey, until the very end of it. Your dedication and knowledge are truly impressive. The walks around the UMCU were a time of enlightenment and brainstorming for me. I learned a lot from your feedback and guidance.

Thank you, **Roel**, for being my co-promotor. You were always willing to help me out in the lab and give me practical advice about my experiments. I learned a lot from your comments on my manuscripts and your structured way of writing. Discussing my experimental results at the Drug Delivery meetings was always a great opportunity to get feedback and insights from you and **Clemens**. You make an excellent team together.

Sabrina, during our collaboration you were always positive and you provided the scientific guidance I needed to accomplish the nanobody project. The way you approach research and your kindness are remarkable.

It was a great pleasure to be part of the OcuTher consortium. I had the opportunity to collaborate with researchers from around the world and travel across Europe for meetings. I would like to express my warmest thanks to **Kai** for the opportunity to spend time at the Ophthalmology department at the University Hospital in Kuopio. Thank you for showing me how patients with retinal diseases are diagnosed and treated in clinical practice, and for discussing together the disadvantages of current treatments. I would like to thank you, **Arto** and **Marika**, for accepting me in your laboratory to conduct my secondment studies. Thank you for the training in various ocular-specific *in vitro* and *ex vivo* methods, and for providing me with your guidance and advice. **Lea**, you are a great lab technician! Thank you for your help in the transwell experiments. Your contribution was invaluable. A big thank you to all my **fellow OcuTher PhD students** for the cooperation and the fun times we had in our trips, and specifically **Amir**, **Anam** and **Anusha** for your warm hospitality in Kuopio. **Karin**, thank you for the excellent organization and assistance during our consortium meetings and my stay in Finland.

Having well-organized, functional and tidy laboratories can be a challenging task, which couldn't be accomplished without the hard work of our technicians. A big thank you to **Roel**, **Joep**, **Mies**, **Louis**, **Imro** and **Esmeralda** for your help in the cell culture and biochemistry laboratories, for taking care of the orders and face any other technical challenges that appeared in the lab from time to time, especially during the COVID-19 pandemic. Special thanks to **Kim** for your help with the flow cytometry experiments. Thank you, **Marcel**, for your help with the HUVEC experiments and the training on cryosectioning. I also appreciate your help, **Nicky**, with going to the slaughterhouse and preparing the *ex vivo* eyes, particularly during the months of my pregnancy. **Barbara**, thank you for your help with the administrative and organizational work.

I owe my thanks to the team from the Rotterdam Eye Hospital and the Rotterdam Eye Institute. My biggest thank you goes to **Piet**, who passed on the knowledge on the *ex vivo* perfused eye model, which turned out to be one of the most powerful tools I used in my PhD. Thank you also to **Koen** and **Netty** for your feedback on the article about the *ex vivo* model. **Sonia** and **Koorosh**, I learned a lot from you about vitreoretinal surgery. Your enthusiasm and dedication to research are truly impressive. Thank you to my collaborators from the PRECEYES team: **Jorrit** and **Elke**, I had a great time in Eindhoven during the feasibility study for the robot and I can't wait to start working together in March!

I also want to thank my students **Mayke** and **Mayang**. It was great guiding you during your internships and you have both taught me a lot.

Thank you to the **PhD students** and **PostDocs** of Pharmaceutics and UIPS for the pleasant atmosphere, the scientific advice and the nice time inside and outside the lab. Special thanks to **Boning**, for your precious help in my last cell experiments and the fruitful scientific discussions. **Blessing**, thank you for the good time during our trips and for your help at the start of my PhD.

Αρχίζω να σκέφτομαι τι θα γράψω για 'σας και ήδη χαμογελάω! Αγαπημένοι μου **Βάσω**, **Σοφία**, **Τάσο** και **Έλσα**, σας ευχαριστώ για τη βοήθεια στο εργαστήριο κυττάρων και τις υπέροχες, γεμάτες γέλιο βραδιές στο κέντρο της Ουτρέχτης. Μαζί σας πέρασα μερικούς από τους πιο όμορφους μήνες του διδακτορικού μου, που είχαν μια ζεστασιά που θυμίζει Ελλάδα. Σας εύχομαι από καρδιάς να προοδεύετε στον τομέα σας. Είμαι σίγουρη πως θα διαπρέψετε!

Πάτερ Αλέξανδρε, Μαρία και **Κωνσταντίνε**, είναι πραγματική ευλογία να σας έχω στη ζωή μου. Σας ευχαριστώ για την καλοσύνη, τη φιλοξενία σας και για όλες τις Κυριακές που γεμίσατε με φως και αισιοδοξία.

My dear UMCU colleagues and friends **Josanne** and **Helen**, you have a special place in my heart! Josanne, you have been my "right hand" in the permeability experiments and I know that without your input I wouldn't have made it! Thank you for your support and encouragement in difficult times. Also, thank you for accepting to be my paranymph! Thank you Helen for your help in the laboratory and the practical tips about cell work in the beginning of my PhD. Your constructive comments and advice during the Drug Delivery meetings were extremely helpful. Thank you both for the cozy outings we had; I am looking forward to many more!

Carel, Rob, Vicky, Lex en **Sara**, jullie hebben van mij gehouden sinds ik in jullie leven kwam en jullie zijn mijn tweede familie geworden. Ik voel me vereerd om deel uit te maken van jullie gezin. Bedankt voor alles dat jullie voor mij hebben gedaan!

Αδερφές μου, **Μαρία** και **Άντρη**, οι υποστηρικτικές και ευγενικές σας προσωπικότητες πάντε με ενέπνεαν. Είναι πραγματικά ευτυχία να σας έχω αδερφές! Σας ευχαριστώ που είσαστε πάντα δίπλα μου και πρόθυμες να με βοηθήσετε.

Λατρεμένοι μου **μπαμπά** και **μαμά**, χάρη στην αφοσίωσή σας μπορώ σήμερα να γράφω το ευχαριστήριο μήνυμα αυτό. Σας ευχαριστώ για την αστείρευτη αγάπη, υπομονή, επιμονή και στήριξη που μου παρείχατε στο ταξίδι αυτό. Είσαστε οι σπουδαιότεροι καθοδηγητές της ζωής μου και σας ευχαριστώ από καρδιάς για όλα όσα μου προσφέρετε με ανιδιοτέλεια κάθε μέρα.

Κοριτσάκι μου, σαν ανοιξιάτικο λουλούδι, γεμίζεις τη ζωή μου με τα πιο φωτεινά χρώματα από τότε που σε γνώρισα κι ακόμη πιο πριν! Τους τελευταίους μήνες του διδακτορικού μου, μου έδινες τόση δύναμη και κουράγιο κάθε μέρα, χωρίς καν να το γνωρίζεις! Ένα άγγιγμα στην κοιλίτσα ήταν αρκετό να με γεμίσει ελπίδα! Σ'ευχαριστώ που μου έδειξες πώς από αγάπη γεννιέται αγάπη, κι αυτή πολλαπλασιάζεται και δυναμώνει κάθε μέρα. Σε λατρεύω, πάντα!

Carl, it is certain, if nothing else, that this journey was worth it to meet you. I could not have completed this life chapter without your support and patience. Your unconditional love and pure kindness have made me a better person. I am extremely grateful for the past few years together and the family we have created. I can't wait to see where life will take us. Thank you very much for everything you do and for being my paranymph. Σ' αγαπώ!

December 2022

ABOUT THE AUTHOR

Charis Rousou was born in 1992 in Nicosia, Cyprus. After obtaining her high school diploma, in 2009 she enrolled in the Mechanical and Manufacturing Engineering program at the University of Cyprus. Simultaneously, she obtained a Minor degree in Biomedical Engineering at the same university. In her bachelors thesis she studied the ultrasound beam parameters that induce inertial cavitation for use in drug delivery applications. Between 2014 and 2016 she continued her studies following the Mechanical Engineering masters program, in the discipline of Biomedical Engineering. During her postgraduate studies she executed a single-arm clinical trial, where she investigated the response of breast cancer patients to neoadjuvant therapy using dynamic contrast enhanced ultrasound (DCEUS), under the supervision of Dr. Mike Averkiou. In 2017 she started her Doctoral studies in the Drug Innovation program at Utrecht University, the Netherlands. The results of her work are presented in this PhD thesis entitled “Microbubble-assisted ultrasound for retinal drug delivery”.



